Διδακτορική διατριβή

Μελέτη των μηχανικών ιδιοτήτων και των φωτογενών μεταβολών τους στο Άμορφο Υδρογονωμένο Πυρίτιο: ο ρόλος του υδρογόνου

Εμμανουήλ Σπανάκης

Τμήμα Φυσικής

Πανεπιστήμιο Κρήτης

Ηράκλειο – 2001

PhD thesis

Mechanical properties and their photo-induced changes in hydrogenated amorphous Silicon: Study of the role of hydrogen.

Emmanuel Spanakis

Physics Department

University of Crete

Heraklion – 2001

Ευχαριστίες

Θα ήθελα να ευχαριστήσω θερμά τον επιβλέποντα καθηγητή μου Παναγιώτη Τζανετάκη για την πολύτιμη πειραματική και θεωρητική καθοδήγηση και βοήθεια στην διάρκεια της εργασίας αυτής.

Επίσης ευχαριστώ τον συνάδελφο μου Μανόλη Στρατάκη για την υποδειγματική συνεργασία, τις συζητήσεις και τις ιδέες που μου προσέφερε καθ' όλη την διάρκεια της μελέτης αυτής.

Σημαντική υπήρξε επίσης η βοήθεια του Νίκου Κοπιδάκη ιδιαίτερα στις αρχές της δουλειάς και τον ευχαριστώ ιδιαίτερα για αυτό. Ευχαριστώ επίσης τους συναδέλφους μου στο εργαστήριο Αντώνη Κονδύλη και Μαρία Σπυριδάκη για την συνεργασία τους.

Πολύτιμη ήταν επίσης η συνεισφορά του καθηγητή Hellmut Fritzsche με τον οποίο είχαμε συνεχείς ανταλλαγές απόψεων στην διάρκεια των τεσσάρων χρόνων της δουλειάς αυτής. Τον ευχαριστώ για τις πάντα εύστοχες επισημάνσεις του τόσο σε θεωρητικό όσο και σε πειραματικό επίπεδο. Επίσης ευχαριστώ τον Howard Branz για τις συζητήσεις που είχαμε κατά την διάρκεια της εδώ παραμονής του.

Θέλω να ευχαριστήσω τον Qi Wang από το National Renewable Energy Laboratory και τους J. Yang και S. Guha από την United Solar Systems για την συνεργασία και τα δείγματα που μας παρείχαν.

Το μεγαλύτερο μέρος των μετρήσεων πραγματοποιήθηκε στα εργαστήρια της Ομάδας Μικροηλεκτρονικής του ΙΤΕ. Θέλω να ευχαριστήσω θερμά την Κατερίνα Τσαγκαράκη για τον απεριόριστο χρόνο που μας παραχώρησε στο Ατομικό Μικροσκόπιο Σάρωσης Ακίδος (AFM) και την βοήθεια που μας παρείχε, μαζί με την Αργυρώ Πατενταλάκη, στην εκμάθηση του Ηλεκτρονικού Μικροσκοπίου Σάρωσης (SEM). Ευχαριστώ επίσης την Μαρία Ανδρουλιδάκη για την βοήθεια της στις μετρήσεις απορρόφησης υπέρυθρου. Τέλος ευχαριστώ τους Μιχάλη Σφενδουράκη και Ηλία Απεραθίτη για τις εναποθέσεις δειγμάτων άμορφου πυριτίου και ηλεκτρικών επαφών αντίστοιχα.

Τέλος θέλω να ευχαριστήσω τους εργαζόμενους στο μηχανουργείο του ΙΤΕ και στη ομάδα κατασκευών Αργύρη Κασσωτάκη, Γιώργο Παπαδάκη, Μιχάλη Βισκαδουράκη και Μιχάλη Σμυρνάκη για την τεχνική υποστήριξη τους στην προετοιμασία των πειραματικών διατάξεων. Ιδιαίτερα ευχαριστώ επίσης τον Γιάννη Τσάμπο για την βοήθεια του σε ηλεκτρονικές κατασκευές.

Acknowledgements

I want to express my gratitude to Prof. Hellmut Fritzsche with whom I had the fortune of collaborating during the four years of this work. His help and guidance throughout this study, both in terms of experimental research and in understanding the physics of Hydrogenated Amorphous Silicon, was invaluable.

I also want to thank Dr. Howard Branz from the National Renewable Energy Laboratory (NREL) for the many stimulating discussions especially during the five months of his stay in the University of Crete.

Finally I wish to thank Dr. Qi Wang from NREL and Drs. Jeff Yang and Subhendu Guha from United Solar Systems Corp. (USSC) for their general contribution in this work and especially for the state-of-the-art samples they provided.

Περίληψη

Αντικείμενο της εργασίας αυτής είναι η πειραματική μελέτη των φωτογενών αλλαγών στις μηχανικές ιδιότητες του Άμορφου Υδρογονωμένου Πυριτίου (a-Si:H) που ανακαλύφτηκαν πρόσφατα. Μελετήθηκαν διεξοδικά τόσο οι στατικές ελαστικές ιδιότητες του υλικού όσο και το φαινόμενο της φωτογενούς διαστολής του, κάτω από ισχυρό συνεχή φωτισμό. Η εργασία εστιάζεται κυρίως στο ρόλο του υδρογόνου στην δομή του υλικού και μέσω αυτής, στα φαινόμενα που σχετίζονται με τη δημιουργία μετασταθών ατελειών.

Στο **Κεφάλαιο 1** παρουσιάζεται μια γενική περιληπτική εισαγωγή στο Άμορφο Υδρογονωμένο Πυρίτιο. Γίνεται μια σύντομη αναφορά στη δομή του υλικού, την πυκνότητα καταστάσεων, την φωτοαγωγιμότητα και τα κανάλια επανασύνδεσης των φωτο-φορέων. Περιγράφονται εκτενέστερα οι διαφορετικές φάσεις που υπάρχουν στο υλικό όσον αφορά την περιεκτικότητα τους σε υδρογόνο και τα πειράματα από τα οποία έχουν αντληθεί πληροφορίες σχετικά με τις φάσεις αυτές και τις ιδιότητες τους.

Στο **Κεφάλαιο 2** περιγράφεται το φαινόμενο υποβάθμισης της αγωγιμότητας και δημιουργίας μετασταθών ατελειών, το γνωστό ως φαινόμενο Staebler-Wronski (SW) και παρουσιάζονται δύο μοντέλα που έχουν προταθεί για την ερμηνεία του. Στην συνέχεια γίνεται αναφορά σε πρόσφατα πειράματα που αποδεικνύουν ότι τα μοντέλα αδυνατούν να περιγράψουν τον πραγματικό μηχανισμό του φαινομένου. Γίνεται μια σύντομη εισαγωγή σε άλλες φωτοδομικές αλλαγές που παρατηρούνται στο υλικό και σχετίζονται με το υδρογόνο, η μελέτη των οποίων πιστεύεται ότι μπορεί να βοηθήσει στην κατανόηση του μηχανισμού του SW. Τέλος αναφερόμαστε στις πρώτες εργασίες που δημοσιεύτηκαν και έδιναν αντικρουόμενα αποτελέσματα σχετικά με την παρουσία μετασταθούς φωτογενούς διαστολής ή συστολής στο υλικό.

Στο **Κεφάλαιο 3** γίνεται εκτενής περιγραφή της πειραματικής τεχνικής «μέτρησης της κάμψης και της συχνότητας συντονισμού διμεταλλικής μικροράβδου» που για πρώτη φορά χρησιμοποιείται για την μελέτη των μηχανικών ιδιοτήτων του άμορφου υδρογονωμένου πυριτίου και παρουσιάζονται τα πλεονεκτήματα της, σε σχέση με τις άλλες τεχνικές που έχουν χρησιμοποιηθεί μέχρι σήμερα. Αναφέρονται τα σημεία εκείνα στα οποία η υπάρχουσα θεωρία γύρω από το πείραμα αυτό ήταν ελλιπής ή έπρεπε να τροποποιηθεί ώστε να μπορούν τα πειραματικά αποτελέσματα να δώσουν με ακρίβεια τις ιδιότητες του υλικού. Τα σημεία αυτά σχετίζονται με την τραπεζοειδή διατομή που χαρακτηρίζει τις διμεταλλικές μικροράβδους που χρησιμοποιήσαμε. Στην συνέχεια περιγράφεται αναλυτικά η μεθοδολογία που ακολουθήσαμε για την εξαγωγή των αναγκαίων τύπων και οι παραδοχές που έγιναν. Στο τέλος του κεφαλαίου γίνεται μια σύντομη εισαγωγή στο φαινόμενο της παρουσίας εσωτερικών τάσεων σε υμένια και παρουσιάζεται ένας αναλυτικός υπολογισμός για την εύρεση της εσωτερικής τάσης ενός υμενίου, εναποθετημένου σε ράβδο ορθογώνιας ή τραπεζοειδούς διατομής από την κάμψη που παρουσιάζει η τελευταία εξαιτίας της τάσης αυτής, στην γενική περίπτωση όπου τα δύο υλικά έχουν συγκρίσιμα πάχη και διαφορετικές ελαστικές ιδιότητες.

Το **Κεφάλαιο 4** χωρίζεται σε δύο μέρη.

Το **πρώτο μέρος** αναφέρεται στην μελέτη των ελαστικών ιδιοτήτων υμενίων με διαφορετική περιεκτικότητα σε υδρογόνο. Μετρούμε τη συχνότητα συντονισμού μικροράβδων στις οποίες έχουν εναποτεθεί υμένια a-Si:H κατασκευασμένα με διάφορες τεχνικές και κάτω από διαφορετικές συνθήκες εναπόθεσης. Προσδιορίζουμε το μέτρο ελαστικότητας του Young όλων αυτών των υλικών. Στην συνέχεια παρουσιάζουμε περιληπτικά ένα απλό μοντέλο για συνεχές τυχαίο δίκτυο (CRN) ατόμων, που έχει προταθεί για να εξηγήσει πως εξαρτάται το μέτρο αυτό από την περιεκτικότητα ενός υμενίου σε υδρογόνο. Συγκρίνοντας τα αποτελέσματα μας με τις προβλέψεις του μοντέλου συμπεραίνουμε ότι το άμορφο υδρογονωμένο πυρίτιο παρουσιάζεται γενικά πιο μαλακό από ότι αναμένεται για υλικό CRN. Εξετάζουμε πιθανούς λόγους για την συμπεριφορά αυτή. Καταλήγουμε ότι τα υλικά με τις καλύτερες οπτοηλεκτρονικές ιδιότητες είναι ανομοιογενή τουλάχιστον όσον αφορά την κατανομή υδρογόνου στο εσωτερικό τους.

Το **δεύτερο μέρος** είναι αφιερωμένο στην εκτεταμένη μελέτη του φαινομένου διαστολής του υδρογονωμένου αμόρφου πυριτίου κάτω από φωτισμό. Μετρούμε την κάμψη που παρουσιάζουν μικροράβδοι κρυσταλλικού πυριτίου, εξαιτίας της διαστολής των υμενίων που έχουν εναποτεθεί σε αυτές. Αποδεικνύουμε ότι το φαινόμενο αυτό χαρακτηρίζει όλα τα υλικά ανεξαρτήτως κατασκευαστικής τεχνικής και περιεκτικότητας σε υδρογόνο. Παρατηρούμε, για πρώτη φορά, την ύπαρξη συγκεκριμένης κινητικής, που χαρακτηρίζει όλα τα ενδογενή δείγματα. Στην συνέχεια μελετούμε την εξάρτηση του φαινομένου από την περιεκτικότητα των δειγμάτων σε υδρογόνο. Εξετάζουμε την μεταστάθεια του φαινομένου και αποδεικνύουμε ότι το φαινόμενο αναστρέφεται σε ποσοστό που εξαρτάται από την θερμική ιστορία των δειγμάτων. Μελετούμε επίσης δείγματα μη υδρογονωμένου άμορφου πυριτίου (a-Si) και μερικώς αφυδρογονωμένου a-Si:H και συμπεραίνουμε ότι το φαινόμενο δεν παρουσιάζεται σε δείγματα αυτού του τύπου. Τέλος συζητούμε πιθανούς μηχανισμούς φωτογενούς διαστολής και αποδεικνύουμε ότι αυτή δεν μπορεί να προέρχεται από την δημιουργία μετασταθών ατελειών. Παρουσιάζουμε ένα απλό μοντέλο που έχει προταθεί για να περιγράψει το φαινόμενο και προτείνουμε τροποποιήσεις που εξηγούν τα ευρήματα μας. Τέλος συζητούμε έναν πιθανό συσχετισμό ανάμεσα στην φωτογενή διαστολή και τη δημιουργία μετασταθών ατελειών και αναπτύσσουμε ένα απλό μοντέλο που συνδέει τα δύο φαινόμενα μεταξύ τους και δίνει σωστά ποσοτικά αποτελέσματα σχετικά με το πείραμα.

Table of contents

CHAPTER 1: INTRODUCTION…………………………………………………………………1

1.1. THE AMORPHOUS SILICON BONDING STRUCTURE……………….……..2

1.2. DENSITY OF STATES OF HYDROGENATED AMORPHOUS SILICO………………………………………………………………………….3

1.3. THE HYDROGEN BONDING STRUCTURE……………………………..…6

1.3.1. INFRA-RED ABSORPTION……………………………….…….7

1.3.2. NUCLEAR MAGNETIC RESONANCE………………………...8

1.3.3. HYDROGEN EVOLUTION…………………………….……10

1.4. PHOTOCARRIER RECOMBINATION IN a-Si:H…………………………11

1.5. PHOTOCONDUCTIVITY IN a-Si:H……………………………………...12

REFERENCES…………………………………………………………………….…16

CHAPTER 2: LIGHT INDUCED STRUCTURAL CHANGES IN a-Si:H……………….…..17

2.1. INTRODUCTION……………………………………………………...….18

2.2. KINETICS OF THE STAEBLER-WRONSKI EFFECT……………...…..18

2.2.1. THE SJT MODEL…………………………………..……...19

2.2.2. THE H-COLLISION MODEL…………………………..………21

2.2.3. DIFFICULTIES IN DESCRIBING THE MICROSCOPIC MECHANISM OF THE SW EFFECT…………………………….24

2.3. OTHER PHOTOSTRUCTURAL CHANGES IN a-Si:H…………………….26

2.3.1. PHOTO-INDUCED STRAIN IN a Si:H…………………………...27

REFERENCES……………………………………………………………………….29

<u>CHAPTER 3: THE CANTILEVER BEAM BENDING AND OSCILLATION METHOD…</u>31

3.1. EXPERIMENTAL SETUP…………………………………………………32
3.2. CALCULATION OF FILM PROPERTIES FROM THE QUANTITIES MEASURED…………………………………………………………35
3.2.1. STRESS – STRAIN CONSIDERATIONS UNDER UNI-AXIAL LOADING……………………………………………………………….36
3.3. PHYSICAL QUANTITIES CHARACTERIZING A BEAM OF UNIFORM CROSS-SECTION …………………………………..37
3.3.1. NEUTRAL AXIS, BENDING MOMENT AND STIFFNESS…….37
3.3.2. APPLICATION: NEUTRAL AXIS AND STIFFNESS OF A BEAM OF TRAPEZOIDAL CROSS-SECTION…………………………..40
3.4. FREE FLEXURAL VIBRATIONS OF AN UNDAMPED TRAPEZOIDAL CANTILEVER BEAM……………………………………………………43
3.4.1. EFFECT OF TIP MASS, DAMPING AND INITIAL BENDING ON THE MEASURED RESONANT FREQUENCY…………………..48
3.5. COMPOSITE CANTILEVER BEAM BENDING UNDER INTERNAL STRESS……………………………………………………………………..52
3.5.1. INTERNAL STRESSES IN FILMS……………………………….52
3.5.2. CALCULATION OF THE INTERNAL STRESS OF A FILM FROM THE CURVATURE IT INDUCES ON A CANTILEVER SUBSTRATE……………………………………………………….55
REFERENCES…………………………………………………………….…62

CHAPTER 4: MECHANICAL PROPERTIES AND THEIR LIGHT-INDUCED

CHANGES IN a-Si:H………………………………………………63
4.1. EFFECT OF HYDROGEN ON THE RIGIDITY OF a-Si:H FILMS………..64
4.1.1. INTRODUCTION…………………………………………………64

4.1.2. THE YOUNG'S MODULUS OF CRYSTALLINE SILICON AND HOT-WIRE HYDROGENATED AMORPHOUS SILICON WITH VARIABLE HYDROGEN CONCENTRATION………………….65
4.1.3. A THEORETICAL APPROACH TO THE ISSUE OF RIGIDITY OF A CONTINUOUS RANDOM NETWORK OF ATOMS……...68
4.1.4. YOUNG'S MODULUS AND FILM STRUCTURE………………70
4.1.5.CONCLUSIONS……………………………………………………75
4.2. PHOTO-INDUCED STRESS IN a-Si:H……………………………….…77
4.2.1. INTRODUCTION…………………………………………………77
4.2.2. KINETICS OF PHOTO-INDUCED STRESS………….…………78
4.2.3. STUDY ON HW SAMPLES WITH VARIABLE HYDROGEN CONCENTRATION………………………………………………….81
4.2.4. METASTABILITY…………………………………………………..82
4.2.5. STUDY OF ΔS(T) IN UNHYDROGENATED a-Si……………...86
4.2.6. STUDY OF ΔS(T) IN HIGH TEMPERATURE ANNEALED a-Si:H……………………………………………………………………….88
4.2.7. DISCUSSION………………………………………….…….……..91
4.2.7.1. Possible origins of photo-induced stress in a-Si:H….……..91
4.2.7.2. H-flip in H-clusters: a modification of the Biswas model to account for our results…………….………………………94
4.2.7.3. Correlation of ΔS(t) with light-induced defect creation…....96
4.2.7.4. Linked kinetics of volume expansion and defect creation………………………………………………………..97
4.2.8. CONCLUSIONS…………………………………………………102
REFERENCES……………………………………………………………….104

Chapter 1: Introduction

CHAPTER 1: INTRODUCTION 10

1.1. THE AMORPHOUS SILICON BONDING STRUCTURE 11

1.2. DENSITY OF STATES OF HYDROGENATED AMORPHOUS SILICON 12

1.3. THE HYDROGEN BONDING STRUCTURE 15

1.3.1. INFRA-RED ABSORPTION 16

1.3.2. NUCLEAR MAGNETIC RESONANCE 18

1.3.3. HYDROGEN EVOLUTION 20

1.4. PHOTOCARRIER RECOMBINATION IN a-SI:H 21

1.5. PHOTOCONDUCTIVITY IN a-Si:H 22

REFERENCES……………………………………………………………………………………
…………...16

3.1. THE AMORPHOUS SILICON BONDING STRUCTURE

The difference between amorphous and crystalline solids is that the former exhibit long range order in the position of the atoms in the lattice, while in the latter the atoms are arranged in such a way that there is only short range order. This means that almost all silicon atoms in amorphous silicon (a-Si) are 4-fold coordinated having bond lengths and average bond angles identical to crystalline silicon (c-Si). However in amorphous solids the correlation between the atomic positions disappears as we move to the second and further nearest neighbors. Therefore the long- range picture of amorphous solids gives the impression of a continuous random network of atoms. A two dimensional comparison sketch between the ordered structure of crystalline

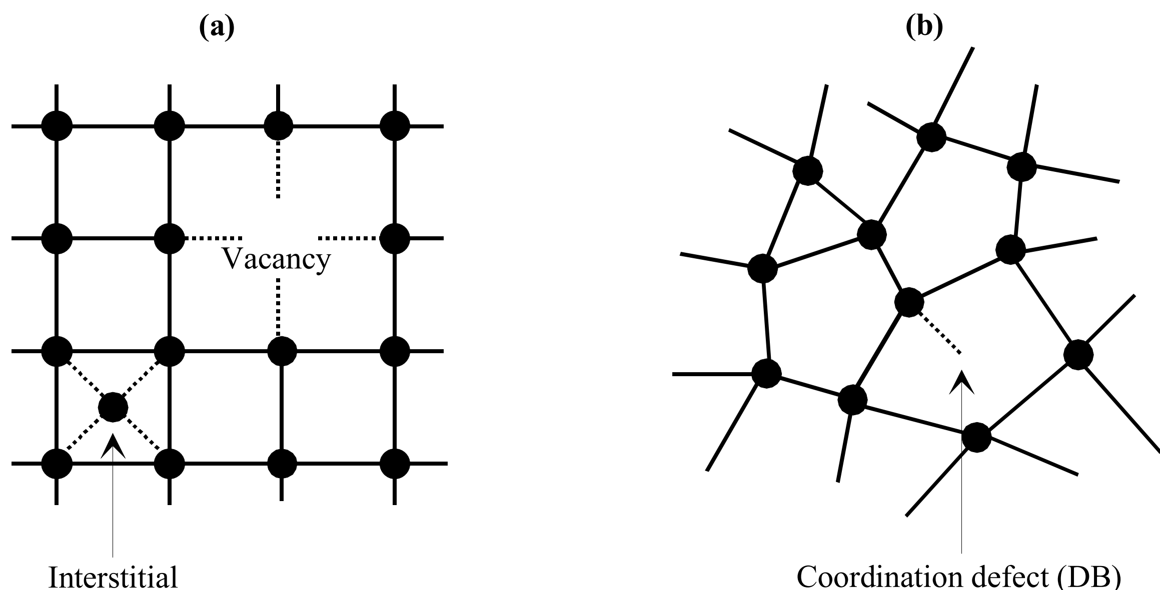

material and the disordered structure of amorphous material is presented in Fig. 1.1.

Fig. 1.1 *Structure and defects in (a) crystalline and (b) amorphous solids.*

The structural disorder influences the electronic properties in several ways. The identical covalent silicon bonds in c-Si and a-Si lead to similar overall electronic structure; amorphous and crystalline phases of the material tend to have comparable band-gaps. However, in amorphous materials there are no sharp band edges. The disorder represented by deviations in the bond lengths and bond angles broadens the distribution of electronic states, producing localized states inside the gap. These states form the conduction and valence band tails. (Fig. 1.2)

A real crystal contains defects such as vacancies and interstitials (Fig. 1.1). In amorphous solids with random network of atoms and no periodicity, the only distinguishable feature is the bonding configuration of an atom to its nearest neighbors. Therefore the elementary defect in amorphous semiconductors is the *coordination* defect, appearing when an atom has too many or two few bonds. It has been shown that a random network with each atom four fold coordinated has very high internal stresses.[i] Such a network will have a natural tendency to break Si-Si bonds and create three-fold coordinated atoms in order to relief stress. These are the dominant coordination defects in amorphous silicon and are usually called *dangling bond* (DB) defects (Fig. 1.1). It has been proposed by Pantelides[ii] that the floating bond, i.e. a 5-fold coordinated atom may also be present in the material. All coordination defects in a-Si form a broad distribution of states near midgap (Fig. 1.2)

The atomic structure of the real a-Si and hydrogenated amorphous Silicon (a-Si:H) films has features with a range of length scales. The shortest length is that of the atomic bonds and the structure is defined by the orientation of the bonds and the coordination of each atom to its nearest neighbors. The intermediate range order involves the topology of the network at the level of second, third or fourth nearest neighbors and is described by the size and distribution of rings of silicon atoms. The next larger scale is the void structure, which has typical dimensions of 5 - 10 Å in a-Si:H and is generally larger in a-Si. Finally there is the growth morphology which can have feature sizes of larger than 100 Å. These different structural features are almost independent.

3.2. DENSITY OF STATES OF HYDROGENATED AMORPHOUS SILICON

In amorphous materials the band structure theory based on Bloch's theorem is not applicable, since there is no periodicity in the amorphous lattice. This means that the density of states in amorphous solids represents an average number of states over the disordered lattice and cannot be parametrised with inverse lattice vector $\boldsymbol{k}$. The density of states in hydrogenated amorphous Silicon (a-Si:H) is shown in (Fig. 1.2).

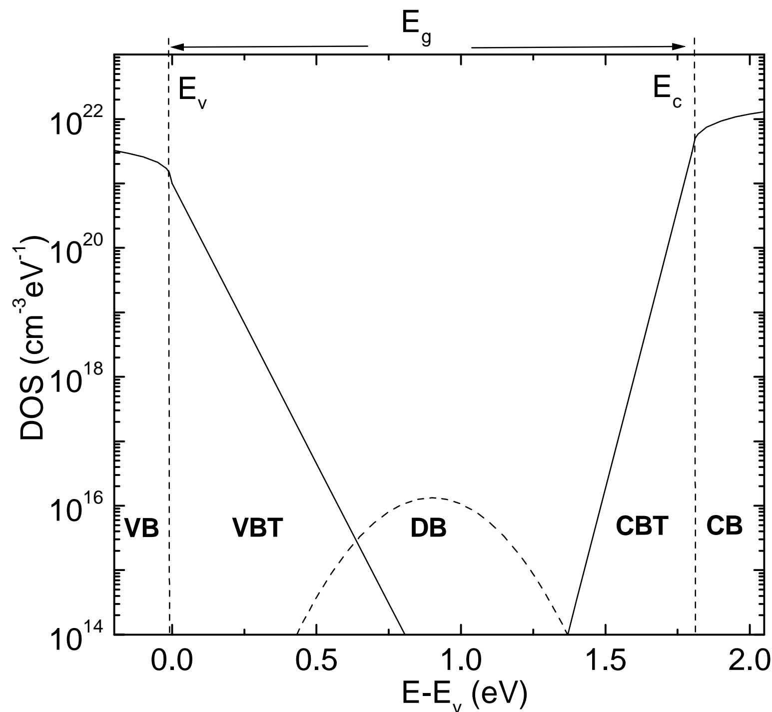

As the silicon atoms are brought together to form a covalently bonded solid, the neighboring bonding and non-bonding orbitals that hold all the valence electrons interact, overlap and eventually spread into a band of states. In the case of a crystal, the overlapping results to electron wave functions that extend over the entire volume of the solid. Extended wave functions are formed in an amorphous solid too, however, disorder produces also states that are localized with a typical localization radius of a few bond lengths. Bonding extended states

Fig. 1.2 *Density of states in a-Si:H.*

form the so called *valence band* (VB), while localized states form the *valence band tail* VBT), shown in Fig. 1.2. Likewise, antibonding orbitals of neighboring atoms interact, overlap, and form extended and localized wave functions. Their states are spread into bands which are called *conduction band* (CB) and *conduction band tail* (CBT) respectively (Fig. 1.2).

The extended wave-functions are not of the Bloch type, due to the lack of translational symmetry in amorphous solids. In a-Si the band tails can be described accurately with exponential functions. The slopes of the tails are different, reflecting the fact that the p-like states of the top of the valence band are more influenced by disorder than the spherically symmetric s-like states of the bottom of the conduction

band. The slopes of the exponential tails in high-quality a-Si:H are about 25 meV for the CBT and 45 meV for the VBT (Fig. 1.2). The energy that separates the localized tail states from the extended band states is called the mobility edge because at very low temperatures an electron should still be mobile in an extended state while it is immobile in a localized state. In Fig. 1.2, E_c and E_v denote the conduction and valence band mobility edges respectively. Their energy separation defines the mobility gap of the material E_g.

The dangling bond (DB) states are represented with a distribution near midgap (Fig. 1.2). In the first attempts to deposit a-Si, with the sputtering technique, the material produced had a very high density of defects, 10^{18} cm^{-3} or higher. Due to this high defect density this material exhibited very poor electronic properties and could not be used in devices. The development of methods for producing films which incorporate hydrogen atoms (hydrogenated a-Si or a-Si:H films) was a major breakthrough for the use of a-Si in devices. The main beneficiary effect of hydrogen is the passivation of dangling bonds, which reduces the total defect density to (1-5)x10^{15} cm^{-3}. However even with the incorporation of H, the defect density cannot be reduced to values lower than about 10^{15} cm^{-3}. Still the reduction of DB density brought a serious improvement in a-Si:H properties compared to a-Si, one of them being the high photoconductivity. This fact together with the observation that a-Si:H can be effectively doped by incorporation of Boron or Phosphorous was a critical step in the use of a-Si:H in device applications.

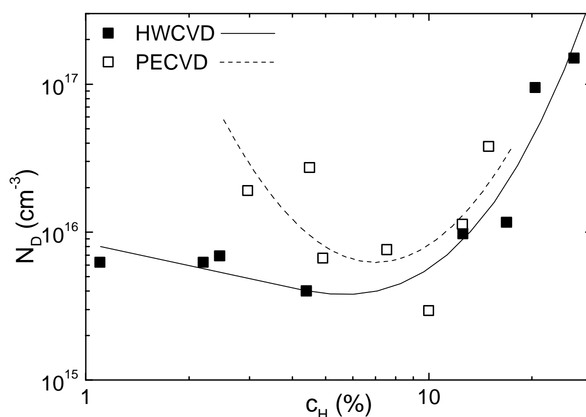

Two are the main techniques used nowadays for the production of high quality a-Si:H films; Plasma Enhanced Chemical Vapor Deposition (PECVD) and Hot Wire Chemical Vapor Deposition (HWCVD). In the first method the film is deposited after glow discharge decomposition of Silane (SiH_4) gas at a pressure of 0.1 – 1 Torr, which is the optimum pressure to sustain the plasma. In the second method the Silane gas

decomposes thermally near a tungsten filament at 1900 °C. The filament is heated by dc current. The temperature is selected to be high enough to prevent silicide formation on the filament and low enough to prevent evaporation of the filament.

The hydrogen concentration, c_H, of the film decreases with increasing substrate temperature. A-Si:H films with concentrations varying from lower than 1 at % to almost 40 % have been

Fig. 1.3 *Relation of defect density, N_D, and Urbach parameter, E_u, with the hydrogen content, c_H of Hot Wire (HWCVD) and Plasma Enhanced (PECVD) a-Si:H material.*

deposited, but the best quality films, in terms of low defect density, have a more limited range of hydrogen contents. In Fig. 1.3 we show the defect density, N_D, of HW and PE films as a function of their hydrogen content c_H (after Ref. [iii]). The best PE films have c_H varying from 7 % to 9 % while high quality HW material can have hydrogen concentration in a much wider range (c_H = 1 – 10%). Hydrogen has also an important effect on the disorder of the amorphous material. In the same figure (Fig. 1.3) we show the dependence of the Urbach parameter on the hydrogen concentration for the same deposition methods (after Ref [iv]). The Urbach parameter is equal to the slope of the VBT of the density of states (Fig. 1.2) which, as we have already mentioned, is a measure of the disorder in the material. Fig. 1.3 reveals that the best ordered materials are roughly the less defected materials. It is seen that hydrogen plays an important role in the quality of a-Si:H but this does not mean that the more the incorporated hydrogen the best the material. The hydrogen bonding configurations in a-Si:H is the topic of the next section.

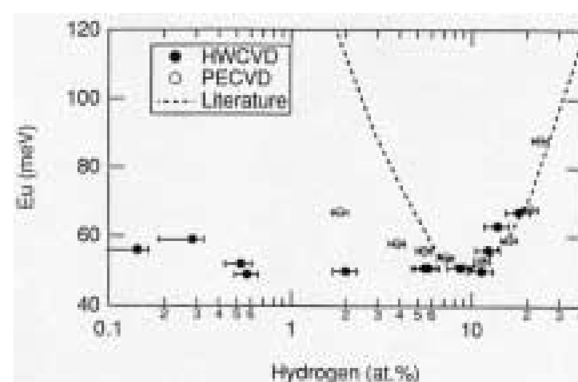

3.3. THE HYDROGEN BONDING STRUCTURE

Hydrogen and silicon in a-Si:H have different bonding properties. The silicon structure is described in terms of a rigid network with a high strain energy. There is negligible diffusion of the silicon and no apparent relaxation of the strain after growth. In contrast the hydrogen is more weakly bound and can diffuse

within the material and effuse across the surface at elevated T. The hydrogen bonding is very sensitive to the deposition conditions and its diffusion is closely associated with the many metastable changes of the electronic properties. As growth proceeds and silicon is bonded into the network the different characters of the silicon and hydrogen begin to develop. The silicon forms a rigid non-equilibrium structure whereas the hydrogen has a more mobile structure closer to equilibrium.

Hydrogen partially penetrates the silicon network. The stable bonding configurations are the Si-H bonds and Si-Si bonds which are too strongly bonded to be broken by hydrogen. Highly strained Si-Si bonds which have energies close enough to the chemical potential of hydrogen are broken and either remain as Si-H bonds or are reconstructed into stronger Si-Si bonds. Thus the hydrogen scavenges the growing film of its weak strained bonds resulting in a less disordered network. Such a process occurs only when there is a significant hydrogen diffusion at the surface during growth and is a reason why an elevated growth temperature is needed to grow the best films.

The available information about Si-H bonds comes from three major types of experiments:

a) Infra-Red (IR) absorption measurements provide information on the hydrogen concentration and the local Si-H bonding
b) Nuclear Magnetic Resonance of protons gives information about the local environment in which the hydrogen atoms reside and
c) Hydrogen evolution at elevated temperatures is a direct measurement of hydrogen concentration and provides additional information on hydrogen diffusion.

In the following we describe briefly the experiments and the pieces of information that each one provides. From the combination of these pieces we form the best possible picture on the H-bonding structure used in the discussion of our results.

3.3.1. Infra-Red absorption

Hydrogen is a light atom and since the phonon frequency is given by $(k/m)^{1/2}$, where k is the force constant and m is the reduced mass, the frequencies of the hydrogen modes are above the silicon network modes making them easy to observe. The vibration is almost confined to the hydrogen atom, so the analysis of the modes is

relatively simple. Phonon modes occur in three energy bands; a broad peak at 630-640 cm^{-1} which is always present along with a band of modes in the range of 2000-2200 cm^{-1} and a group of sharp lines at 800-900 cm^{-1} whose existence and intensity depend on deposition conditions.[v] All of the above bands originate from the Si-H vibrational modes of the ≡Si-H, $=Si=H_2$ and $-Si≡H_3$ configurations which are always present in a-Si:H in different concentrations:

a) The 630 cm^{-1} band consists of *rock* and *wag* bending modes[v] and is attributed to all of the three silicon-hydrogen groups.

b) The bands at 800 – 900 cm^{-1} originate from bending modes of only $=Si=H_2$ and -$Si≡H_3$ bonding configurations.[v] The higher energy compared to the previous modes is the combined displacement of the bonds which increases the force constant of each.

c) The 2000-2200 cm^{-1} band comes from bond streching vibrations in which the hydrogen moves along the direction of the Si-H bond. It is well established that Si-H configurations result in a peak at 2000 cm^{-1} whereas 2100 cm^{-1} modes arise from structures involving $=Si=H_2$ and $-Si≡H_3$ arrangements provided that the 800 – 900 cm^{-1} band is also present.

The integrated IR absorption of a band, I_w, is proportional to the concentration of hydrogen in the configurations associated with this band, N_H^w :

$$N_H^w = AI_w \quad where \quad I_w = \int_w \frac{a(w')}{w'} dw'$$

[1.1]

where A is a constant which depends on the local field, experienced by each Si-H bond of the $Si\text{-}H_n$ configuration, inside the local network. Combinatorial studies of IR absorption and hydrogen evolution reveal that the total hydrogen concentration is directly proportional to I_{640},[vi] while the same is true for the stretching band but with two different constants for the 2000 cm^{-1} and 2080-2100 cm^{-1} peaks[vii]

$$N_H = A_{640} I_{640} = A_{2000} I_{2000} + A_{2100} I_{2100}$$

[1.2]

The general results from the IR measurements are:

a) The total hydrogen concentration increases always with decreasing deposition temperature.

b) The absorption at 800 – 900 cm^{-1} emerges for hydrogen concentrations higher than 10-12 %. This indicates that material with c_H = 1-10 % is free from SiH_2 and SiH_3 structures while the opposite is true for a-Si:H with higher c_H. For very high c_H, polymeric chains of SiH_2 groups are produced, giving rise to columnar structure.

c) The stretching mode at 2100 cm^{-1} can not be fully attributed to SiH_2 and SiH_3 structures since it may not be accompanied by the 800 – 900 cm^{-1} lines. This is almost always the case in samples having c_H < 10 %.[vii,viii,ix] It is suggested[vii,viii] that this mode is also present when Si-H bonds are aggregated forming $(Si\text{-}H)_n$ clusters possibly in the surface of voids or decorating vacancy type defects.

3.3.2. Nuclear Magnetic Resonance

Nuclear Magnetic Resonance (NMR) of protons gives more information about the local environment in which the hydrogen atoms reside. NMR arises from transitions between the different spin states of the nucleus, which are split by an applied magnetic field. An isolated proton has a precisely defined resonance frequency, but the interactions between atoms in a solid modify the resonance by a variety of mechanisms. Modern NMR experiments are fairly complex and no attempt is made here to present a detailed treatment (see Refs. [x],[xi]). We will proceed immediately to summarize the widely accepted information that NMR provides for the H-bonding structure.

NMR detects two distinct local environments for hydrogen in a-Si:H where the dipolar couplings differ. The first environment is characterized by dispersed Si-H bonds, in which the H-atoms are separated from each other by 5 – 8 Å irrespective of the total hydrogen concentration of the sample and the deposition technique used.[viii,xii,xiii] This is an extraordinary result which shows that the hydrogen solubility in the amorphous matrix is constant. From the average separation it is calculated that the number density of randomly distributed hydrogen is always of the order of c_{Ho} = 2 – 4 %.[viii,xii] Therefore if the total c_H of a sample is higher than c_{Ho} the remaining hydrogen must be bonded in structures with higher than average c_H which are the hydrogen clusters. This is actually the second environment detected by NMR.

NMR provides additional information on these hydrogen clusters. It shows that hydrogen atoms are either bonded to the same silicon atom or to neighboring atoms within approximately 2 Å.[xii,xiii] This distance is independent of the deposition technique and total H-concentration and is partly increased because of the electrostatic repulsion between H atoms which are charged when bound to Si. The fraction of hydrogen concentration in clusters is always more than 50 % of the total and in some cases it can reach 90%.[xiii] Furthermore there are NMR experiments which find that the number of strongly interacting H-atoms is at least 5 – 7 in device quality PECVD material[xi] (c_H = 8 - 10 %) and at least 14 in low c_H (2 – 3 %) HW material.[xiii] A hydrogenated multivacancy or void is the most obvious interpretation of the clustered hydrogen.[xii,xiii] For c_H > 10 % the H-cluster fraction comprises Si-H_2 bonding configurations already distinguished from IR measurements. It has been proposed that H-clusters may be formed in regions of the network, which are under tension during the growth process.[xiv] The cluster is then the sum of the pairs of hydrogen atoms, which break and passivate the distorted bonds in those regions.

Finally a new important result from NMR was reported by Wu *et al.*[xiii] in 1996. They found that the HW material with 2 - 3 % hydrogen concentration has both dispersed hydrogen of 3 – 4 % concentration and a 90 % of the total hydrogen atoms in clusters. The only way that this is possible is that this film contains a large volume fraction of hydrogen deficient material. They concluded that at least 60 % of the volume of this film is pure a-Si. In Table 1.I we show the

Sample	Material 1 (vol. %)	Material 2 (vol. %)	Material 3 (vol. %)
HW (c_H = 2-3 %)	20-30, with c_H = 3-4 %	< 10, H-clusters of 14 atoms	> 60, H-deficient
PE (c_H = 8-10 %)	70-80, with c_H = 3-4 %	~ 20, H-clusters of 6 atoms	< 10, H-deficient

Table 1.I *H-bonding environments in a-Si:H.*

results of their analysis on this sample and a device quality PECVD film which was used for comparison.

Summarizing the NMR results for hydrogen bonded to silicon atoms we conclude that a-Si:H is an inhomogeneous structure with three well defined phases:

a) Randomly dispersed hydrogen, of constant concentration, which is approximately 2 – 4 %.

b) Hydrogen clusters, which comprise more than 50% of the hydrogen concentration. They are aggregates Si-H or, for high c_H, Si-H_2 structures and are always present in a-Si:H material.
c) Hydrogen deficient material or pure amorphous silicon

The constant concentration of dispersed H along with the constant presence of clusters, dictates that the volume fraction of hydrogen deficient material decreases with increasing c_H until $c_H \approx$ 8-10 % At this region the H-dispersed volume fraction reaches a maximum value and the H-deficient becomes practically zero. For $c_H > 10$ % the H-dispersed fraction starts to decrease and Si-H_2 clusters become the dominant phase.

Finally NMR measurements at low temperatures (20 – 30 K)[xv,xvi] reveal that molecular hydrogen is present at a concentration of about 0.1 - 1 at %. The molecular hydrogen is immobile, trapped in small voids, and it is estimated that there are about 10 H_2 molecules in each void. Annealing to high temperatures, which tends to remove bonded hydrogen from the a-Si:H network, increases the amount of molecular hydrogen in the voids.

3.3.3. Hydrogen evolution

The ability of hydrogen to move into, out of, and within a-Si:H has both beneficial and undesirable properties. The low defect density is a beneficial result of the movement and bonding of hydrogen to weak or broken silicon bonds. Hydrogen is, however, responsible for the instability of a-Si:H at elevated temperatures. Hydrogen is completely removed from a-Si:H above about 400 ^oC, degrading the properties in a way that can not be reversed unless hydrogen is deliberately reintroduced. Hydrogen evolution experiments have been used for the accurate measurement of the hydrogen concentration of a sample. However since this is a destructive technique, it is mainly utilized for the calibration for other non-destructive methods such as IR absorption.

Hydrogen evolution studies in the temperature range from 400-500 ^oC reveal a higher effusion rate from clustered than for dispersed Si-H. Clustered hydrogen is always the first to evolve from a-Si:H material.[xvii] Furthermore, samples with $c_H > 10$ % loose

hydrogen at temperatures lower than 400 °C. This is a characteristic of a columnar material i.e. a material with significantly larger and oriented clustered phase, which provides additional paths, among columns, for hydrogen evolution. It is also observed that near 350 °C hydrogen begins to effuse from a-Si:H without significantly changing the dangling bond defect concentration.[xviii] This means that broken Si bonds left behind must be close pairs and reconstruct to a Si-Si bond, albeit weak and stretched. Removing H from this pair of atoms leaves behind a dangling bond, which costs energy. Taking two Hs costs less because a Si-Si bond is formed. This feature leads to a negative effective correlation energy of H-pair states in clusters[xix] and thus verifies the NMR result that most of the hydrogen concentration must be in the form of clusters. Finally NMR studies in device quality PECVD material deposited at 270 °C reveal that hydrogen rearranges prior to evolution.[xi] It was observed that annealing at 300 °C and 387 °C causes either greater interactions between small clusters or the formation of larger clusters resulting from cluster migration and coalescence.[xi]

3.4. PHOTOCARRIER RECOMBINATION IN a-SI:H

When a-Si:H is illuminated with photons having energy larger than the band gap, electron-hole pairs are generated, the former in the CB and CBT and the latter in the VB and VBT of the density of states of Fig. 1.2. Under steady state conditions, thermal equilibrium is established between the free carriers in the bands and the trapped carriers in the localised band tail states. This equilibrium implies the following approximate[xii] proportionalities:

$$n_t \propto n \quad and \quad p_t \propto p$$

[1.3]

where n,n_t are free and trapped electrons densities and p,p_t are the respective densities for holes. The occupancy of the tail states is determined by Fermi-like functions, where the chemical potential is the so-called trap quasi-Fermi level. Steady state conditions mean that all of the above densities remain constant with time or that the rate of photogeneration of carriers G is equal to the recombination rate R of electron-hole pairs. The recombination rate is generally described by the simple relationships $R = n / \tau_n = p / \tau_p$ where τ_n, τ_p are called the *lifetimes* of electrons and hole respectively.

There are two main recombination paths in a-Si:H: the immediate band to tail recombination and the recombination through defects.

When either the dangling bond density in a film is low or the generation rate is high the band to tail recombination is the dominant recombination path in a-Si:H. In this case the recombination rate can be written as $R \propto np_t + c_2pn$ and with the help of Eqs [1.3] it is found that $R \propto np \propto n^2$. The latter proportionality holds mainly for relatively high photogeneration rates and temperatures and through the equality of generation and recombination it shows that the free carrier density in the material will be given by the relation $n \propto G^{1/2}$. This recombination path involves two carriers simultaneously, and is called "bimolecular" recombination. With increasing light intensity and thus generation rate, the trap quasi-Fermi levels move closer to the band edges, and since bimolecular recombination involves states always in the vicinity of these levels, the energy released by a single event will be higher. Bimolecular recombination energy is the major driving force for photostructural changes described in following sections.

Defects are electronically active sites. This means that they can capture carriers, electrons or holes, and become charged. Recombination at defects is a two step procedure. At first a carrier is captured by a defect and then a carrier of the opposite type is subsequently captured at the same site, resulting in loss of both carriers i.e. recombination. This procedure is dominant at normal illumination conditions and substantial defect densities. Let us denote the defect density as N_D and assume for simplicity that the defect states are not completely filled with electrons or holes and thus can capture carriers of either sign. Then the recombination rate will be given by $R \propto nN_D \propto pN_D$ and since $G = R$ the free carrier density in the material will be given by $n,p \propto G / N_D$. Recombination at defects is also referred to as "monomolecular" recombination.

3.5. PHOTOCONDUCTIVITY IN a-Si:H

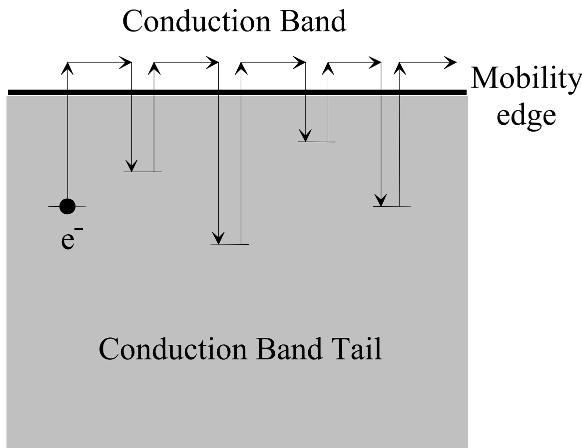

Device quality a-Si:H is highly photoconductive. In the dark, at room temperature, the conductivity of a-Si:H is as low as $10^{-10}\ \Omega^{-1}cm^{-1}$ while under bandgap illumination it can increase by orders of magnitude depending on the intensity of the light used.

The conduction mechanism in a-Si:H is strongly influenced by the presence of tail states. Carrier transport proceeds according to a multiple trapping mechanism in which a carrier gets trapped in shallow band tail states and thermally re-emmited during transport. This procedure is presented schematically in
Fig. 1.4. The term shallow can be understood as follows. The characteristic time for thermal emission of a carrier trapped in a tail state becomes larger as we move away from the band edge. Thus a carrier trapped in a tail state near the band edge i.e. a shallow state, will be re-emitted in the band and contribute to conduction while a carrier trapped deep in the tail will remain there for a time sufficiently long for a carrier of the opposite sign to be captured at the same state. The latter procedure results in loss of both carriers i.e. a recombination event. From the trap-limited transport it follows that both the free and the shallow trapped carriers contribute to conductivity and that the average mobility of these carriers, usually denoted as *drift mobility*, μ_d, is lower that the usual extended state

Fig. 1.4 *Multiple trapping conduction in a-Si:H.*

mobility, μ_o. The drift mobility is defined as the free carrier mobility reduced by the fraction of time that the carrier spends in the traps or in other words by the fraction of the free to total carrier density:

$$\mu_{dn} = \mu_{on} \frac{n}{n_{tot}} \quad and \quad \mu_{dp} = \mu_{op} \frac{p}{p_{tot}}$$

[1.4]

where $n_{tot} = n + n_{st}$ and $p_{tot} = p + p_{st}$ are the total electrons and holes contributing to conduction and n_{st}, p_{st} are the shallow trapped carriers. The conductivity and photoconductivity of a-Si:H can then be written in general as

$$\sigma = e(n_{tot}\mu_{dn} + p_{tot}\mu_{dp}) = e(n\mu_{on} + p\mu_{op})$$

[1.5]

The second equality comes from the use of Eq. [1.4]. As we see there are two ways to describe conduction; either by using the free carriers and respective mobilities or the total carriers and drift mobilities. In a-Si:H $\mu_{on} \cong 10\mu_{op}$ and thus in undoped material, electrons dominate the carrier transport.

One of the major problems in a-Si:H that has limited its applications in devices and especially solar cells, is the so-called Staebler – Wronski (SW) effect. The first observation by Staebler and Wronski[xx] was that both the photoconductivity and the dark conductivity of a-Si:H samples decrease after exposure of the samples to intense illumination with band-gap light. At first the effect was attributed to an increase in the defect density of gap states (Fig. 1.2), which act as recombination centers. Staebler and Wronski concluded that these light-induced changes shift the dark Fermi level towards midgap, thus decreasing the dark conductivity and act as recombination centers, decreasing the photocarrier lifetime and the photoconductivity. Subsequent studies, employing various experimental techniques, verified that under intense illumination the dangling bond density increases, reaching saturation at a value that can be two orders of magnitude higher than the native defect density. Great effort is being devoted to understand the mechanism behind the SW effect and find ways to prevent degradation of the material. Several different models have attempted to describe the kinetics or time dependence of the SW effect assigning the phenomenon fully to defect creation. Hydrogen is involved either directly or indirectly in all of these models We describe briefly the two most widely accepted models in the next chapter.

All present models for the SW effect have difficulties in explaining the experimental observations especially at the limiting cases of low temperatures, high illumination intensities and long exposure time. These difficulties along with two major facts described below are the main reasons which prove that despite the twenty years of research of the SW effect, the mechanism behind the phenomenon is still poorly understood.[xxi] The first fact comes from the reversibility of the SW effect. It has been observed than one can eliminate the light-induced defects and recover the

photoconductivity of the a-Si:H material by annealing the films at sufficiently high temperature, usually around 190 ^{o}C, for about 2 hours. However, experiments on reversibility proved that no single-valued functional relation between defect density and photoconductivity exists. In other words the SW effect cannot be fully described by light-induced defect generation.

The second fact which proves that there is more to the SW effect than defect creation is that there are changes in other physical properties of the material which appear to be too large to be explained by the measured concentrations of light induced defects. In some of these changes there is certain involvement of hydrogen and will be described in the next chapter. The other counter intuitive observation was that although the recombination energy of just a single event is high enough to create a dangling bond, defect creation is very inefficient; light exposures involving about 10^{25} cm^{-3} recombination processes yield only 10^{17} cm^{-3} dangling bonds.[xxii] It was proposed that all of these problems can be resolved by assuming that illumination not only creates dangling bond defects but in addition changes the whole structure of the material in a way that a more strained, higher energy network is obtained.[xxii]

Our experiments detailed in the following chapters proved for the first time that under intense illumination major photostructural changes occur inside a-Si:H resulting in the increase of stress inside the material which is too large to be assigned to defect sites only. We have made a detailed study of the creation and annealing kinetics of photo-induced stress in samples with variable hydrogen concentration in order to explore the role of hydrogen in these photo-structural changes. This study provides new ideas regarding the primary mechanism responsible for the SW effect.

Chapter 2: Light induced structural changes in a-Si:H

CHAPTER 2: LIGHT INDUCED STRUCTURAL CHANGES IN A-SI:H 26

2.1. INTRODUCTION 27

2.2. KINETICS OF THE STAEBLER-WRONSKI EFFECT 27

2.2.1. THE SJT MODEL 28

2.2.2. THE H-COLLISION MODEL 30

2.2.3. DIFFICULTIES IN DESCRIBING THE MICROSCOPIC MECHANISM OF THE SW EFFECT 34

2.3. OTHER PHOTOSTRUCTURAL CHANGES IN a-Si:H 36

2.3.1. PHOTO-INDUCED STRAIN IN A-SI:H 37

REFERENCES………………………………………………………………………………………………………...29

3.6. INTRODUCTION

In this chapter we first summarize the basic experimental results concerning light-induced defect creation in a-Si:H. After that we review the two most widely accepted models which describe theoretically these results but suggest two completely different microscopic mechanisms driving the phenomenon. We also note the difficulties encountered by these models in explaining certain experimental results. These difficulties arise mainly from the role of hydrogen in the respective mechanisms. Subsequently we present some light-induced photo-structural changes other than defect creation involving hydrogen, which were discovered in the last five years and attracted a lot of interest. Finally we introduce our experimental results on light-induced volume expansion. This phenomenon is our main subject of study in hydrogenated amorphous Silicon.

3.7. KINETICS OF THE STAEBLER-WRONSKI EFFECT

As we have already mentioned in the previous chapter, the primary observation associated with the light-induced degradation of the photoconductivity of a-Si:H (the Staebler-Wronski -SW- effect) is the increase in the defect density of the material. These defects act as additional recombination centers for the photo-carriers, thus reducing the carrier lifetime and the photo-conductivity. At this point we wish to note that excess defect concentration can also be created by charge injection or by bombardment with keV electrons. In all cases the state of the sample after degradation is metastable, and minimum defect density is achieved after annealing at sufficiently high temperature.

One of the basic experimental findings concerning the kinetics i.e. the time evolution of the SW effect is that under illumination with CW light, the defect density N_D increase with time t as[xxiii]

$$N_D(t) \propto G^{0.6} t^{0.3}$$

[2.6]

G, being the photo-carrier generation rate of the soaking light. This is the best known relation for the SW effect in a-Si:H. It is proved experimentally over a range of CW

generation rates reaching 10^{21} cm^{-3}s^{-1} and temperatures from as low as 4.2 K to as high as 400 K.[xxiii,xxiv,Error! Bookmark not defined.] The generation rate exponent of Eq. [2.6], however, is not proved to be universal since there are many experimental studies which find it between 0.4 and 0.5.[xxiv,xxv] The two models that we are going to present, account for the power law dependencies of Eq. [2.6], but are based on very different assumptions for the microscopic origin of the phenomenon.

3.7.1. The SJT model

The first widely accepted model for the SW effect was proposed by Stutzmann, Jackson and Tsai in 1985.[xxiii] We will hereafter refer to it as the SJT model. This model is based on two simple assumptions:

1. Mono-molecular recombination is the dominant path for photo-carrier recombination. This means that the photocarrier lifetime is determined by recombination through dangling bonds.
2. Excess defect creation is driven by band-to-tail, i.e. bimolecular recombination, which is the only event, releasing sufficient energy to break weak Si-Si bonds and create dangling bonds. This bimolecular recombination path is present although the dominant path is the one through defects, as stated in assumption 1.

As we have already discussed in Section 1.4, the lifetime of either photo-generated electrons or holes which recombine through defects will be inversely proportional to the defect density N_D so that the respective photo-carrier densities will be

$$n \propto p \propto \frac{G}{N_D}$$

[2.7]

for steady-state illumination with generation rate G. In the same section (1.4) we have shown that the band-to-tail recombination rate R is proportional to the electron-hole density product, np. The second assumption of the SJT model is written as:

$$\frac{dN_D}{dt} = c_{sw} np$$

[2.8]

where, t, is the illumination time and c_{sw} is a constant which determines the efficiency of defect creation via bimolecular recombination. Substituting the photo-carrier densities from Eq. [2.7] to Eq. [2.8] we get the basic differential equation for defect creation in the SJT model

$$\frac{dN_D}{dt} \propto \frac{G^2}{{N_D}^2}$$

[2.9]

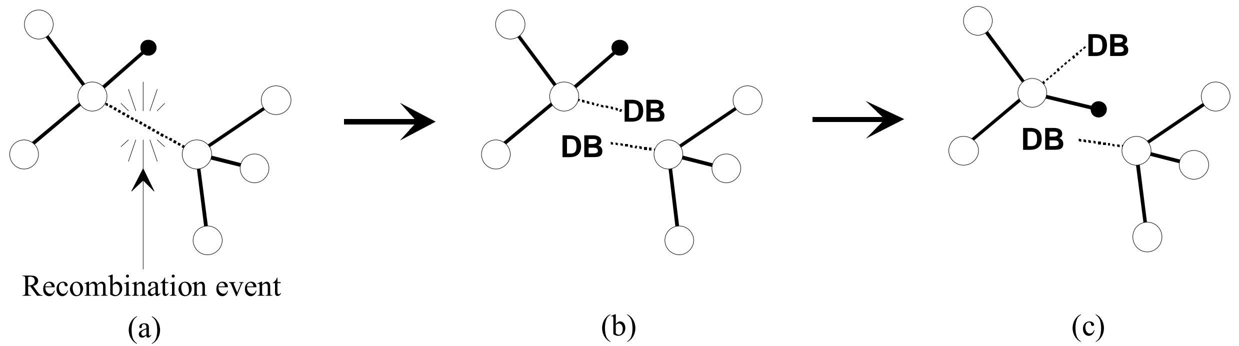

which can be solved analytically to give

$$N_D(t)^3 - N_D(0)^3 \propto G^2 t$$

[2.10]

where $N_D(0)$ is the initial or native defect density of the material. For sufficiently long illumination, for which $N_D(t) >> N_D(0)$, Eq. [2.10] is simplified to

$$N_D(t) \propto G^{2/3} t^{1/3}$$

[2.6]

The SJT model was the first model to account for the observed time evolution of light induced defect creation; equation [2.6], which is the prediction of the model, is in agreement to experimental observations[xxiii] on the kinetics of the SW effect. The model also gives physical insight on why the rate of defect creation decreases with exposure time. As the defect density increases more recombination events decrease the carrier densities which are the driving force for defect generation.

Fig. 2.5 *The microscopic mechanism of the SW effect in the SJT model: a recombination event (a) results to breaking of a weak bond (b) to two dangling bonds (DBs) which stabilize (c) with the aid of an H atom (black sphere) located nearby.*

The microscopic mechanism of the creation of an additional dangling bond by breaking a weak S-Si bond, proposed by SJT, is shown in Fig. 2.5. It consists of three

steps. In the first step a bimolecular recombination event takes place in the vicinity of a weak Si-Si bond. The energy released causes the breaking of this weak bond in two temporary dangling bonds, and this is the second step of the process. Normally these two bonds will recombine to reform the initial Si-Si bond and this is the most probable outcome of the process. However there are cases in which the two bonds are prevented from recombining by a hydrogen atom as shown in Fig. 2.5. It is a prediction of the model that a hydrogen atom must be near a weak Si-Si site in order to stabilize the dangling bonds that are newly formed. Therefore light-induced dangling bonds must always be near hydrogen atoms.[xxiii]

3.7.2. The H-collision model

In 1997 Branz[xxvi] proposed a new model for the SW effect which attracted the interest of a lot of researchers for experimental investigation since it was based on a completely different mechanism of defect creation. This model attributed light induced defect generation to a process which involves hydrogen motion and interaction in a straightforward manner.

The first assumption of this model is that when a-Si:H is exposed to light, a H-atom can be excited from a Si-H bond when the energy of a recombination event dissipates in the vicinity of this bond. This excitation leaves behind a dangling bond. The excited hydrogen reaches a new state, which can be viewed as a Si-H/DB complex, as shown in Fig. 2.6. This process can be described by a chemical reaction equation of the form

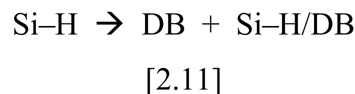

$$\text{Si–H} \rightarrow \text{DB} + \text{Si–H/DB}$$

[2.11]

The Si-H/DB complex is considered to be a mobile state of hydrogen, having energy 1.5 eV higher than that of the Si-H bond. Therefore only high-energy recombination events i.e. band-to-tail recombination, can drive this excitation.[xxvi] This mobile-H complex travels through the material by hopping between Si-Si sites a process that is enhanced by photo-carrier recombination (Fig. 2.6). Each broken bond reforms as the mobile-H hops away. When this complex meets a DB, then the Si-H bond is immobilized through the recombination of the two DB’s

$$\text{Si-H/DB} + \text{DB} \rightarrow \text{Si-H}$$

[2.12]

Fig. 2.6 *The excitation and transfer mechanism of the Si-H/DB complex or mobile-H in the H-collision model. The complex is shown inside the dashed circle and the H-atom is represented by a black sphere.*

This is the inverse process of Eq. [2.11] and the main source of loss of mobile-H species during illumination. The combination of processes [2.11] and [2.12] forms a cycle which does not result in a net creation of new DBs. However there is also another process which immobilizes Si-H/DB complexes but is far less frequent than normal recombination. Two mobile-H complexes can meet and then both of them are immobilized by the annihilation of their DBs according to the reaction

$$\text{Si-H/DB} + \text{Si-H/DB} \rightarrow M(\text{Si-H})_2$$

[2.13]

Where $M(\text{Si-H})_2$ is a metastable complex containing a pair of Si-H bonds in close

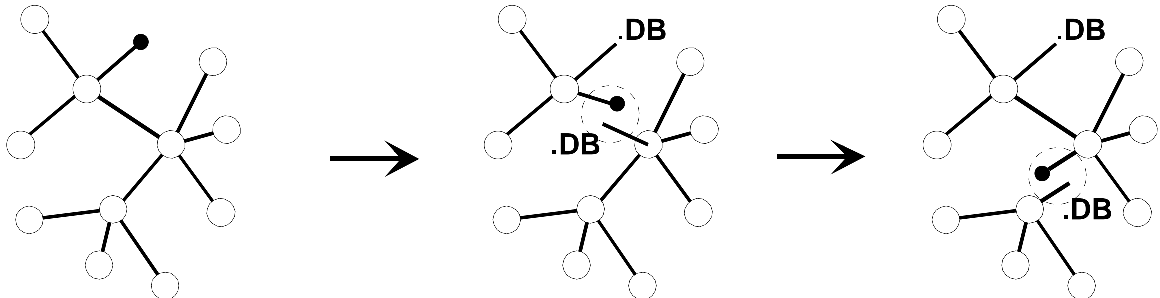

proximity (Fig. 2.7). The process of Eq. [2.13] results in the net creation of two dangling bonds, which are those left behind in the Si-H bonds, from which H was originally excited to form the interacting mobile-H complexes (Fig. 2.7). The complete equation for dangling bond creation in the H-collision model is

$$2\ \text{Si-H} \rightarrow 2\ \text{DB} + 2\ \text{Si-H/DB} \rightarrow 2\ \text{DB} + M(\text{Si-H})_2$$

[2.14]

The main *ansatz* of the H-collision model is that the rate of emission of mobile hydrogen from Si-H bonds (Eq. [2.11]) is proportional to the generation rate *G*. Therefore the creation rate, R_m, of mobile-H density, N_m,, from a hydrogen density, N_H, in the sample is

$$R_m = k_H N_H G$$

[2.15]

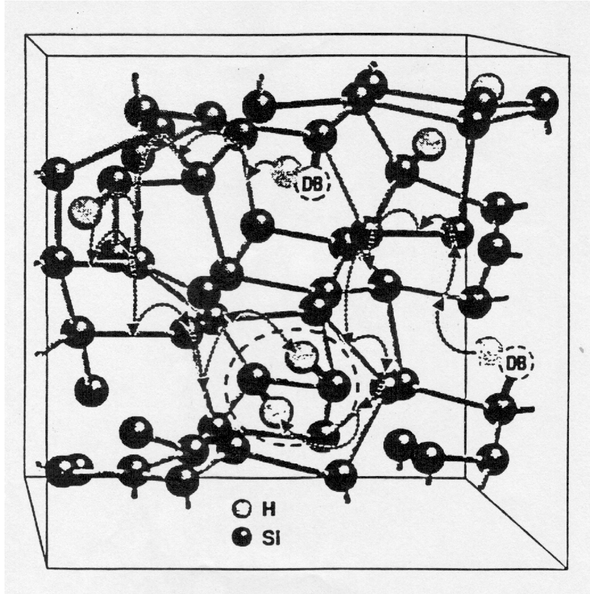

where k_H is a proportionality constant. The complete rate equation for the creation and loss of mobile hydrogen concentration is

$$\frac{dN_m}{dt} = k_H N_H G - k_{db} N_m N_D - 2k_c N_m^2$$

[2.16]

Fig. 2.7 *The DB formation mechanism in the H-collision model.*

where t is the illumination time, N_D is the dangling bond density and k_{db} and k_c are constants. The first term stands for mobile-H creation as mentioned above. The second term represents the recombination of mobile-H to ordinary DBs according to Eq. [2.12]. The third term describes the rate of loss of mobile-H species due to collision and annihilation of pairs of Si-H/DB complexes (Eq. [2.13]). Under CW illumination a steady state of mobile-H density is reached, i.e. $dN_m/dt = 0$. At the low hydrogen excitation limit, the density of dangling bonds is higher than the density of mobile hydrogen and the density of the total Si-H bonds, N_H, stays approximately constant. Therefore the major loss of mobile hydrogen comes through isolated DBs and not through the collision of two Si-H/DB complexes, i.e. $2k_c N_m << k_{db} N_D$.

Following the discussion of the previous paragraph, Eq. [2.16] can be simplified to

$$N_m = \frac{k_H N_H G}{k_{db} N_D}$$

[2.17]

which gives the mobile-H concentration under steady state illumination conditions. The final step is the connection between dangling bond creation and mobile hydrogen

concentration. According to Eq. [2.13] the rate of dangling bond creation must be equal to the rate of mobile-H collision i.e.

$$\frac{dN_{db}}{dt} = 2k_c N_m{}^2$$

[2.18]

Substituting Eq. [2.17] into the previous rate equation and solving for N_D one finds

$$N_{db}(t) = (3C_{sw})^{1/3} G^{2/3} t^{1/3} \quad where \quad C_{sw} = 2k_c k_H{}^2 N_H{}^2 / k_{db}{}^2$$

[2.19]

which, as in the SJT model, is in agreement with the experimental observations of Stutzmann *et al.*[xxiii] However the H-collision model makes an additional prediction, compared to the SJT model. It implies that the SW effect will be intensified with increasing hydrogen concentration. Until now no experimental results are found in the literature concerning the hydrogen dependence of the SW defect creation.

Finally one has to point out here the completely different mechanism of defect formation compared to the SJT model. The outcome, however, of both models is the same kinetics of light-induced defect creation. The main differences are summarized as follows:

1. The SJT model suggests that a dangling bond comes from the breaking of a weak bond, while the H-collision model suggest that dangling bonds originate from the breaking of Si-H bonds.
2. In the Branz model, it is the mobile density that determines the rate of defect creation and not the photo-carrier density as in the SJT model.
3. The SJT model predicts that light-induced dangling bonds are in close proximity with stabilizing H atoms while in the H-collision model, DBs can be far away from each other and far from any H atoms. Hydrogen is not needed for DB stabilization.
4. Finally one must not forget that a major step in the process described by the Branz model is the enhancement of diffusion of the mobile-H in the material due to recombination energy. In the SJT model, DB creation is a purely localized process.

3.7.3. Difficulties in describing the microscopic mechanism of the SW effect

Before discussing the difficulties concerning the above models we must refer to the fact that among the first models which tried to resolve the microscopic mechanism behind the SW effect were the impurity related models. These models assumed that an impurity atom is associated with each silicon dangling bond. The entire class of these models were eliminated by the work of Kamei *et al.*[xxvii] By carefully controlling and measuring the purity of their a-Si:H samples they observed SW defect densities orders of magnitude greater than the densities of their C, N, and O impurity densities. Thus the SW effect is positively intrinsic to the a-Si:H network.

Some of the problems with both the SJT and the H-collision models arise from the low temperature kinetics of the SW effect. Light-induced defect creation is observed at a temperature as low as 4.2K with the same efficiency as that observed at room temperature; not only the magnitude but also the kinetics of the SW effect are the same at these two temperature conditions.[xxiv] This is incompatible with the SJT model because DB's do not participate significantly in carrier recombination; at these temperatures the dominant recombination path for photo-carriers is the band-to-tail recombination discussed in section 1.4 and not monomolecular recombination.[xxvi.xxviii] Therefore the first assumption of this model stated in Section 3.7.1 is not valid. The 4.2 K kinetics of the SW effect do not support the H-collision model as well. The reason is that long range H diffusion, which is one of the main assumptions of this model, is not believed to be possible at such low temperatures even under illumination.[xxix] However this is a topic of still ongoing experimental research.

One of the main problems of the bond-breaking SJT model is the need of hydrogen for stabilization. As we have discussed in Section 3.7.1 the main mechanism of DB creation in this model is the breaking of weak Si-Si bonds due to photo-carrier recombination energy release in the vicinity of these bonds, which leads to the production of DBs in pairs. A hydrogen atom stabilizes these bonds by a switching process shown in Fig. 2.5. This means inevitably that all light-induced DBs are in close proximity to hydrogen atoms. The local environment of hydrogen or deuterium around DBs has been studied by electron-spin-echo envelope modulation (ESEEM) of pulsed Electron Spin Resonance (ESR).[xxx] By this technique, small hyperfine and

nuclear quadrupole interactions can be extracted from within the ESR line broadened by random orientations and structural fluctuations. It was found that no hydrogen or deuterium atoms are closer than 4 Å to dangling bonds. Therefore the H-atoms are not spatially correlated to DBs and this is a major argument against the SJT model; without H-stabilization it is difficult to understand why the broken Si-Si bond of the model would not simply reform.

Until now we have discussed the main models that have been developed in order to explain the experimental results on the kinetics of light induced defect creation. Although significant steps have been made towards understanding the phenomenon it was made clear that the basic microscopic mechanism behind defect creation still remains elusive. At this point we wish to remind the reader that the SW effect is by definition the phenomenon of light induced degradation of the photoconductivity, σ_p, of the a-Si:H material. The entire research in a-Si:H, however, was devoted to dangling bond creation under illumination, because the photoconductivity degradation was *entirely* attributed to the creation of new defects. However it was proved that this is not the case by metastability studies in a-Si:H

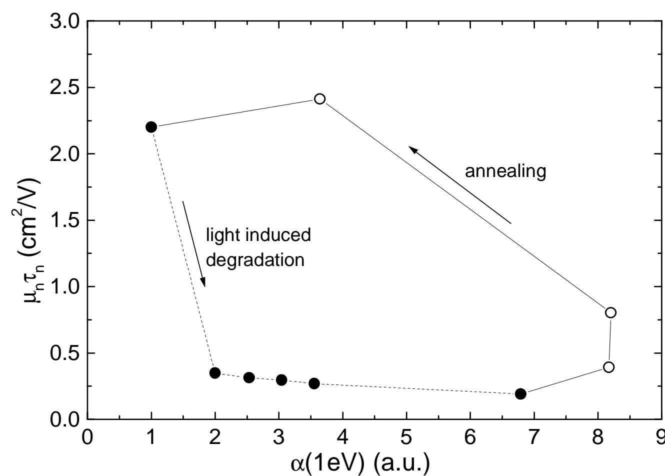

Metastability or reversibility is a key property of the SW effect light induced defects are eliminated and the photoconductivity is recovered after annealing the material at high temperatures. Fig. 2.8 shows the relation between the mobility lifetime product, $\mu_n\tau_n$, and the optical absorption, $\alpha(1eV)$, of the defect (DB) band of the density of states during light-exposure and subsequent annealing of an a-Si:H sample.[xxxi] The $\mu_n\tau_n$ product is proportional to the photoconductivity of the sample, whereas $\alpha(1eV)$, is proportional to the dangling bond density inside the material. This figure proves that there is no unique relation between the number of defects and the photoconductivity; the first defects created and the first to anneal correlate with a much greater change in the

photoconductivity than the majority of light-induced effects. Other studies have shown that the same number of light-induced defects created by short pulses[xxxii] decrease the photo-conductivity more than those created by CW light. The lack of a correlation between changes in photoconductivity and defect concentration in these experiments strongly suggests that

Fig. 2.8 *Mobility-lifetime product of electrons as a function of the change in defect absorption a at hν = 1eV during exposure and annealing.*

some other photo-structural changes must occur besides defect generation, which have a degrading effect on the photoconductivity.[xxxiii] This suggestion is strongly supported by recent experimental results described in the next section.

3.8. OTHER PHOTOSTRUCTURAL CHANGES IN a-Si:H

In this section we will present briefly two of the experiments which could not be explained by the creation of about 10^{17} dangling bond defects. These experiments imply a direct involvement of hydrogen in large-scale photo-structural changes inside hydrogenated amorphous silicon

Kong *et al.*[xxxiv] observed a light induced increase of the Si:H stretching mode at the wavenumber of 2000 cm^{-1}. An exposure for 342 h to a white light flux of 400 mW/cm^2 produced a 1.3 % increase in the stretching mode absorption. There are about $3x10^{21}$ cm^{-3} Si-H bonds in the annealed state. The authors argued that this increase cannot to be due to an increase in the oscillator strength (proportional to the A_{2000} constant defined in Section 1.3.1) of those Si-H bonds which are involved in the creation of the $N_D \sim 10^{17}$ cm^{-3} dangling bond defects or which are in the immediate vicinity of these defects. The increase in oscillator strength would have to be unrealistically large if the concentration of Si-H bonds affected were of the same order of magnitude as N_D.[xxxiv] On the other hand it was proposed[xxxiii] that the increase in the stretching mode absorption could be due to a 1.3 % increase of the effective bond charge e^* of the pre-existing Si-H bonds which is caused by the light induced increase of strain or structural disorder in the environment of these bonds.

Hari *et al.*[xxxv] observed changes in the proton NMR dipolar spin lattice relaxation time resulting from light exposures of a-Si:H. These changes must involve more than 10 % of the $3x10^{21}$ cm^{-3} hydrogen atoms which are bonded in this material. There is no way that this phenomenon, which involving more than 10^{20} cm^{-3} H-atoms, could be caused by the generation of 10^{17} cm^{-3} metastable dangling bonds and by the hydrogen nuclei in their vicinity.[xxxiii] For a review of all photo-structural changes observed in hydrogenated amorphous silicon see Refs. [xxix,xxxiii]

Fritzsche[xxxiii] suggested that both the large changes observed in physical properties of a-Si:H and the absence of a single-valued functional relation between the photoconductivity and defect density can be resolved and explained by assuming that the exposing light not only creates dangling bonds but in addition changes the structure of the whole material. He proposed that the mechanism behind these changes must produce a more strained (or stressed) and disordered structure of higher energy. If light actually induces strain then this strain could be detected mechanically i.e. in a straight-forward manner. This concept led to the two first attempts to observe light-induced strain in a-Si:H described in the following.

3.8.1. Photo-induced strain in a-Si:H

In 1998 Gotoh *et al.*[xxxvi] reported for the first time that hydrogenated amorphous Silicon expands after exposure to light. They used PECVD samples deposited on 1.5 cm long and 100 μm thick quartz substrates, which were rigidly clamped at one end and exposed them for several hours to 0.3 W/cm^2 of green Ar^+ laser light at room temperature. This exposure produced a permanent bending of the substrates, which was detected by an optical lever method. A He-Ne laser probe beam was reflected off the free end of the substrates to a position sensitive detector and any deflection of this end could be measured by the displacement of the probe beam on a detector. Gotoh *et al.*[xxxvi] found that a-Si:H samples are under *compressive* stress of 350 MPa after deposition, which increases by 0.2 MPa after 10 hours of exposure showing no sign of saturation. Compressive stress means that the film has a tendency to expand and this tendency increases after illumination. They also found that the phenomenon is metastable. After 1 hour in-situ annealing at 200 ^{o}C the film contracts to its original as-deposited shape and the substrate acquires its initial position. Finally their data

showed a one-to-one correlation of the inverse of the photoconductivity with the bending effect. From that result they speculated that the defect creation is linked to the photo-induced expansion.

In the same year Shimizu *et al*[xxxvii] reported that hydrogenated amorphous Silicon contracts after exposure to light. These authors used exactly the same technique as Gotoh *et al.* for measuring the bending of a-Si:H films deposited on 5 cm long and 50 μm thick fused silica substrates. This time a 50 mW/cm^2 white light source was used for exposure of the films. These authors found that a-Si:H samples are under internal compressive stress of 50 – 300 MPa which decreases by about 1 % at max. after exposure for 5 min. No change in the stress of the sample is observed with further exposure i.e. the phenomenon saturates. Finally by measuring the dangling bond-density with ESR during exposure, they found that the defect density of their samples increases with decreasing compressive stress, but also that it continues to increase more rapidly, after the stress has saturated. From these results, the authors speculated that light induces a structural distortion of the a-Si:H lattice. This distortion reaches a maximum allowable value after which, dangling bond defects are created in the highly strained regions of the material.

From the discussion of these two studies it is obvious that they have reached to contradicting results. Gotoh *et al* found a light induced increase of compressive stress in a-Si:H which does not saturate after several hours of exposure, whereas Shimizu *et al* showed a light induced reduction of compressive stress which saturates after 5 min exposure. The main problems with the measurements made in these studies where

a) the low sensitivity of the beam bending methods utilized
b) the heating of the samples by the exposing light due to poor thermal conductivity of the substrates. This heating produced large unwanted deflections of the substrates during the exposures and proves that the films were at elevated temperatures during these exposures.
c) the illumination intensities used were too weak to produce sizeable and thus less amenable to experimental error, results.

For this study we have developed an extremely sensitive cantilever beam bending and oscillation technique to measure accurately the mechanical properties and their light-

induced changes in a-Si:H samples. This technique eliminates the problems encountered by previous investigations and is presented in the next chapter. Finally in Chapter 4 we present our experimental results from an extensive study of the photo-induced stress in hydrogenated amorphous silicon, discuss their implications and propose a new direction in the search of the microscopic mechanism of metastability in a-Si:H.

Chapter 3: The cantilever beam bending and oscillation method.

CHAPTER 3: THE CANTILEVER BEAM BENDING AND OSCILLATION METHOD............................. 40

EXPERIMENTAL AND THEORETICAL ESTABLISHMENT. .... ERROR! BOOKMARK NOT DEFINED.

3.1. EXPERIMENTAL SETUP 41

3.2. CALCULATION OF FILM PROPERTIES FROM THE QUANTITIES MEASURED. 44

3.2.1. STRESS – STRAIN CONSIDERATIONS UNDER UNI-AXIAL LOADING 45

3.3. PHYSICAL QUANTITIES CHARACTERIZING A BEAM OF UNIFORM CROSS-SECTION 47

3.3.1. NEUTRAL AXIS, BENDING MOMENT AND STIFFNESS 47

3.3.2. APPLICATION: NEUTRAL AXIS AND STIFFNESS OF A BEAM OF TRAPEZOIDAL CROSS-SECTION 51

3.4. FREE FLEXURAL VIBRATIONS OF AN UNDAMPED TRAPEZOIDAL CANTILEVER BEAM 54

3.4.1. EFFECT OF TIP MASS, DAMPING AND INITIAL BENDING ON THE MEASURED RESONANT FREQUENCY 59

3.5. COMPOSITE CANTILEVER BEAM BENDING UNDER INTERNAL STRESS 64

3.5.1. INTERNAL STRESSES IN FILMS 64

3.5.2. CALCULATION OF THE INTERNAL STRESS OF A FILM FROM THE CURVATURE IT INDUCES ON A CANTILEVER SUBSTRATE 68

REFERENCES……...62

3.9. EXPERIMENTAL SETUP

All properties reported here have been measured with the help of samples consisting of a-Si:H films deposited on crystalline silicon (c-Si) microcantilevers (MCLs) of the type commercially available as probe in Scanning Probe Microscopy (SPM). Fig. 3.9 shows a Scanning Electron Microscope (SEM) side-view photograph of a typical compound MCL, that is, an MCL on which a-Si:H has already been deposited. The probe tip is also visible. These MCLs are fabricated by micro-lithography and chemical etching techniques out of single-crystalline Si wafers providing ideal stiffness and positioning accuracy at their clamped end. Before any experiment, we took SEM photographs of all cantilevers, in order to measure their dimensions, as accurately as possible. This is crucial for minimizing the error on the quantities to be calculated i.e the stress and theYoung's modulus. The MCLs have a free length L of 130-140 μm, trapezoidal cross section, and thickness t_s in the range of 4-5 μm. The ratio of the parallel faces of the trapezoid was $w_l / w_h \approx 0.47$, where w_l and w_h are the narrow and wide face respectively. The measuring accuracy obtained from the SEM photographs was 1 μm for the length and 0.1 μm for the thickness. The films are always deposited on the narrower side of the cantilevers. Finally it should be mentioned that c-Si MCLs were found to be completely straight, since they have curvature always lower than our detection limit of R^{-1}_{min} = 0.5 cm^{-1}, at the SEM magnification used.

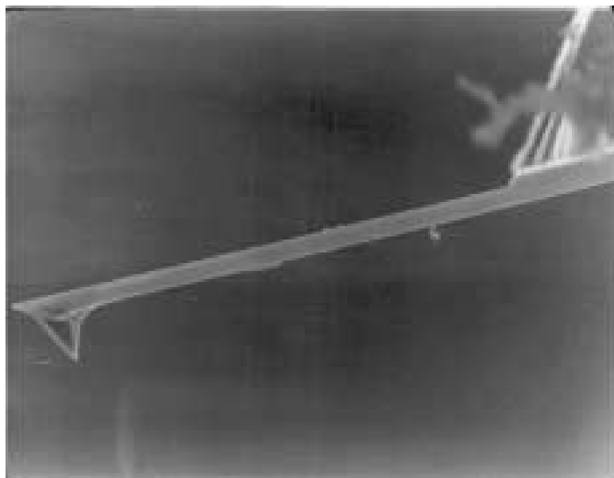

The static deflection of the MCL beam as well as its oscillation amplitude and frequency were measured with the help of the detection system of a commercial SPM shown in Fig. 3.10. In this system, the MCL is rigidly clamped to a holder, which is in turn attached to a piezoelectric actuator. A laser diode probe beam reaches the free end of the cantilever, from which it is reflected

Fig. 3.9 *Scanning Electron Microscopy photograph of a typical micro-cantilever.*

towards a position sensitive photodiode (PSD). Every movement of the lever's free end, results to a movement of the probe beam along the plane of the PSD. The PSD produces an electrical signal, which is proportional to the illumination difference among its four segments, and is thus

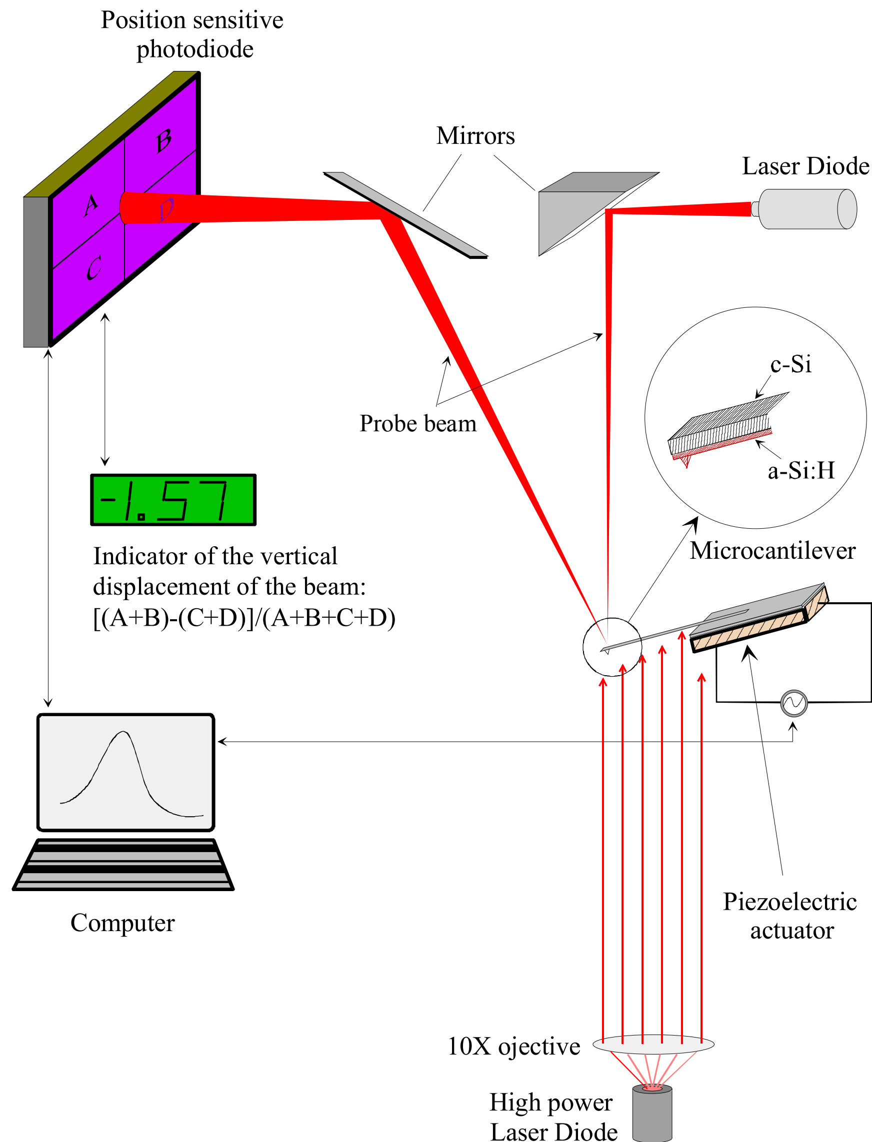

Fig. 3.10 *Cantilever beam bending and oscillation measurement setup.*

a measure of the position of the beam on its plane and, in turns, a measure of the deflection of the beam's free end. The resonant frequency, f_o, of the MCL can be measured automatically by sending a harmonic electric signal to the actuator, thus driving it to oscillate at constant amplitude. The MCL is then forced to vibrate at a frequency, which is varied continuously, by the input signal, within a range of 200-500 kHz and the r.m.s. amplitude of vibration of its free end is monitored. When the maximum amplitude is reached, the control electronics lock the frequency of the input

signal, which is the resonant frequency of the beam. The resonant frequency of an MCL is measured both before and after the deposition of the a-Si:H film. These measurements along with the measured of the lever are used to calculate the Young's moduli of c-Si and a-Si:H. The accuracy of deflection, amplitude and frequency measurements is 1 nm, 1 nm (rms) and 0.1 kHz respectively. The resonant frequency of the uncoted MCLs, f_o, was measured to range from 250 to 350 kHz. We must point out here the first major advantage of our detection system. The detection limit i.e. the lowest static deflection that can be measured, is only 1 nm. This value is the lowest compared to the values reported for the setups used in the previous studies of photo-induced stress.[xxxviii,xxxix]

The photo-induced stress experiments were done by exposing the cantilevers, from the side that the films are deposited, to intense light produced by a 35mW CW laser diode (LD) emitting at 658nm. The treatment was always done at room temperature and the laser beam was focused onto the MCL with a 10X-microscope objective, reaching an intensity of 20 W/cm^2. This value is among the highest values of continuous monochromatic light ever used for photodegradation experiments in hydrogenated amorphous Silicon. The high intensity offers the chance to produce intense photo-induced phenomena which can be measured beyond any experimental uncertainty. High intensity illumination is easily implemented in our setup because of the extremely small dimensions of the cantilevers and the high focusing ability of the laser light. Finally the monochromatic red light of 1.9 eV (658nm) offers another advantage. Since the photon energy is just above the band gap of a-Si:H (1.7 – 1.8 eV) the absorption coefficient is low enough for the light to be absorbed uniformly inside the sample. This means that any observed effect will originate from the bulk of the film and not only from the surface. The effect of non-uniform absorption was not taken into account in previous studies of photo-induced stress.[xxxviii,xxxix]

Very few exposures of a-Si:H films have been done to such high light intensity, because the poor thermal conductivity of the usual substrates resulted in substantial heating of the films. In our case, thanks to the good thermal conductivity of the c-Si MCLs, the temperature of the films at the free end did never rise more than 5 ^oC compared to the clamped end, the latter assumed to be always at room *T*. This was

calculated approximately through the formula[xl] given for a simple orthogonal bimetallic cantilever:

$$\Delta T = \frac{L^2}{2} \frac{I}{\lambda_s t_s + \lambda_f t_f}$$

[3.20]

where ΔT is the temperature difference between the two ends of the lever, I is the laser intensity, assumed to be uniformly distributed and fully converted to heat, L is the length of the MCL, λ, t are the thermal conductivity and thickness, respectively, of either the a-Si:H film (f) or c-Si MCL substrate (s). For the calculation we used λ_f = 1.5 W/mK[xli] and λ_s = 124 W/mK[xlii]. Before measuring the deflection of the cantilevers, after each soaking interval, we allowed sufficient time in the dark for complete thermal equilibration. This time was always less than 5 min. We have verified that there was no measurable change in the deflection signal during periods of several hours in the dark, at ambient temperature. The absence of heating of the samples despite the high illumination intensity ensures that one measures light-induced changes which happen with the sample being at room temperature during exposure and not at some unknown elevated temperature.

3.10. CALCULATION OF FILM PROPERTIES FROM THE QUANTITIES MEASURED.

In the analysis of our experiments we need: a) a formula giving the dependence of the resonant frequency of a cantilever on its elastic properties and b) a formula for the accurate calculation of the stress present in a film of thickness comparable to that of the substrate, from the induced. In the literature one can readily find accurate calculations of the resonant frequency of either a simple or a composite cantilever beam with orthogonal cross-section but, to our knowledge, none of these calculations has ever been published for a lever with trapezoidal section. Furthermore the effect of the tip of the cantilever (Fig. 3.9) to that frequency has always been disregarded as negligible.

For the case of the stress-curvature relation the situation is even more complicated. The only well accepted equation is the so-called 'modified Stoney's formula', and is

applicable only for a composite beam of orthogonal section with the added assumption that the film has negligible thickness compared to the substrate. We will see in the following, that there is a large amount of literature giving corrections for non-negligible film thickness, which sometimes have significant differences among each other. Again nothing is available for trapezoidal cross-section.

In the sections to follow, we describe the derivation of formulae for cantilevers of trapezoidal cross-section. Since definitions, theories and models used, are taken from several different sources, we present our derivation in a way that recurring to these sources is not required. In Section 3.10.1 we give briefly the definitions of the quantities used throughout this derivation in the simple and intuitive case of uni-axial loading, but we will return to a more rigorous and general mathematical formulation in Section 3.13 [after Refs [xliii],[xliv]]. In Section 3.11 we define and determine the neutral axis and stiffness of a beam with trapezoidal cross-section utilizing the approach given in Ref xliii, but in a more comprehensive way, for the case of a composite beam. These quantities are necessary for the derivation of the stress and resonant frequency formulae. In Section 3.12 we review [after Refs xliv,[xlv]] the derivation of the differential equation describing the flexural vibrations of a cantilever, and we find the resonant frequency for the trapezoidal case. We also make corrections for the tip mass and damping. Finally Section 3.13 presents our attempt to derive an approximate formula for the stress present in a film deposited on a trapezoidal lever.

3.10.1. Stress – Strain considerations under uni-axial loading

If a bar is subjected to a uniform tension or compression, i.e. a direct force, F, (Fig. 3.11) which is uniformly or equally applied across a cross section, $A = w \cdot t$, then the internal forces set up, are also distributed uniformly and the bar is said to be subjected to a uniform *external stress*, σ, defined as $\sigma = F / A$. In some cases the loading situation is such that the stress will vary across any given cross section and in such cases the stress at any point is given by the limiting value of $\delta F / \delta A$ as δA tends to zero. A bar subjected to direct stress would change in length. The strain, ε, produced in the bar is defined as $\varepsilon = \delta L / L$, where δL is the change in the original length, L, of the bar. Strain is thus a measure of the deformation of the material.

A material is said to be elastic if it returns to its original, unloaded dimensions when load is removed. A particular form of elasticity, which applies to a large range of materials, at least over part of their load range, leads to deformations, which are proportional to the loads producing them. This implies that, whilst materials are elastic, stress is proportional to strain or in other words the Hooke's law is valid: $\sigma = E \cdot \varepsilon$. The proportionality constant, E, is called the *modulus of elasticity* or *Young's modulus* and

Fig. 3.11 *Deformation of a rectangular bar subjected to uni-axial tension.*
is generally assumed to be the same in tension or compression. The Young's modulus is expressed in the same units as stress. Finally, the "elastic limit" of the material is generally defined as the stress, over which the Hooke's law is no longer valid.

Let us now consider a rectangular bar of width, w, thickness, t, and length, L, subjected to a tensile load along its length (Fig. 3.11). Under the action of this load the bar will increase in length by an amount δL giving a longitudinal strain in the bar of $\varepsilon_L = \delta L / L$. The bar will also exhibit, however, a decrease in dimensions laterally, i.e. its width and thickness will decrease. The associated lateral strains will both be equal and will be given by $\varepsilon_{lat} = - \delta w / w =- \delta t / t$. Provided the load on the material is retained within the elastic range, the ratio of the lateral to longitudinal strains will

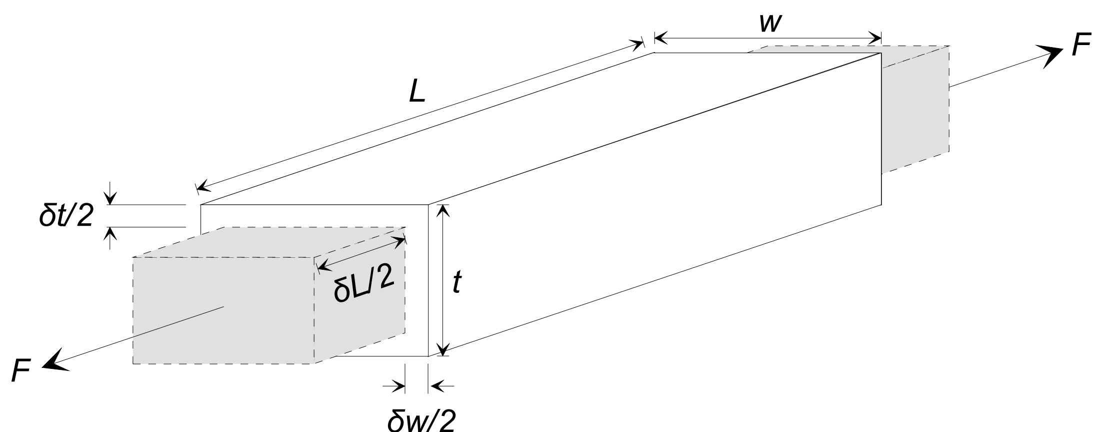

always be constant. This ratio is termed the *Poisson's ratio*, $\nu = \varepsilon_{lat} / \varepsilon_L$.

Fig. 3.12 *Shear stress (τ) and strain (γ).*

Finally consider a block of material, as shown in sideview in Fig. 3.12(a), subjected to a set of equal and opposite forces *Q*. There is then a tendency for the upper layer of the material to slide over the lower one. The resistance of the material to this sliding corresponds to the build up of a *shear stress*: $\tau = Q/B$ where *B* is the area of the block which resists to shear. Thus shear stress will always be *tangential* to the area on which it acts. If the material cannot withstand to the action of the forces, it will deform to the shape of Fig. 3.12(b), the angle of deformation, γ, being the so-called *shear strain.* For materials within the elastic limit, the equation $\tau = G\gamma$, is valid. The proportionality constant, *G*, is called the *shear modulus* and is always directly comparable to the Young's modulus.

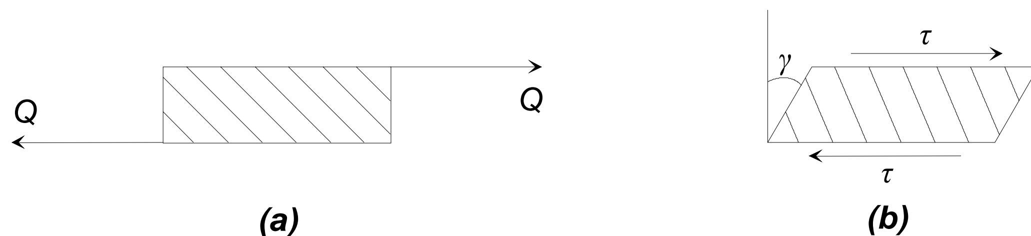

3.11. PHYSICAL QUANTITIES CHARACTERIZING A BEAM OF UNIFORM CROSS-SECTION

3.11.1. Neutral axis, bending moment and stiffness

Let us consider a beam initially straight and unstressed, having a uniform cross-section along its length, and, for the time speaking, the same density and elastic properties throughout (Fig. 3.13(a)). When the beam is subjected to a constant bending moment, i.e. pure bending, as would be obtained by applying equal couples at each of the free ends, it will bend to a radius *R* as shown in Fig. 3.13(b)**.** For the discussion to follow, we must also assume that the elastic limit is nowhere exceeded that plane cross sections remain plane before and after bending and that there is no resultant force perpendicular to any cross section of the beam. As a result of the bending the top fibers of the beam will be subjected to tension and the bottom to compression. It is reasonable to suppose, therefore, that somewhere between the two, there are points at which the stress is zero. The locus of all such points is termed the *neutral axis* (N.A), and to this, is the *radius of curvature, R,* measured.

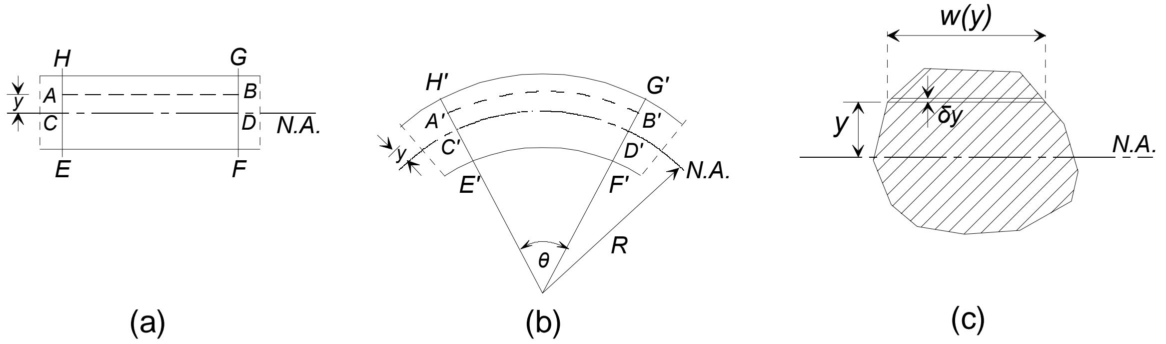

Fig. 3.13 *α) Side-view of a section of a straight and uniform beam. b) The same section under bending of radius R. c) Cross sectional view of the same beam.*

Let us take now two cross sections of the beam, HE and GF, originally parallel (Fig. 3.13(a)). When the beam is bent it is assumed that these sections remain plain; i.e. H'E' and G'F', the final positions of the sections, are still straight lines (Fig. 3.13(b)). They will then subtend some angle θ. Every fiber between the two cross-sections will change in length after bending, except for that located on the N.A., i.e CD = C'D'. A fiber, AB, of distance, y, from the N.A. will stretch to A'B' when the beam is bent. The strain in that fiber, for which: AB = CD, will be

$$\varepsilon(y) \equiv \frac{A'B' - AB}{AB} = \frac{A'B' - C'D'}{C'D'} = \frac{(R+y)\vartheta - R\vartheta}{R\vartheta} = \frac{y}{R}$$

[3.21]

and thus the stress on the fiber will be $\sigma(y) = E \cdot \varepsilon(y) = E \cdot y/R$. The force δF acting on the strip of area δA, located on the cross-section HE of the beam, at distance, y, from the N.A. (Fig. 3.13(c)) is

$$\delta F(y) = \sigma(y) \cdot \delta A(y) = \frac{y}{R} \cdot E \cdot w(y) \cdot \delta y$$

[3.22]

where $w(y)$ and δy is the width and thickness of the strip at this distance.

Until now we have introduced what is called the *simple bending theory* which holds strictly only when a beam is constructed by a material which has the same Young's modulus, E, throughout. This theory can be found in textbooks dealing with the subject of mechanics of materials. A composite beam is one, which is made from a combination of materials in a way that maintains a uniform cross-section along its length but a non-constant E across this section. In this case the simple theory must be modified. This is done in Ref. [xliii] in a more or less schematic way. Following the

reasoning of this reference we will describe the modifications that must be performed in this theory in a more mathematical manner. This will help us in developing the formulae for bending and oscillation of cantilevers with trapezoidal cross-section.

Let us consider a beam with a cross-section as shown in Fig. 3.14(a). The method of solution in such a case, is to replace one of the materials, let's say that with *E'*, by an equivalent section of the other, so that the force δF at any given δy in the equivalent beam is equal to that at the strip it replaces:

$$\sigma(y)\cdot w(y)\cdot \delta y = (\sigma_a(y)\cdot w_a(y) + \sigma_b(y)\cdot w_b(y) + \sigma_c(y)\cdot w_c(y))\cdot \delta y$$

or

$$E\cdot w(y) = E'\cdot(w_a(y) + w_c(y)) + E\cdot w_b(y)$$

[3.23]

We then produce an equivalent beam with the cross-section of Fig. 3.14(b). This way, we can generalize Eq. [3.22] for the case of a composite beam by writing it as

$$\delta F(y) = \frac{y}{R}\cdot\left(\sum_i E_i\cdot w_i\right)_y\cdot \delta y$$

[3.24]

where the term in brackets stands for the equivalent of the strip at distance *y* from the N.A. The total force acting parallel to the composite beam axis i.e. perpendicular to the cross section of Fig. 3.14(b), will be given by the sum of all the δF components along the y-axis. In the infinitesimal limit: $\delta y \rightarrow$ dy, this sum is replaced by the integral

$$F \equiv \int dF \equiv \int \sigma(y)\cdot dA(y) \Rightarrow F = \frac{1}{R}\int y\left(\sum_i E_i w_i\right)_y dy$$

[3.25]

Now one of the basic assumptions listed earlier, states that when the beam is in equilibrium there can be no resultant force across the section, i.e. the tensile force on one side of the N.A. must exactly balance the compressive force on the other side, or $F \equiv 0$.

$$\int y \cdot \left(\sum_i E_i \cdot w_i \right)_y dy = 0$$

[3.26]

The equation above is the principal formula used to locate the N.A. across a section of a composite beam, since it holds only when the integration takes place with respect to that axis.

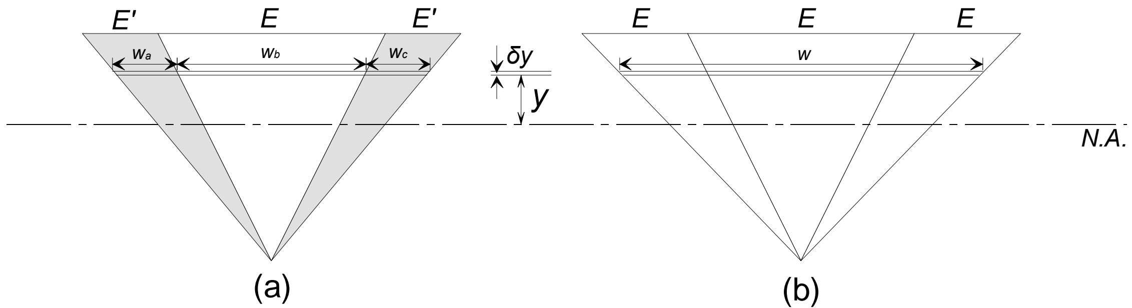

Fig. 3.14 *Cross section of a composite beam (a) and its equivalent (b) acquired as described in the text.*

Every elemental force δF(y) will contribute to a bending moment about the N.A. which will be the external product of the distance and force vectors: $\delta \boldsymbol{M}(y) = \boldsymbol{y} \times \delta \boldsymbol{F}(y)$. The magnitude of total moment, M, for the whole cross section of (a) is therefore the sum of all the elemental moments and in the infinitesimal limit: $\delta y \rightarrow$ dy is given by

$$M \equiv \int y \cdot \sigma(y) dA(y) \Rightarrow M = \frac{EI}{R}$$

[3.27]

where EI is called the "stiffness" of the beam. EI can be written in the form:

$$EI = \int y^2 \cdot \left(\sum_i E_i \cdot w_i \right)_y dy$$

[3.28]

and as we will see in the following, it is a measure of the beam's flexibility under external stimulation. The bending moment of a uniform and unstressed beam is zero. The stiffness of a uniform beam is always constant. When the beam is bent, this moment stands as the reaction of the beam to the bending load. If it is constant throughout, then the radius of curvature, R, will also be constant. Therefore the beam

will deflect into a circular arc and in that case the term "circular bending" is often used.

3.11.2. Application: Neutral axis and stiffness of a beam of trapezoidal cross-section

Throughout our study of the light-induced modifications of the mechanical properties of a-Si:H we used micro-cantilevers of trapezoidal cross-section as substrates for the a-Si:H films. These cantilevers are straight c-Si beams, which have an isosceles-trapezoidal cross-section (Fig. 3.15(a)), uniform along their length, except for a small region near one end where the tip

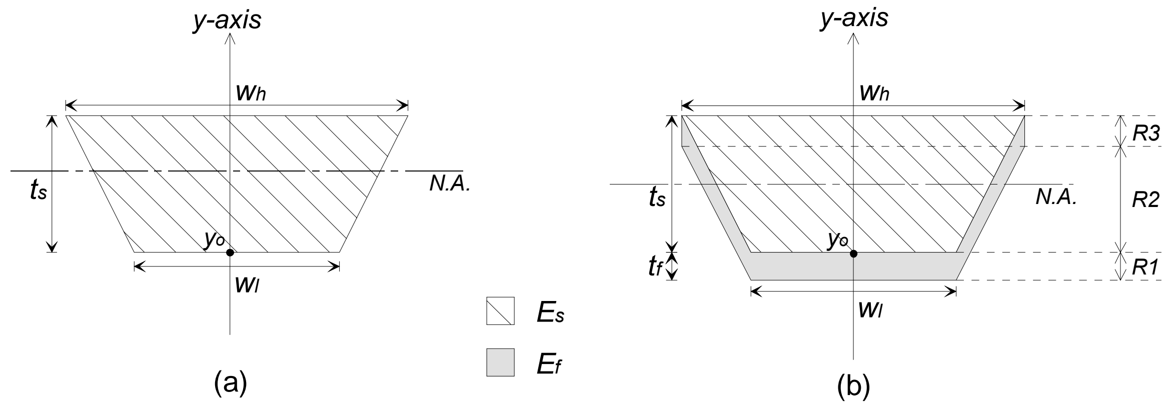

Fig. 3.15 *Cross sectional view of a beam with trapezoidal cross-section. a) "simple" case, b) "composite" case.*

is located (Fig. 3.9). They are clamped rigidly at one end while the other is free to bend or oscillate. The a-Si:H films were always deposited on the narrower side of the trapezoid modifying their cross-sectional view to that shown in Fig. 3.15(b). As we will see in the following, in order to study the elastic properties of the films, we need to calculate the stiffness of the cantilevers before and after the deposition of the a-Si:H material.

Let us consider a beam with the cross-section of Fig. 3.15(a) and a constant Young's modulus, E_s, throughout. In order to find a formula for the stiffness of the beam we need to locate the N.A. using the Eq.[3.26]. The method is to select a reference on the y-axis, let's say the narrow side of the trapezoid, and state that this point is at distance

y_o from the N.A (Fig. 3.15(a)). The integration function and limits are then taken with respect to that point. We first find a form for the term in the brackets

$$\left(\sum_i E_i w_i\right)_y = E_s\left(\frac{w_h - w_l}{t_s}\left(y - y_o\right) + w_l\right)$$

[3.29]

Utilizing the above we turn Eq. [3.26] into

$$\int_{y_o}^{y_o+t_s} yE_s\left(\frac{w_h - w_l}{t_s}\left(y - y_o\right) + w_l\right)dy = 0$$

[3.30]

and solve the equation for y_o:

$$y_o = -\frac{1}{3}\frac{r_w + 2}{r_w + 1}t_s$$

[3.31]

where $r_w = w_l / w_h$ is the width ratio of the parallel faces of the beam. The absolute value of y_o gives the distance of the reference point from the N.A. while the negative sign dictates that this point is located on the negative portion of the y-axis that we assumed. There is, then, only one possible location for the neutral axis. For $r_w = 1$, which stands for a beam with orthogonal cross section, the N.A. is placed at the middle of the section as expected from symmetry considerations. The stiffness of the beam may be given from Eq.[3.28] in which the integral is calculated again with respect to the N.A. or with respect to the reference point at y_o, since the exact position of the latter is known. The result is

$$EI = \frac{1}{36}\left(1 + r_w + \frac{2r_w}{1 + r_w}\right)E_s w_h t_s^{\,3}$$

[3.32]

Let us now consider the more complex case of a composite beam with the cross-section shown in Fig. 3.15(b). Following the methodology described earlier, we will locate the N.A,, taking the plane which divides the film (E_f) from the substrate (E_s), as the reference, y_o, and solving the equation

$$\int_{y_o-t_f}^{y_o+t_s} y\left(\sum_i E_i w_i\right)_y dy = 0$$

[3.33]

In order to solve the equation we need to break the integration range into the three regions *R1, R2, R3,* shown in Fig. 3.15(b), in which the term in brackets, is much easier to find. After some calculations we reach the result:

$$\left(\sum_i E_i w_i\right)_y = \begin{cases} E_f\left[\dfrac{w_h - w_l}{t_s}\left(y - y_o + t_f\right) + w_l\right] \ldots\ldots R1 \\ E_f\left(w_h - w_l\right)\dfrac{t_f}{t_s} + E_s\left[\dfrac{w_h - w_l}{t_s}\left(y - y_o\right) + w_l\right] \ldots\ldots R2 \\ E_f\dfrac{w_h - w_l}{t_s}\left(y_o + t_s - y\right) + E_s\left[\dfrac{w_h - w_l}{t_s}\left(y - y_o\right) + w_l\right] \ldots\ldots R3 \end{cases}$$

[3.34]

Replacing the above into Eq.[3.33] and solving for y_o, we find:

$$y_o = -\frac{1}{3}\frac{2 + r_w + 3\varepsilon\chi\left(1 - r_w\right) - 3\varepsilon\chi^2}{1 + r_w + 2\varepsilon\chi} t_s$$

[3.35]

where $r_w = w_l / w_h$, $\varepsilon = E_f / E_s$ and $\chi = t_f / t_s$. For thin films, the N.A. will always intersect the substrate, as we see from the negative sign of y_o. When the film's thickness goes to zero ($\chi \rightarrow 0$), then y_o takes the same value as that found earlier for the homogeneous beam (Eq.[3.31]). Knowing the position of the N.A., we can find the "stiffness" of the composite beam, using Eq.[3.28]. Dividing again the integral in the same three regions we derive the formula:

$$EI = \frac{w_h E_s t_s^3}{12} \cdot \frac{1 + 3r_w + \dfrac{\left(1 + r_w\right)^2 + 2r_w}{6\varepsilon\chi} + \varepsilon\chi\left(\chi^2 + 1 + 2r_w - 3r_w^2\right) + \chi\left[\left(1 + r_w\right)\left(1 + r_w + 2\chi\right) + 2r_w^2\right]}{1 + \dfrac{1 + r_w}{2\varepsilon\chi}}$$

[3.36]

The stiffness of the composite beam, which originated from the deposition of a film onto a simple beam, is always higher than that of the simple beam.

3.12. FREE FLEXURAL VIBRATIONS OF AN UNDAMPED TRAPEZOIDAL CANTILEVER BEAM

The problem of finding the free flexural vibrations of a cantilever beam with orthogonal cross-section has been extensively studied in the past. In the literature one can find accurate formulae for the resonant frequencies of all the flexural vibration modes of an undeposited orthogonal cantilever beam[xlv] and for the resonant frequency of at least the first vibration mode of the corresponding composite beam.[xlvi] However we have not found any analytiacal calculation, regarding either one of these cases, for a cantilever of trapezoidal cross-section such as ours. In this section we will try to find a formula giving the principal resonant frequency, f_o, of the free flexural vibrations of an undamped uniform cantilever beam of trapezoidal cross-section. The value of f_o will be a function of the elastic properties of the cantilever's constituents. Therefore by measuring the resonant frequency of a cantilever before and after the deposition of an a-Si:H film we will be able to calculate dynamically the Young's modulus of both the c-Si substrate and the a-Si:H material. We will first review the extraction of the differential equation for the flexural vibrations of an ideal undamped uniform cantilever beam and then make the necessary modifications in order to account for the real case.

Let us consider a straight, uniform, composite cantilever beam, which is initially curved from the action of an external force. The force is then removed and the beam is left to oscillate freely. Fig. 3.16 is a sideview snapshot, showing the beam curved at a time point, t. We will try to find the differential equation describing the motion of small segment, δs, of the beam (Fig. 3.16) located at distance, x, from the clamped end of the lever.

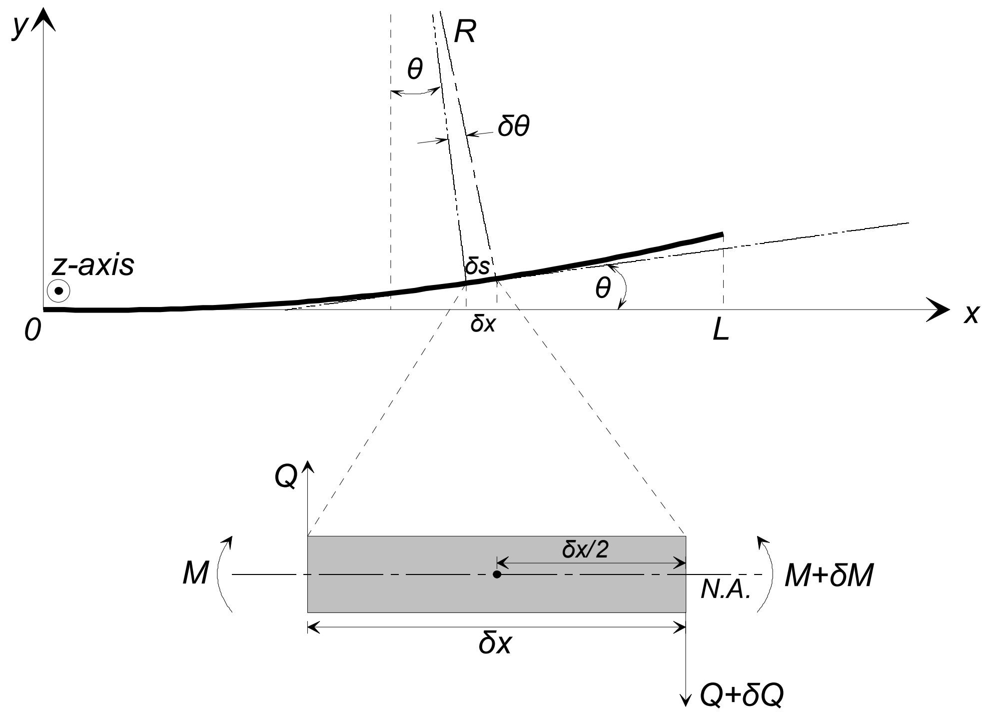

Fig. 3.16 *Side-view snapshot of an oscillating cantilever showing the beam curved at a time point, t.*

In the limit of small deformations, this motion lies on a straight line, perpendicular to the axis of the beam (the y-axis in Fig. 3.16). The slope at any point along the bent beam will be given by $\theta = dy/dx$, since for small deformations: $tan(\theta) \cong \theta$. For the same limit, the length, *ds*, of an infinitesimal piece of the beam will be equal to *dx* and, since $ds = Rd\theta$ (Fig. 3.16), we can easily find that the *curvature,* R^{-1}, at that point, will be given by the expression:

$$R^{-1} = 1/R = d^2y/dx^2$$

[3.37]

Inserting this relation into Eq.[3.27], we find the basic differential equation for the deflection of beams which is:

$$M = EI\frac{d^2y}{dx^2}$$

[3.38]

Every time that the cantilever is bent away from the straight line, a “spring” type force will act along the beam trying to bring it to its original position. For small deformations, this force will act always perpendicular to the axis of the lever. Considering the small segment of the beam, $\delta s \approx \delta x$, shown in Fig. 3.16, we observe that this force, *W*, may be taken as the sum of the opposite shearing forces acting at

the two cross-sections of the segment or $W = Q-(Q+\delta Q) = -\delta Q$. To the first approximation, $\delta Q = (dQ/dx)\cdot\delta x$, so

$$W = -\frac{dQ}{dx}\delta x$$

[3.39]

The shear force Q at point x may be found by the condition that the total moment around an axis in the z-direction, passing through the center of the element, must be zero. There are four components of moment in that segment: two are the bending moments (Fig. 3.16), $-M$ and $M+\delta M$, and two are the moments produced by the shearing forces: $Q\cdot(-\delta x/2)$ and $(-(Q+\delta Q))\cdot(\delta x/2)$. Having in mind that to the first approximation: $\delta M = (dM/dx)\cdot\delta x$ and neglecting the small δx^2 terms, the condition described previously will give for Q the result:

$$Q = \frac{dM}{dx}$$

[3.40]

Combining Eqs. [3.38], [3.40] with Eq. [3.39] we conclude that the total force acting to the segment, δs, of the beam, perpendicular to the beam's axis is

$$W = -EI\frac{d^4 y}{dx^4}\delta x$$

[3.41]

Under the action of this force, the segment will move along the y-axis. This motion can be described by Newton's second law: $W = \delta m\cdot(d^2y/dt^2)$, where, δm, is the mass of the segment. In the general case of a composite beam of uniform cross-section, δm will be given by

$$\delta m = \left(\sum_i \rho_i A_i\right)\delta x$$

[3.42]

where the sum is taken over all areas, A_i, of different density material, ρ_i, composing the cross-section of the segment and thus of the cantilever. Finally, combining Eqs. [3.41], [3.42] with Newton's law, we arrive at the general differential equation describing the deflection of the beam $y(x,t)$ which is

$$EI\frac{\partial^4 y}{\partial x^4}+\left(\sum_i \rho_i A_i\right)\frac{\partial^2 y}{\partial t^2}=0$$

[3.43]

Such an equation will have a general solution of the type:

$$y(x,t)=\left(a_1 e^{kx}+a_2 e^{-kx}+a_3 e^{ikx}+a_4 e^{-ikx}\right)e^{-i\omega t}$$

[3.44]

where α_i ($i = 1\text{-}4$) are constants. The wave number, $k = 2\pi/\lambda$, and angular frequency, $\omega = 2\pi f$, obey the following dispersion relation

$$EI\cdot k^4-\left(\sum_i \rho_i A_i\right)\cdot\omega^2=0$$

[3.45]

which can be obtained by inserting Eq. [3.44] into Eq. [3.43]. In order to calculate all the constants one has to fulfill the following boundary conditions:[xlv] at the clamped end of the cantilever, the deflection and slope of the beam must always be zero,

$$y = 0 \text{ and } \frac{\partial y}{\partial x}=0 \text{ at } x=0$$

[3.46]

while at the free end, the bending moment and shear force must be zero. The latter condition is expressed with the help of Eqs. [3.38], [3.40] by the relations:

$$\frac{\partial^2 y}{\partial x^2}=0 \text{ and } \frac{\partial^3 y}{\partial x^3}=0 \text{ at } x=L$$

[3.47]

where, L, is the length of the cantilever. Inserting the general solution for $y(x,t)$ into the four boundary conditions leads to the formation of four equations which can be solved for the coefficients α_i only when the characteristic equation

$$\cos(k_n L)\cdot\cosh(k_n L)+1=0$$

[3.48]

is fulfilled. The solutions $\{k_n L,\ n = 1,2,\ldots\}$ of this equation give the wavenumbers k_n of an infinite set of flexural vibration modes, where n is the mode number. The solution for the first or principal mode, which is of immediate interest to us, is $k_1 L =$

1.875. With the help of the dispersion relation Eq. [3.45], the first or principle resonant frequency f_o of the cantilever can be calculated:

$$f_o = \frac{1.875^2}{2\pi L^2}\sqrt{\frac{EI}{\left(\sum_i \rho_i A_i\right)}}$$

[3.49]

This is an equation, which will be used extensively in our studies. Let us calculate, the Young's modulus of a c-Si micro-cantilever of trapezoidal cross-section as that shown in Fig. 3.15(a), as a function of its resonant frequency f_o. The stiffness of this beam is given by Eq. [3.32]. Since the beam is homogeneous, the sum of Eq. [3.49] will just be equal to $\rho_s t_s(w_h+w_l)/2$ (Fig. 3.15(a)) where ρ_s is the density of c-Si. Inserting the latter and Eq. [3.32] into Eq. [3.49] and solving for E_s we find

$$E_s = \frac{57.5\rho_s}{1+\frac{2r_w}{\left(1+r_w\right)^2}}\left(\frac{f_o L^2}{t_s}\right)^2$$

[3.50]

where $r_w = wl / wh$. After the deposition of an a-Si:H film the resonant frequency of the cantilever will change. The beam is now composite, having the cross-section presented in Fig. 3.15(b) and it can be shown easily that

$$\sum_i \rho_i A_i = w_h\left(\rho_f t_f + \rho_s t_s \frac{1+r_w}{2}\right)$$

[3.51]

The stiffness of the beam has also been altered and is now given by Eq. [3.36]. Inserting the relations [3.36], [3.51] into Eq. [3.49] and solving for the Young's modulus of the a-Si:H film, E_f, we derive the complicated formula

$$E_f = E_s \frac{-\left(c_1 - r_f c_5\right) + \sqrt{\left(c_1 - r_f c_5\right)^2 - 4c_3\left(c_2 - c_4 r_f c_5\right)}}{2c_3}$$

[3.52]

The constants c_i, $i = 1\text{-}5$ are given by

$$\left.\begin{aligned}
c_1 &= 1+3r_w+\chi\left[1+2r_w+3r_w^2+2(1+r_w)\chi\right]\\
c_2 &= \frac{(1+r_w)^2+2r_w}{6\chi}\\
c_3 &= \chi\left(1+2r_w-3r_w^2+\chi^2\right)\\
c_4 &= \frac{1+r_w}{2\chi}\\
c_5 &= \frac{1+r_w}{2}+\chi\frac{\rho_f}{\rho_s}
\end{aligned}\right\}$$

[3.53]

where $\chi = t_f / t_s$, ρ_f, ρ_s are the densities of the film and substrate respectively and $r_f = (f_o / f)^2$, with, f_o, being the new resonant frequency for the composite cantilever and, f, a "unit" frequency defined by

$$f = 0.1615\frac{t_s}{L^2}\sqrt{\frac{E_s}{\rho_s}}$$

[3.54]

It is therefore clear that by measuring accurately the dimensions and the resonant frequency of the cantilever before and after the deposition of the film we can readily calculate the Young's moduli of both the crystalline Silicon substrate and the a-Si:H film by use of Eqs. [3.50], [3.52]

3.12.1. Effect of tip mass, damping and initial bending on the measured resonant frequency

The accuracy of the calculated Young's moduli for c-Si and a-Si:H is of great importance, especially in the comparison with previously published values obtained by different experimental procedures. Besides any experimental errors, discussed elsewhere, care must be taken with the assumptions, made for the derivation of Eq. [3.49], which are not met in a real cantilever oscillation experiment. The uniformity of the cantilever is everywhere obeyed except for the region of the free end where the tip is located (Fig. 3.9). The mass of the tip is expected to reduce the resonant frequency. Damping, due to internal friction and the presence of fluid resistance from the surrounding medium, will have the same result. Finally one has to explore the potential effect of initial bending, since this situation almost always emerges after the deposition of the amorphous film.

To calculate the tip mass and damping effects we replace the uniform, straight and undamped cantilever by an equivalent spring-mass system. The equivalent is such that the displacement of the mass under the action of a force, *W*, parallel to the axis of the spring, is equal to the deflection of the beam at its free end, *y(L)*, when the same force is acting at that point perpendicular to the axis of the beam. This procedure is actually used to find the so called "spring constant" of the cantilever. Let us consider the cantilever of Fig. 3.16 and imagine it being bent by a load, *W*, acting at its free end, towards the direction of the y-axis. The moment produced by this force, about an axis in the z-direction, at distance, *x*, from the clamped end of the beam is *W(L-x)*. For the beam to lie in static equilibrium, this moment must be equal and opposite to the bending moment of Eq. [3.38], giving the following differential equation for the deflection *y(x)*:

$$EI\frac{d^2y}{dx^2} = -W(L-x)$$

[3.55]

Applying the boundary conditions of Eqs. [3.46], which are always valid at the clamped end of the lever, we find for *y(x)* the solution:

$$y(x) = -\frac{Wx^2}{EI}\left(\frac{L}{2} - \frac{x}{6}\right)$$

[3.56]

For $x = L$, the equation above takes the form: $W = -\left(3EI / L^3 \right) \cdot y(L)$. The term in brackets, is that, defined as the "spring constant", k^*, of the cantilever

$$k^* = 3EI/L^3$$

[3.57]

The effective mass, m^*, of the equivalent spring-mass system, is obtained from the calculated (Eq. [3.49]) resonant frequency, f_o, of the beam through the definition: $2\pi f_o \equiv (k^* / m^*)^{1/2}$. It is now very easy to imagine that the tip attached to the free end of the lever, would have the same effect to its resonant frequency, as if the mass of the tip, m_{tip}, was added to the effective mass of the equivalent. The modified frequency, f_{tip}, of the (cantilever + tip) system will then be given by:

$$f_{tip} = \frac{f_o}{\sqrt{1+\frac{m_{tip}}{m^*}}} = f_o\left(1+4\pi^2 f_o^2 \frac{m_{tip}}{k^*}\right)^{-\frac{1}{2}}$$

[3.58]

The frequency of Eq. [3.58] corresponds to the true resonance of a real cantilever when damping is negligible. The effect of damping is to remove energy from a freely vibrating system and dissipate it to heat, reducing the amplitude of oscillation with time. The most common origins of damping is internal friction, a phenomenon very likely to occur in a-Si:H coated cantilevers, and viscous resistance coming from the surrounding medium. The latter is much more pronounced under the presence of increased humidity and is greatly reduced when the oscillating system is placed in vacuum. Damping in a harmonically excited oscillating cantilever, may be treated effectively using again the equivalent spring-mass system in which the displacement of the total mass, $m^* + m_{tip} \equiv M^*$, is described by the usual differential equation

$$M^* \frac{d^2 y}{dt^2} + c\frac{dy}{dt} + k^* y = F_o \sin(2\pi f t)$$

[3.59]

where $c(dy/dt)$ is the damping term, and F_o is the harmonically exciting force. In the real case of a cantilever, the harmonic excitation arises from the movement of the piezoelectric actuator to which the lever is attached. The solution of Eq. [3.59] is of the form $y(t) = y_o(f)\cdot sin(2\pi ft - \varphi(f))$. The amplitude and phase of oscillation are given by

$$y_o(f) = \frac{y_{oo}}{\sqrt{\left[1-\left(\frac{f}{f_{tip}}\right)^2\right]^2 + \left[2\zeta\left(\frac{f}{f_{tip}}\right)\right]^2}} \quad \text{and} \quad \tan\varphi(f) = \frac{2\zeta\frac{f}{f_{tip}}}{1-\left(\frac{f}{f_{tip}}\right)^2}$$

[3.60]

where $y_{oo} = F_o / k^*$ and $2\zeta = 2\pi f_{tip} c / k^*$. The resonant frequency, f_{damp}, of the damped cantilever oscillator is then the frequency, which maximizes the amplitude y_o of Eq. [3.60]. After some simple calculations one finds:

$$f_{damp} = f_{tip}\sqrt{1-2\zeta^2} \qquad [3.61]$$

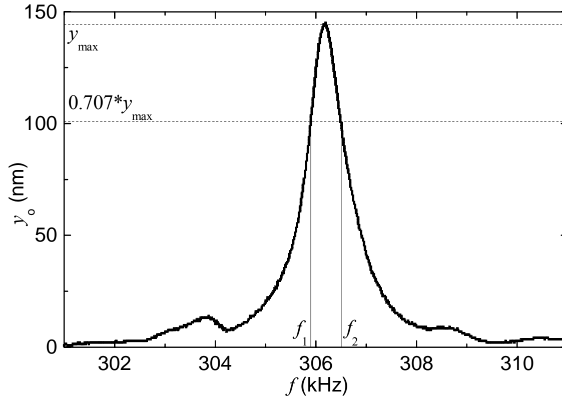

and for the peak amplitude: $y_{max} \cong y_{oo} / 2\zeta$. We observe that damping reduces the resonant frequency of the cantilever. The graphic representation of Eq. [3.60] corresponds to the experimentally determined "cantilever tune curve" a typical example of which, is shown in Fig. 3.17. The two frequencies f_1, f_2 on either side of

Fig. 3.17 *Cantilever resonance curve. y_o is the deflection of the free end of the beam.*

resonance, where $y_o = y_{max} / \sqrt{2}$, are referred to as the *half-power points*. Substituting y_o with $y_{max} / \sqrt{2}$ in Eq. [3.60] and solving for f, we find that for weak damping ($\zeta << 1$) the half-power points are given by $(f_{1,2} / f_{tip})^2 = 1 \pm 2\zeta$ and therefore their distance can be given by the relation:

$$\frac{1}{Q} \equiv \frac{f_2 - f_1}{f_{tip}} = 2\zeta$$

[3.62]

The quantity Q is called the *quality factor* and is a measure of the sharpness of the resonance. The higher the factor Q is, the weaker is the effect of damping on the oscillation of the cantilever. This is clearly seen when one inserts Eq. [3.62] into Eq. [3.61]:

$$f_{damp} = f_{tip} \sqrt{1 - \frac{1}{2Q^2}}$$

[3.63]

In Table 3.II we present a quantitative estimation of the relative magnitude of the effect of tip mass and damping on A) the Young's modulus of the substrate E_s and B) the Young's modulus of the film E_f when E_s is known. All of the values used for the cantilever substrate and film parameters, for the mass of the tip and for the damping factor are typical measured values from our experiments. As we observe from the table, damping (case (iii)) has generally a negligible effect on the calculation of the Young's modulus when the mass of the tip has been taken into account (case (ii)).

However if the latter is omitted (case (i)) the error made is substantial especially when the Young's modulus of the film is considered. The last column of Table 3.II gives the estimations, from previously published formulae, in the case where the cantilever is considered to have orthogonal instead of trapezoidal cross-section. The large relative error values justify the need for the derivation of formulae analyzing the correct trapezoidal case.

A) *substrate only*: f_{res} = 310 kHz	i) Eq. [3.50] $f_o = f_{res}$	ii) Eq. [3.58] $f_{tip} = f_{res}$	iii) Eq. [3.63] $f_{damp} = f_{res}$	$f = f_{res}$ [after Ref. xlv]
E_s (GPa)	148	160	160	141
Relative error	8 %	~0 %	-	12 %
B) *film + substrate*: f_{res} = 350 kHz	i) Eq. [3.52] $f_o = f_{res}$	ii) Eq. [3.58] $f_{tip} = f_{res}$	iii) Eq. [3.63] $f_{damp} = f_{res}$	$f = f_{res}$ [after Ref. xlvi]
E_f (GPa)	86	109	109	63
Relative error	21 %	~0 %	-	42 %

Table 3.II: *Calculated values of the Young's modulus, from the resonant frequency f_{res}, when the cantilever is considered: i) ideal, ii) with a tip of mass m_{tip} and iii) under damping of quality factor Q. Case **A**: undeposited trapezoidal c-Si cantilever with L = 135 μm, t_s = 4.5 μm, w_l = 17 μm, w_h = 36.5 μm, ρ_s = 2.33 gr/cm^3 $m_{tip} \approx 7.8 \cdot 10^{-10}$ gr, Q = 300. Case **B**: the cantilever of Case A, with the correct E_s = 160GPa, after deposition of an a-Si:H film with t_f = 1μm, ρ_f = 2.25gr/cm^3, $m_{tip} \approx 1 \cdot 10^{-9}$ gr. Q = 300. The relative error is taken with respect to the correct value when damping is concerned. The last column contains the values estimated from the formulae found in the corresponding references.*

From Table 3.II it is obvious that measured the resonant frequencies of SPM cantilevers, are actually the values of f_{tip}. It is thus imperative that the tip mass is always accounted in the calculation of the Young's moduli of c-Si and a-Si:H. Fortunately this can be done easily by inserting in Eqs. [3.50]or [3.52] the value

$$f_o = f_{tip}\sqrt{1 + 4.12\frac{m_{tip}}{L\left(\sum_i \rho_i A_i\right)}}$$

[3.64]

for the resonant frequency of the tip-less cantilever where f_{tip} is the measured resonant frequency. Eq. [3.64] was derived combining Eqs. [3.49], [3.57], [3.58].

Finally one has to consider the case where the beam is originally curved to a circular arc of radius R_o. This is the most common case in our composite cantilever beams and in fact the maximum static slope we have observed at the free end of a cantilever was $\theta_{max} = 5^o$. This value is well within the limit of small deformations as expressed from the relation $tan(\theta) \cong \theta$ (Fig. 3.16). Since the amplitude of vibration of that end produces an additional slope which is 20 times smaller that θ_{max} it is concluded that this limit was never violated. The only difference in the analysis leading to the differential equation of flexural vibrations (Eq. [3.43]) is that y must be replaced with $y' = y - x^2 / 2R_o$ but this change does not have any effect in the differential equation itself and thus to the resonant frequency of the cantilever. As we will see in a following section there was also an experiment in which an a-Si:H coated cantilever had an initial curvature that changed sign after the end of this experiment. We observed, however, that this extreme change in the static curvature of the lever, did not have any effect on its resonant frequency.

3.13. COMPOSITE CANTILEVER BEAM BENDING UNDER INTERNAL STRESS

3.13.1. Internal stresses in films

Nearly all films, by whatever means they are deposited, are found to be in a state of non-zero internal stress. This stress may be compressive (i.e. the film tends to expand parallel to the surface) so that in extreme cases it may buckle up on the substrate. Alternatively the film may be under tensile stress (i.e. the film tends to contract) and in certain cases the forces may be high enough to exceed the elastic limit of the film, so that it breaks up. In technological applications it is of great importance that the internal stresses are kept small. Device quality a-Si:H films are generally under compressive stress, while non-hydrogenated a-Si films are reported to be almost always under tensile stress.

The total internal stress of a film is generally the sum of more than one components with different origins. When the coefficients of thermal expansion of a film and its

substrate are different, heating or cooling always produces stress. This stress contribution is known as thermal stress, and its sign and magnitude depend on the difference between the thermal expansion coefficients of the film and the substrate. Even after accounting for the thermal stress, many films are found to have residual internal stress. This part is called the intrinsic stress and it forms during the deposition of the film. Finally, structural changes taking place inside the material may result to the build-up of stress. These changes are usually induced by external factors such us light or interactions of the film with the surrounding medium.

In Chapter 2 we have already mentioned that one of the motivations of this study was the preliminary but also conflicting reports on the presence of photo-induced stress in hydrogenated amorphous Silicon films. The problem in these reports came from the fact that the phenomenon they detected was very small and thus amenable to experimental error. When a small stress becomes present in a film deposited on a thin substrate, then the latter will be bent, but a very sensitive apparatus will be needed for someone to measure it. One of the most sensitive methods of measuring stresses is films is by using a thin cantilever beam as a substrate and calculating the radius of curvature of the beam and hence the stress, from the deflection of the free end. In the following we will try to derive an approximate formula with which, we will calculate the stress present in the film from the light-induced curvature of the composite cantilever.

In Section 3.10.1 it was stated there that when a rectangular bar, such as that shown in Fig. 3.11, is subjected to a tensile load along its length, then the latter will increase but this will be accompanied by a decrease of its width and thickness. This happens because no load is acting on the lateral planes of the bar. When a tensile load is acting *simultaneously* along the direction of the width and length of the bar, then *both* of these dimensions will increase. Therefore it is expected that the stress-strain relations will be modified depending on the *boundary* conditions present. A similar situation exists in a

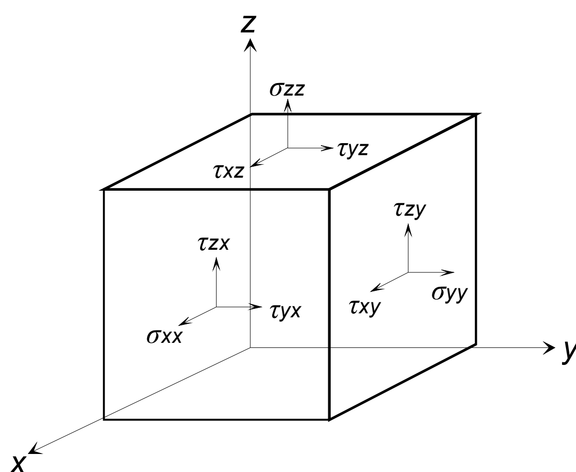

film, which is under internal stress. This stress is built up because the substrate prevents the film from retrieving its dimensions by exerting forces along both principal directions within the film plane.

Fig. 3.18 *Normal and shear components of stress in an element of a material in three dimensions*

Consider an element of material subjected to a complex stress system in three dimensions. Whatever the type of applied loading, the resulting stresses can always be reduced to the nine components, i.e. three normal and six shear, shown in Fig. 3.18. For each component the first suffix gives the direction of the stress while the second stands for the direction of the normal to the plane on which this stress acts. The *cartesian stress components* considered here relate to the three mutually perpendicular axes X,Y and Z. By taking moments, it may be seen easily that for equilibrium $\tau_{xy} = \tau_{yx}, \tau_{xz} = \tau_{zx}$ and $\tau_{yz} = \tau_{zy}$, so that only six dependent components of stress remain. The Hooke's law is then stated mathematically as: *each of the six components of stress is, at any point, a linear function of the six components of strain* and written as:

$$\begin{pmatrix} \sigma_{xx} \\ \sigma_{yy} \\ \sigma_{zz} \\ \tau_{yz} \\ \tau_{zx} \\ \tau_{xy} \end{pmatrix} = \begin{pmatrix} c_{11} & c_{12} & \cdot & \cdot & \cdot & c_{16} \\ c_{21} & c_{22} & & & & \cdot \\ \cdot & & \cdot & & & \cdot \\ \cdot & & & \cdot & & \cdot \\ \cdot & & & & \cdot & \cdot \\ c_{61} & \cdot & \cdot & \cdot & \cdot & c_{66} \end{pmatrix} \begin{pmatrix} \varepsilon_{xx} \\ \varepsilon_{yy} \\ \varepsilon_{zz} \\ \gamma_{yz} \\ \gamma_{zx} \\ \gamma_{xy} \end{pmatrix}$$

[3.65]

where $\varepsilon_{xx}, \varepsilon_{yy}, \varepsilon_{zz}$ are the normal strain and $\gamma_{yz}, \gamma_{zx}, \gamma_{xy}$ are the shear strain components. In an isotropic solid the values of the coefficients must be independent of the set of rectangular axes chosen, and if this condition is applied to the equations then only two independent constants remain.[xliv] These will be denoted by λ and μ. We then have:

$$c_{12} = c_{13} = c_{21} = c_{23} = c_{31} = c_{32} = \lambda,$$

$$c_{44} = c_{55} = c_{66} = \mu,$$

$$c_{11} = c_{22} = c_{33} = \lambda + 2\mu,$$

and the other twenty four coefficients all become zero. Eqs. [3.65] may then be written:

$$\left.\begin{matrix} \sigma_{xx} = (\lambda + 2\mu)\varepsilon_{xx} + \lambda(\varepsilon_{yy} + \varepsilon_{zz}) & \sigma_{yy} = (\lambda + 2\mu)\varepsilon_{yy} + \lambda(\varepsilon_{xx} + \varepsilon_{zz}) & \sigma_{zz} = (\lambda + 2\mu)\varepsilon_{zz} + \lambda(\varepsilon_{xx} + \varepsilon_{yy}) \\ \tau_{yz} = \mu\gamma_{yz} & \tau_{zx} = \mu\gamma_{zx} & \tau_{xy} = \mu\gamma_{xy} \end{matrix}\right\}$$

[3.66]

The two elastic constants, λ and μ, are known as Lame's constants, and they completely define the elastic behavior of an isotropic solid. From the three shear stress – strain relations it is easily seen that μ is identical with the rigidity modulus, G [see also Section 3.10.1]. The Young's modulus and Poisson ratio may be defined in terms of λ and μ, by applying the boundary conditions that no shear stress is present in the element of Fig. 3.18 and that normal stress is present only along one direction (let's say the X-axis) i.e. an identical situation with that shown in Fig. 3.11. Mathematically the conditions are: $\sigma_{xx} \neq 0$, $\sigma_{yy} = \sigma_{zz} = \tau_{yz} = \tau_{zx} = \tau_{xy} = 0$. Inserting them in Eqs. [3.66] and solving for the normal strains we find:

$$\varepsilon_{xx} = \frac{\lambda + \mu}{\mu(3\lambda + 2\mu)}\sigma_{xx} \text{ and } \varepsilon_{yy} = \varepsilon_{zz} = -\frac{\lambda}{2\mu(3\lambda + 2\mu)}\sigma_{xx}$$

[3.67]

where the signs stand for the relative direction among the different strains. The Young's modulus, E, is defined to be given by $\sigma_{xx} / \varepsilon_{xx}$, and the Poisson ratio, v, by – $\varepsilon_{yy} / \varepsilon_{xx}$, so that

$$E = \frac{\mu(3\lambda + 2\mu)}{\lambda + \mu} \text{ and } v = \frac{\lambda}{2(\lambda + \mu)}$$

[3.68]

Now let us consider the most interesting case in which the element of Fig. 3.18 is under bi-axial stress i.e $\sigma_{xx}, \sigma_{yy} \neq 0$ and $\sigma_{zz} = \tau_{yz} = \tau_{zx} = \tau_{xy} = 0$ and furthermore that the stress is the same along the two dimensions, $\sigma_{xx} = \sigma_{yy} = S$, which is the case assumed to be valid in thin internally stressed films deposited on substrates. Inserting these relations into Eqs. [3.66] and solving for the strains we find

$$\varepsilon_{xx} = \varepsilon_{yy} = \frac{\lambda + 2\mu}{2\mu(3\lambda + 2\mu)}S \text{ and } \varepsilon_{zz} = -\frac{\lambda}{\mu(3\lambda + 2\mu)}S$$

[3.69]

Using Eqs. [3.68] we can rewrite the strains in terms of E and v as

$$\varepsilon_{xx} = \varepsilon_{yy} = \frac{1-v}{E} S \text{ and } \quad \varepsilon_{zz} = -\frac{2v}{E} S$$

[3.70]

These are the basic stress-strain equations of the bi-axially stressed system. The quantity $E' = E / (1-v)$ is called the modified or bi-axial Young's modulus and is defined such that $\varepsilon_{xx} = \varepsilon_{yy} = S / E'$. Comparing Eqs. [3.67],[3.68] with Eqs. [3.69],[3.70] we observe that for the same absolute stress, the strain in the direction of loading gets less in the bi-axial case, while the strain in the stress-free direction is doubled.

3.13.2. Calculation of the internal stress of a film from the curvature it induces on a cantilever substrate

There have been many attempts for calculating the intrinsic stress of a film in terms of the deflection or curvature it induces at the free end of a cantilever. For a review see Ref. [xlvii]. The earliest analysis was made by Stoney[xlviii] and provided the most widely known formula:

$$S = \frac{E_s t_s^2}{6 t_f R}$$

[3.71]

where R is the radius of curvature, t, E, are the thickness and Young's modulus of the film, f, and substrate, s, respectively. This analysis assumed that $E_s = E_f$, that the stress in the film is homogeneous but deploys only along the length of the cantilever and not bi-axially and that the thickness of the film is negligible compared to that of the substrate. The calculations that followed this pioneering paper tried to account for the cases in which some or all of these assumptions failed to describe the real situation. In our study none of the assumptions made by Stoney is correct, therefore we need an analysis covering the problem in the most general case. Brenner and Senderoff[xlix] have obtained a 'more accurate' derivation of Eq. [3.71] considering both the comparable thickness and the difference in elastic moduli, of the film and the substrate. Their result was[l]

$$S = \frac{E_s t_s^2}{6 t_f R} \frac{1 + \varepsilon\chi\left(4 + 6\chi + 4\chi^2 + \varepsilon\chi^3\right)}{1 + \chi}$$

[3.72]

where $\varepsilon = E_f / E_s$ and $\chi = t_f / t_s$. Based on the basic method followed by these authors, we derive a further improvement taking into account the effect of *isotropic stress* along the plane of the substrate.

At first we define as intrinsic stress, *S*, the stress developed in a film deposited on a cantilever substrate that is held *straight* at exactly its *original free dimensions*. This stress will be equal to that developed by the film deposited on a thick, unbendable substrate. Fig. 3.19(a) represents this situation, for a section of an orthogonal cantilever, showing also the intrinsic, stress components in the film which are assumed to be compressive. At this phase the substrate remains stress-free. The total forces acting at the cross-sections of the film (Fig. 3.19(a)) will have a magnitude given, through the definition of Eq. [3.25], by

$$F_{xx} = Swt_f \text{ and } F_{zz} = SLt_f$$

[3.73]

where, w, L are the width and length of the lever which are along the z and x directions respectively in Fig. 3.19. The suffixes of the forces follow the notation of Fig. 3.18. The absolute magnitude of the total bending moments (Fig. 3.19(a)), is given through Eq. [3.27], by

$$M_z = \int_{|y_o|}^{|y_o|+t_f} Swydy = \frac{1}{2} Swt_f (2|y_o| + t_f), and, M_x = \int_{|y_o|}^{|y_o|+t_f} SLydy = \frac{1}{2} SLt_f (2|y_o| + t_f)$$

[3.74]

where the suffixes of the moments denote the respective N.A. about which they act, while y_o is the distance of the film-substrate interface from the neutral plane (N.P. in Fig. 3.19(a)). The theory of Brenner and Senderoff is based on the principal that when the constrains are relieved, the cantilever will gain an equilibrium position that will satisfy two basic conditions:

a) the total force taken with respect to the N.A. over any cross-section of the beam will be zero

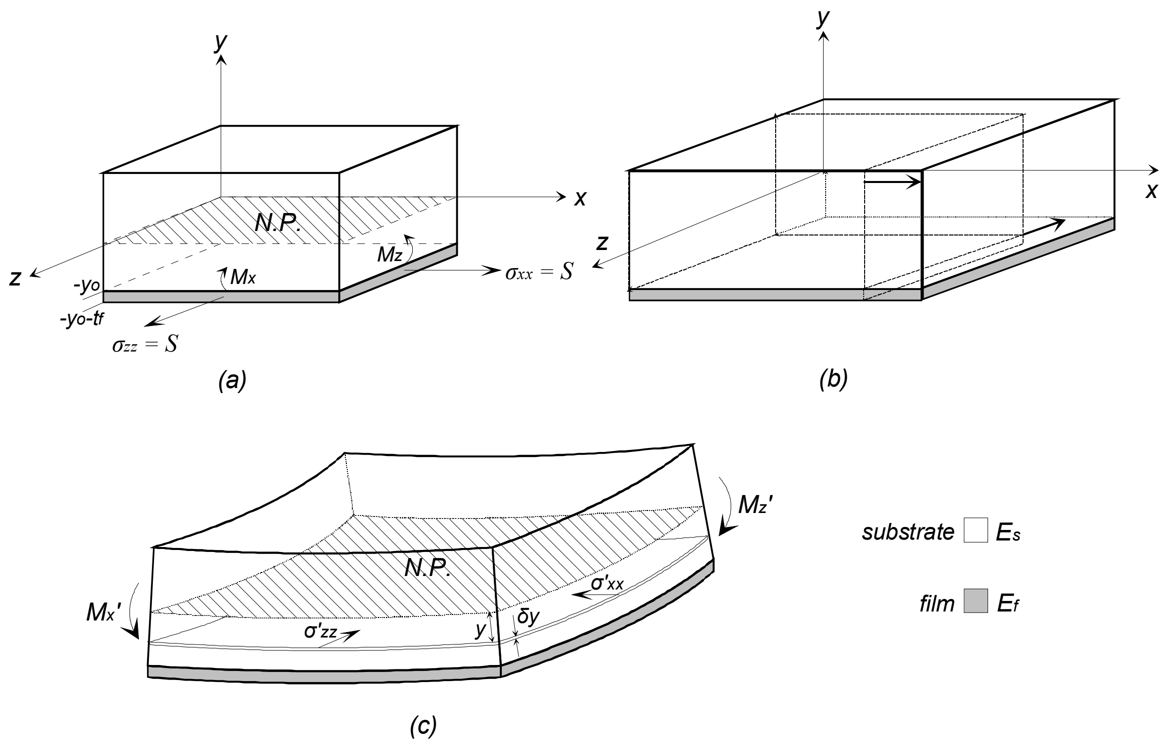

b) the total bending moment about the N.A. of any cross-section of the beam will be zero.

Equilibrium is assumed to be restored in two steps,[xlix] one of pure stretching of the beam, which will satisfy the first condition and one of pure bending, which will satisfy the second. Fig. 3.19(b) shows the piece after the first step is completed. The cantilever has still no curvature but it has expanded along the *xz* plane, until there are no resultant forces across the *yz* and *xy* planes. This means that the compressive stress in the film is somewhat relieved, while tensile isotropic

Fig. 3.19 *Section of a composite beam at the three states described in the text.*

stress has emerged across the *yz* and *xy* planes of the substrate. All of the stress components involved, still have constant values across the cross-sections that they act. This step is completed

by adding the condition that the total bending moments about the *x* and *z* axes are conserved to the values of Eqs. [3.74]. If the film's thickness is small compared to that of the substrate then the change in length and width will be negligible. We have also neglected the inability of the *yz* cross-section to expand at the clamped end of the lever, as being an extremely local constrain which cannot have a serious effect on the main body of a long beam.

When the straight beam is now allowed to bend, the section of Fig. 3.19(a) will evolve to that of Fig. 3.19(c). The equilibrium position will be acquired when the total bending moments about both of the axes involved, M_x, M_z, are one by one equal to the opposite moments that the composite system would normally develop when, being originally unstressed, externally applied loads forced it to bend. The latter moments are denoted by M_x' and M_z' in Fig. 3.19(c) and their calculation will be the subject of the following paragraph.

The problem of an initially straight and unstressed beam which is bent along one direction only, due to external load, has already been treated in Section 3.11.1. The moment developed by the beam due to bending was given by Eq. [3.27]. Let us imagine that Fig. 3.19(c) shows a section of a beam subjected to external bending moments, that will bend it in two directions and consider the two dimensional slab of thickness δy and distance y from the neutral plane as shown in Fig. 3.19(c). Now we make the assumption that *the stresses, $\sigma_{xx}'(y)$, $\sigma_{zz}'(y)$, that build up at the cross-sections of the slab, remain always equal to each other, so that the condition of "isotropic" stress is universally valid.* The stress-strain relation that will then hold strictly is that of Eq. [3.70], modified for the x and z directions: $\varepsilon_{xx}(y) = \varepsilon_{zz}(y) = \sigma(y) / E'(y)$, where $\sigma(y) = \sigma_{xx}'(y) = \sigma_{zz}'(y)$ and $E'(y) = E(y) / [1-v(y)]$. Since a beam with orthogonal cross-sections is uniform both along its length (x-axis in Fig. 3.19(a)) and along its width (z-axis in Fig. 3.19(a)) we can follow the reasoning of Section 3.11.1 to find that the neutral plane is a section of a sphere of radius, R, and that the bending moments along the x and z directions will be given by relationships of the form of Eq. [3.27]: $M_x' = E'I_x / R$ and $M_z' = E'I_z / R$ where the stiffness in each case contains the modified moduli of the components of the beam. In summary, the neutral plane of the rectangular beam will be located at a position such that the film-substrate interface is at distance

$$y_o = -\frac{1}{2}\frac{1-\varepsilon'\chi^2}{1+\varepsilon'\chi}$$

[3.75]

and the bending moments will be given by

$$\begin{pmatrix} M_x' \\ M_z' \end{pmatrix} = \begin{pmatrix} w \\ L \end{pmatrix} \frac{E_s' t_s^3}{12} \frac{4 + 2\chi\left(3 + 2\chi + \varepsilon'\chi^2\right) + \left(\varepsilon'\chi\right)^{-1}}{1 + \left(\varepsilon'\chi\right)^{-1}}$$

[3.76]

where $\varepsilon' = E_f' / E_s'$ and $\chi = t_f / t_s$. Eqs. [3.75][3.76] were derived from Eqs. [3.35][3.36] of a cantilever of trapezoidal cross-section, by setting $r_w = 1$ and replacing the normal with the modified moduli. As one would observe, the latter replacement has changed the position of the neutral plane comparing to that of the uni-axially bent rectangular cantilever.

Application of the second condition of Brenner and Senderoff for the internally bent beam, leads to the system of the equations: $M_x = M_x'$ and $M_z = M_z'$. Solving this system for S we conclude that the correct formula giving the true intrinsic stress in the film is

$$S = \frac{E_s t_s^2}{6(1 - v_s) t_f R} \frac{1 + \varepsilon'\chi\left(4 + 6\chi + 4\chi^2 + \varepsilon'\chi^3\right)}{1 + \chi}$$

[3.77]

In the limit of negligible film thickness, $\chi \rightarrow 0$, Eq. [3.77] is approximated by:

$$S = \frac{E_s t_s^2}{6(1 - v_s) t_f R}$$

[3.78]

Many authors have derived Eq. [3.78] with several different approaches and thus it is the most common found in the literature.[xlvii] Eq. [3.78] is sometimes referred to as 'the modified Stoney's formula'. Since it is very simple, Eq. [3.78] has many times been used erroneously for cases where the thickness of the film cannot be considered negligible compared to that of the substrate.

The errors in the calculation of the internal stress, from the curvature of a composite cantilever with the elastic characteristics and dimensions given in Table 3.II,[1] are 47 %, 34 % and 20 % for the Stoney (Eq. [3.71]), the modified Stoney (Eq. [3.78]) and

[1] These values are calculated with $v_f \approx v_s = 0.2$ for the Poisson ratio of the film and the substate.

the Brenner/Senderoff formula (Eq. [3.72]) respectively, compared to the correct Eq. [3.77]. The estimated stress is substantially lower than the true value given by Eq. [3.77]. It is concluded that when the effects of comparable film-substrate thickness and bi-axial stressing are disregarded, the internal stress of the film is always underestimated.

Both Eqs. [3.77] and [3.78], give the intrinsic stress, S, in the film, as a function of the radius of curvature, R. The latter must be related to the deflection, δ, of the free end of the cantilever which is the quantity measured experimentally. In Section 3.12.1 we have made the remark that in our experiments we are always in the limit of small deformations. In this limit, the differential equation, which relates R with the deflection of a beam along any distance from the clamped end, is Eq. [3.37]. Solving this equation with the boundary conditions of Eq. [3.46], and substituting for $x = L$ we find that

$$\delta = \frac{L^2}{2R}$$

[3.79]

Bending of curvature 1/R will of course take place along the width of the lever too. However, since the average width, $w \sim 30\mu m$, is much smaller than the length, $L \sim 135\mu m$, of a real cantilever, the deflection produced along the width will be only 5% of that along the length, and is thus negligible.

Comparing the formulae [3.72]and [3.77] derived for the orthogonal cantilever in the uniaxial and biaxial case respectively, we conclude that the only difference between them is that the normal moduli of [3.72] are replaced by the modified moduli in [3.77]. This means that we could easily derive Eq. [3.77], treating the uniaxial case with the correct stress-strain equations [3.70] governing both the materials of the composite beam. In the trapezoidal composite cantilever the film is also stressed biaxially. In the following, we treat this case first in the uniaxial approximation and then we correct for the biaxial strain, by replacing the moduli of the film and of the substrate by the modified counterparts.

In this case, we can consider the cross-section of Fig. 3.15(b) for a cantilever held straight at exactly its original dimensions. The intrinsic stress, *S*, which is developed in the film will produce a force perpendicular to to that section. The moment that this force produces will be given by the integral:

$$M = \int_{y_o - t_f}^{y_o + t_s} SydA = S \int_{y_o - t_f}^{y_o + t_s} y \cdot w_f(y) dy$$

[3.80]

where, $w_f(y)$, is the width of the film at distance *y* from the N.A. This moment is expected to be smaller than in the case of an orthogonal lever with $w = w_h$, because in this case there are sections of the film lying in both the half-planes defined by the N.A. The integral may be calculated by breaking the integration range in the three regions *R1, R2, R3,* of Fig. 3.15(b), and entering for each region the width $w_f(y)$, as given by the quantities multiplying E_f in Eqs. [3.34]. The moment, *M'*, that the beam will develop due to bending, will be given by $M' = E'I / R$, where the stiffness, *E'I*, of a composite trapezoidal cantilever, is given by Eq. [3.36] with the moduli of the film and substrate replaced by the modified values. Equating *M* with *M'*, we conclude that *S* will be given by:

$$S = \frac{E_s' t_s^2}{6 t_f R} \cdot \frac{b_1 + \varepsilon' \chi \left[1 + 3r_w + b_2 \chi + 2(1 + r_w)\chi^2 \right] + (\varepsilon' \chi)^2 (b_3 + \chi^2)}{\frac{b_2}{6} + \frac{1 + r_w}{2} \chi}$$

[3.81]

with

$$b_1 = \frac{1 + 4r_w + r_w^2}{6}, \quad b_2 = 1 + 2r_w + 3r_w^2, \quad b_3 = 1 + 2r_w - 3r_w^2$$

[3.82]

where, as usual, $\varepsilon = E_f' / E_s'$, $\chi = t_f / t_s$, $r_w = w_l / w_s$ and $E_f' = E_f / (1 - v_f)$, $E_s' = E_s / (1 - v_s)$.

The absolute errors in the calculation of the internal stress, from the curvature of a composite trapezoidal cantilever with the elastic characteristics and dimensions given in Table 3.II, and $v_f = v_s = 0.2$, are 42 % and 30 % for the modified Stoney (Eq. [3.78]) and the Brenner/Senderoff formula (Eq. [3.72]) respectively, compared to the

correct Eq. [3.81]. We conclude that both the comparable film-substrate thicknesses and the fact that our levers have a trapezoidal section had to be treated in order to acquire the correct values of stress in the films from the curvature of the cantilevers.

Chapter 4: Mechanical properties and their light-induced changes in a-Si:H

CHAPTER 4: MECHANICAL PROPERTIES AND THEIR LIGHT-INDUCED CHANGES IN A-SI:H 76

4.1. EFFECT OF HYDROGEN ON THE RIGIDITY OF a-Si:H FILMS 77

4.1.1. INTRODUCTION 77

4.1.2. THE YOUNG'S MODULUS OF CRYSTALLINE SILICON AND HOT-WIRE HYDROGENATED AMORPHOUS SILICON WITH VARIABLE HYDROGEN CONCENTRATION 78

4.1.3. A THEORETICAL APPROACH TO THE ISSUE OF RIGIDITY OF A CONTINUOUS RANDOM NETWORK OF ATOMS 81

4.1.4. YOUNG'S MODULUS AND FILM STRUCTURE 84

4.1.5. CONCLUSIONS 90

4.2. PHOTO-INDUCED STRESS IN a-Si:H. 91

4.2.1. INTRODUCTION 91

4.2.2. KINETICS OF PHOTO-INDUCED STRESS 93

4.2.3. STUDY ON HW SAMPLES WITH VARIABLE HYDROGEN CONCENTRATION 96

4.2.4. METASTABILITY 98

4.2.5. STUDY OF $\Delta S(t)$ IN UNHYDROGENATED A-SI 102

4.2.6. STUDY OF ΔS(T) IN HIGH TEMPERATURE ANNEALED A-SI:H. 104

4.2.7. DISCUSSION 108

4.2.7.1. Possible origins of photo-induced stress in a-Si:H *108*

4.2.7.2. H-flip in H-clusters: a modification of the Biswas model to account for our results. *113*

4.2.7.3. Correlation of ΔS(t) with light-induced defect creation *115*

4.2.7.4. Linked kinetics of volume expansion and defect creation *117*

4.2.8. CONCLUSIONS 102

REFERENCES........104

3.14. EFFECT OF HYDROGEN ON THE RIGIDITY OF a-Si:H FILMS

3.14.1. Introduction

One of the topics that attracted the interest of many researchers, throughout the 30 years of research in hydrogenated amorphous Silicon, is the relation between the electronic and structural properties of the material. The optimization of the growth conditions was (and still is) done empirically on the basis of the electronic performance of the films grown in solar cells and other devices. In time however, it was understood that the optimization of different growth processes, produced films which are remarkably independent of the details of these processes; the best films are all similar, while low quality films are "defective" in many ways.[li] However many different experiments show that high quality a-Si:H films have complex, non-homogeneous structure with significant variation among materials with similar electronic properties. Better understanding of the structure can certainly provide a valuable guide to further optimization.

Amorphous materials do not have the regular structure characteristic of a crystal. Instead the specific bonding arrangement within a particular volume represents one of many alternative configurations. A-Si:H has the added variability of the hydrogen content. Therefore, the usual techniques for probing, in a straightforward way, the structure in crystals, give limited information on the structure of the a-Si network. X-ray and neutron scattering for example have established the tetrahedral (sp^3) bonding or short-range order in a-Si:H and that there is a long-range randomness of the network, but have not given much information about the intermediate range order which involves the topology of the network at the level of second, third or fourth nearest neighbor. This is unfortunate because the bonding disorder in this range is the main origin of the band tails of localized electronic states, which, for example, control the electron and hole mobility.

A very interesting way to probe larger scale characteristics in a-Si:H and eventually detect qualitative differences among samples with variable hydrogen concentration is through the combined study of easily measurable structural properties of these

materials. The mechanical and elastic properties of a-Si:H films are closely connected to the silicon bonding configuration, hydrogen content and the presence of voids and can be measured easily and quite accurately.[li,lix] Part of this study was devoted to the determination of the Young's modulus, E_f, of a-Si:H films with different hydrogen content, c_H, deposited on c-Si micro-cantilevers (MCLs) by different deposition techniques. As the elastic properties of the crystalline Silicon substrate, are known with accuracy, the Young's modulus of the amorphous films can be measured through the resonance frequency of the composite cantilevers. We then tried to find out whether there is a relation between E_f and c_H. Finally, through a simple-model, and with the aid of results from other experiments, we formed a qualitative picture on what characterizes the medium range structure of high performance a-Si:H.

3.14.2. The Young's modulus of crystalline Silicon and Hot-Wire hydrogenated amorphous Silicon with variable hydrogen concentration

The theoretical analysis of the problem of vibrations of the free end of a composite beam with trapezoidal cross-section as that shown in Fig 3.7(b), has already been made in Section 3.1.5. This analysis led to the formulae [3.33] and [3.45], the combination of which, is able to give the Young's modulus E_f of the film from the resonant frequency f_{tip} of the undeposited cantilever. Besides knowing the exact dimensions of the MCLs on which the a-Si:H material is deposited, the accuracy of E_f depends linearly from the accuracy with which the Young's modulus, E_s, of the c-Si cantilevers is known. For that reason we measured the dimensions and resonance frequencies of seven different uncoated c-Si MCLs and calculated E_s for each one of them through the formulae [3.31], [3.45]. The results are presented in Table 4.III. The ratio of the narrow to wide face of the trapezoid was always $r_w \cong 0.47$ and the density of c-Si is taken as:[lii] ρ_s = 2.33 gr/cm^3. The tip has the shape of a pyramid of base area, $S \cong 77$ μm^2, and height $h \cong 13$μm, thus its mass is estimated to be $m_{tip} \cong 7.8 \cdot 10^{-10}$ gr.

	A1	A2	A3	B1	C1	C2	C3
L (μm)	138	138	136	136	138	134	132
t_s (μm)	4.4	4.2	4.0	4.4	4.0	4.2	4.2
f_{tip} (kHz)	287.2	273.1	272.6	305.5	257.3	298.0	306.2
E_s (GPa)	156.5	155.9	162.4	167.2	153.2	165.4	164.6

Table 4.III *Resonance frequency, f_{tip}, and Young's modulus, E_f, for seven different uncoated c-Si cantilevers.*

The experimentally determined mean value of the Young's modulus of c-Si is thus $E_s = 161 \pm 6$ *GPa*. This value is only 5% smaller than the value of 169GPa for the Young's modulus of c-Si, along any direction within the (111) plane.[liii] Since commercial MCL probes are etched out of (111) c-Si wafers, we conclude that our measurements of bare MCLs are in very good agreement with the known elastic properties of c-Si.

The characteristics of the HW a-Si:H films used in this study are presented in Table 4.IV. The films marked HW1, HW2, HW3 are intrinsic material, deposited at various temperatures, by hot-wire chemical vapor deposition, as described earlier,[liv] onto MCLs.

	PE	**HW1**	**HW2**	**HW3**
Sample number	5-96-1a	D-357-695	H-824-696	D-357-697
T_{sub} (°C)	230	360	300	225
c_H (%)	8	1 - 2	5 – 6	8 - 10
E_{gap} (eV)	1.68	1.64	1.66	1.70
α_{658} (cm^{-1})	10700	15900	11000	8600
t_f (µm)	1.2	0.83	1.40	0.87
L (µm)	137	135	137	133
t_{sum} (µm)	5.7	5.2	5.7	5.3
f_{tip} (kHz)	349.2	330.0	324.6	355.9
E_f (GPa)	109 ± 10	102 ± 10	80 ± 7	122 ± 12
S_o (GPa)	150 ± 25	500 ± 85	335 ± 50	130 ± 25

Table 4.IV *Characteristics of the first family of samples used in this study.*

The films marked PE-N, PE-L and PE-H in Table 4.V are PECVD material deposited after plasma decomposition of disilane gas (Si_2H_6) diluted with hydrogen (H_2) gas.

	PE-N	**PE-L**	**PE-H**	**HW4**
Sample number	L12510	L11407	L11397	H-825
T_{sub} (°C)	300	300	300	250
Dilution ratio	0 (H_2/Si_2H_6)	25 (H_2/Si_2H_6)	150 (H_2/Si_2H_6)	3 (H_2/SiH_4)

c_H (%)	9 – 10	9 - 10	9 - 10	6 - 7
t_f (μm)	0.80	0.85	0.80	1.1
L (μm)	130	134	133	135
t_{sum} (μm)	5.5	6.0	5.8	5.3
f_{tip} (kHz)	358.2	400.5	375.6	343.4
E_f (GPa)	70 ± 5	120 ± 11	83 ± 7	114 ± 11

Table 4.V *Characteristics of the second family of samples used in this study*

The dilution ratios are given in the same table. Details on the deposition conditions and parameters are provided in Refs [lv,lvi]. The HW4 film shown in the table above is a hot-wire sample deposited after thermal decomposition of silane (SiH_4) gas which was lightly diluted with hydrogen gas. The PE-H film is considered as state of the art material for solar cell fabrication since it produces devices with high efficiency and long-term stability against the SW effect. On the other hand the best hot wire material for device applications is considered to be the one with the lowest hydrogen concentration (HW1).

During the growth of all samples of Table 4.IV films were also deposited on Corning 7059 glass substrates. The latter were used for optical absorption measurements from which we calculated the values for the optical (Tauc) gap, E_{gap}, and absorption coefficient at λ = 658nm, α_{658}, of each sample presented also in Table 4.IV. The hydrogen content, c_H, of all films used in this study was always calculated using IR absorption measurements. By T_{sub} we denote the temperature at which the substrates were held, during deposition. The sample named PE in Table 4.IV is a device quality PECVD sample[lvii] used for comparison. The PE and HW samples were prepared in different labs and the thickness of the films, t_f, along with c_H and T_{sub} were provided by the suppliers. The thickness of the c-Si cantilevers, t_s, is calculated by the difference between the measured total thickness of the deposited MCLs, t_{sum}, and the thickness of the films t_f. The ratio of the narrow to the wide face of the trapezoid remains equal to that of the undeposited MCLs i.e. $r_w = 0.47$, while the mass of the tip increases to the approximate value of $m_{tip} \cong 1.0 \cdot 10^{-9}$ gr due to the presence of the film. The density, ρ_f, of a-Si:H with c_H varying from 1% to 10% is generally reported[lviii,lix,lx] to range from 2.2 to 2.3 gr/cm^3. Since the range of densities is very narrow, we assumed a constant value, within limits covering the above range, for all

samples: ρ_f = 2.25 ± 0.05 gr/cm^3. Inserting the above values into the formulae [3.33], [3.45] we calculate the Young's moduli of the films, presented also in Table 4.IV and Table 4.V. Before discussing the experimental results on the Young's modulus of a-Si:H in general, we need to introduce a simple theory which relates the Young's modulus of amorphous tetrahedrally coordinated material assumed to be a continuous random network of atoms, with the hydrogen concentration of this material. This theory combined with our experimental results will help us to form a better picture on the structure that characterizes high quality a-Si:H material.

3.14.3. A theoretical approach to the issue of rigidity of a continuous random network of atoms

All of the elastic moduli of a material are measures of its rigidity, or, in other words, of the degree of elastic, thus reversible, deformation of the material under different loading conditions. Consider a Continuous Random Network of atoms that is isotropic along each one of its three dimensions, in which every atom is connected with its first neighbors with springs representing the bond-stretching and bond-bending forces. These forces will act on this atom as it moves away from its equilibrium position. No dangling or floating bonds are present. If an external load is applied along one axis of this structure, then the atoms will move towards positions where there is less or no net force acting on them, in order to minimize the total strain energy, U, of the network. The net motion of the atoms results to the strain, ε, that is observed externally. The final energy that the network will acquire relates to the macroscopically observed strain by $U = E_f \cdot \varepsilon^2 / 2$, where E_f is the Young's modulus of the material.

Consider now the case of the same network of atoms in which some of the bonds are removed randomly, as happens when the mean netwok coordination is reduced. This means that the 'springs' corresponding to these bonds must also be removed. Under the action of the same external load the atoms will move again in order to minimize the force acting on them. However in this situation the atoms with broken bonds will perform larger displacements acquiring new positions in which this minimization is much more effective than before, due to the absence of some of the previously acting

forces. Minimization may be more efficient when bonds are removed from neighboring atoms and even more, when two bonds are removed from the same atom. This procedure has an impact also to the atoms away from the regions of broken bonds which will increase strongly with the reduction of network coordination. The net result will be an increase of the macroscopically observed strain and thus a decrease of E_f to a new value, E_f', which can be found through the new minimum in strain energy, U'. The Young's modulus, E_f, has a straightforward dependence on the average network coordination number, r_{Si}: when r_{Si} decreases, E_f, will also decrease.

Based on the above discussion, He and Thorpe[lxi], did numerical calculations by which they tried to establish the relation between the modulus of elasticity and the mean network coordination number, r_{Si}. In order to produce networks with different r_{Si}, they started from a lattice in which all atoms were four-fold coordinated and begun removing bonds randomly but in a way that an atom could have a minimum coordination of $r = 2$. Their calculations led to the very important result that for a given mean network coordination, r_{Si}, E_f does not depend on the fractions of two, three and four fold coordinated sites but only on r_{Si}. These calculations resulted to a set of (r_{Si} , E_f) data which could very well be fitted, in the region $2.4 < r_{Si} < 3.2$, by the function:[lxii]

$$E_f = E_o \left(\frac{r_{Si} - r_{cr}}{4 - r_{cr}} \right)^{1.5}$$

[4.83]

E_o is the Young's modulus of the amorphous network in which all atoms are four-fold coordinated, and r_{cr} is a critical coordination below which E_f becomes zero.

An isotropic amorphous silicon lattice which maintains only short-range order can be imagined as an ideal Continuous Random Network (CRN) of atoms, which are all four-fold coordinated. This lattice will have $E_f = E_o$. Since such an ideal material does not exist, the determination of E_o is rather arbitrary. One approximation comes from the concept that this material would resemble elastically a c-Si lattice in which the elasticity constants for the different crystallographic directions are averaged over the unit sphere.[lxiii] This value has been found experimentally to be 160GPa.[lxiii] We must point out however that there are theoretical models of ideal a-Si CRN's which always

show a softening of the material compared to c-Si.[lxiv] Computational results taken from both materials, predict a 5 % reduction of the Young's modulus of the amorphous compared to the crystalline counterpart.[lxiv] Therefore it is expected that E_o for the four-fold coordinated a-Si will be approximately 150 GPa. This may actually be an upper limit to the real material. It has been reported[lxv] that high density ion-implanted a-Si material exhibits $E_f = 124$ GPa .

When the average coordination number becomes lower than or equal to r_{cr} the value of E_f drops to zero. At these coordination numbers any action of external loads can deform the network with zero energy cost, thus there is no need for it to return to its original position after the removal of the load. This quality characterizes the *floppy* material. A classical example is the network of two-fold coordinated atoms in which the chains can arbirtrarily move with respect to each other, for nothing is holding them apart. The critical coordination separating the floppy from the rigid material is $r_{cr} = 2.4$.[lxi] Finally recent experimental studies made by Ferrari *et al.*[lxvi] on tetrahedral hydrogenated amorphous Carbon (ta-C:H) showed that Eq. [4.83] could actually fit reasonably well their experimental data all the way up to coordination equal to four. Since the calculations leading to Eq. [4.83] treat the atoms as spheres of no specific kind, which are normally four-fold coordinated, we will assume that Eq. [4.83] describes well the full range of $2.4 < r_{Si} < 4$, in all amorphous networks of such atoms, including silicon.

In hydrogenated amorphous Silicon, the presence of the hydrogen imposes a distinction between the atomic and the network silicon coordination. All silicon atoms are four-fold coordinated to another Si or H atom, apart from the negligible concentration of coordination defects. However, the network coordination, that is the mean number of Si-Si bonds per Si atom, r_{Si}, is reduced by the presence of hydrogen which forms a single bond to silicon and so does not help to link the network together. The average network coordination is

$$r_{Si} = 4 - \frac{c_H}{100 - c_H}$$

[4.84]

where c_H is in %. In our samples where c_H = 1-10 %, r_{Si} varies from 3.9 to ~ 4. Since bonded hydrogen deteriorates the cross-linking of the network, it can easily be held responsible for reducing the rigidity of the structure, thus having just the same effect as the removal of Si-Si bonds in a pure silicon network. Under this picture we can predict a simple formula describing the relation between the Young's modulus of a-Si:H and the hydrogen content of the material. Inserting Eq. [4.84] into Eq. [4.83] we find

$$E_f(GPa) = 150\left(1 - 0.625\frac{c_H}{1-c_H}\right)^{1.5}$$

[4.85]

where we have substituted E_o and r_{cr} of Eq. [4.83] with 150 GPa and 2.4 respectively. Eq. [4.85] shows that as the hydrogen content of an a-Si:H sample increases, the Young's modulus is always expected to decrease in the continuous random network approximation. Unhydrogenated a-Si material should exhibit the highest modulus.

<u>3.14.4. Young's modulus and film structure</u>

In Fig. 4.20 we plot the Young's modulus, E_f, of the films shown in Table 4.IV as a function of their hydrogen content c_H. Our results, in solid symbols, are plotted together with those of Kushnereit *et al.*[lix] obtained by a completely different technique, namely, Surface Acoustic Wave Spectroscopy (SAWS). Fig. 4.20 indicates a very good agreement of the absolute values and the general behavior of the Young's modulus, E_f, of our HW films with the PECVD and Laser-CVD films of the study of Kuschnereit *et al.*[lix] The solid line plotted in the same graph is the theoretical prediction of Eq. [4.85] discussed in the previous section.

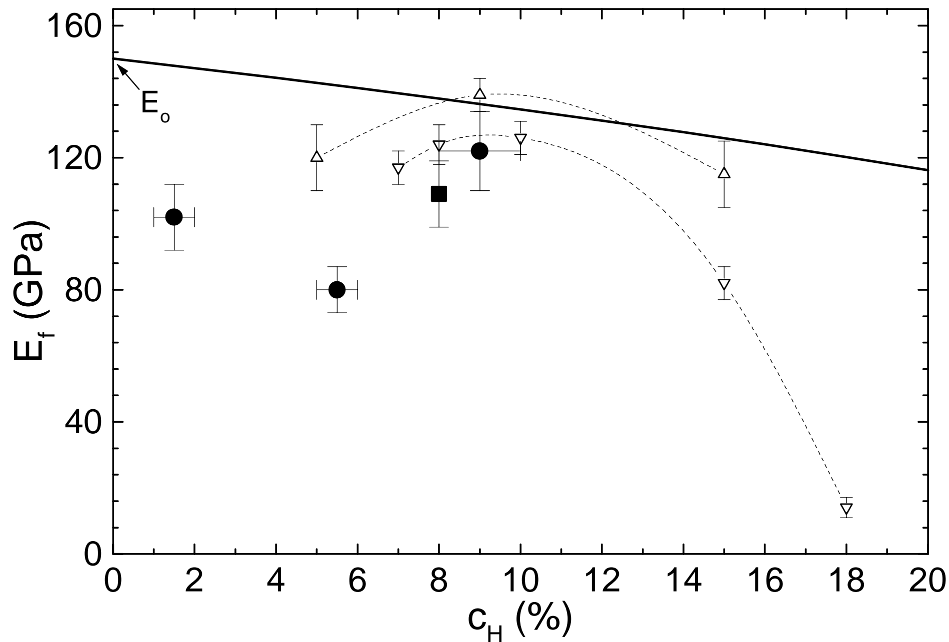

Fig. 4.20 *The Young's moduli E_f of the samples shown in Table 4.IV as a function of their hydrogen content c_H. The solid circles represent the HW samples while the solid square represents the PE sample. The open symbols are results taken from Ref. lix. The solid line is a result of a theoretical calculation discussed in the text.*

We observe that the HW material with 10 % hydrogen has a Young's modulus very close to that predicted theoretically for the amorphous CRN. On the other hand our data reveal that there is a deviation of E_f from the theoretical values in the range of c_H = 1-5 %, which shrinks as the hydrogen content increases from 5 to 10 %. Our results together with those of Kushenereit *et al.* form a unified picture for a-Si:H prepared under regular conditions (i.e. from silane - SiH_4 - gas with no hydrogen dilution): a-Si:H material with c_H ~ 10 % is the closest to the theoretical approximation of a continuous random network. It is also clear that any deviation from this network results in softening and not hardening of the material.

In Fig. 4.21 we plot the Young's modulus, E_f, of the films shown in Table 4.V as a function of their hydrogen content c_H. In this figure the key parameter is not the hydrogen concentration but the dilution ratio i.e. a difference in the deposition conditions of the samples which does not effectively alter their concentration in hydrogen atoms. We observe that a great change in the Young's modulus of a-Si:H can occur without altering c_H. This is true for both the PE and the HW series. In

general we can conclude that provided that c_H is constant, weak dilution increases the rigidity of a-Si:H. On the other hand heavy dilution must have a softening effect on the films as seen from the reduction of E_f for the PE-H sample in which the dilution ratio is 150 (Table 4.V). It seems quit safe to predict that there exists a certain dilution ratio, in which a-Si:H shows maximum rigidity. This ratio may depend on the hydrogen concentration and the parameters of the deposition technique utilized. Such a parameter may be the type of the gas used for the deposition. PE material deposited

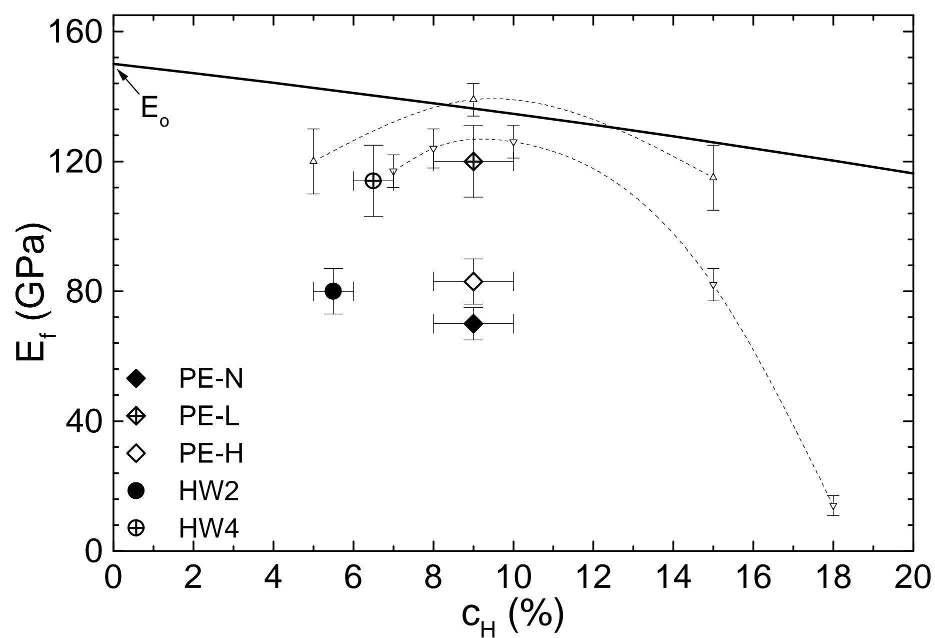

from SiH_4 gas has good rigidity without dilution (*E_f = 109 GPa*) whereas PE material prepared from Si_2H_6 gas acquires substantial rigidity only when prepared under moderate dilution conditions (compare PE-N with PE-L samples of Fig. 4.21)

Fig. 4.21 *The Young's moduli E_f of the samples prepared under different hydrogen dilution, conditions shown in Table 4.V, as a function of their hydrogen content c_H. HW2 is taken from Table 4.IV. The open symbols are results taken from Ref. lix. The solid line is a result of a theoretical calculation discussed in the text.*

In general we conclude that a-Si:H appears to be softer than expected from a continuous random network of atoms, which means that its lattice deviates from this ideal consideration. This deviation depends on a combination of deposition parameters and not only on the hydrogen concentration of the sample. It also seems certain that a high quality a-Si:H material in terms of electronic properties and

stability does not need to be a continuous random network of atoms exhibiting high rigidity; the best HW and PECVD films (HW1 and PE-H respectively) are softer than expected. In the following we will suggest some sources of rigidity reduction which may play a significant role in a-Si:H and discuss their significance in different cases comparing with other experimental results found in the literature.

The first and most straightforward cause of rigidity reduction could be a reduction of the spring constant of the bond-bending and/or bond-stretching forces in a-Si:H compared to that of c-Si. This means that there is a possibility that the network of a-Si:H is continuous and random but the springs connecting the silicon spheres of the Thorpe's model,[lxi,lxii] are weaker in a-Si:H compared to c-Si. As we have already mentioned, weakening is suggested theoretically to occur in four-fold coordinated a-Si, compared to c-Si.[lxiv] In fact the absolute value of E_f found for our lowest c_H sample (HW1, $E_f = 102\ GPa$), which contains an 80 % volume fraction of hydrogen deficient, a-Si material (see Section 1.3.2), is very close to the theoretical prediction of Ref. lxiv (E_f(a-Si) ≅ 90 GPa). On the other hand it is difficult to explain why the HW3 material, which is deposited at lower temperature and has higher c_H, has "stronger" bonds. It was suggested by Hishikawa[lxvii] that weakening of Si-Si bonds may be detected by a reduction of the TO Raman peak which is not observed in either HW samples[lxviii] or PECVD material prepared with H-dilution.[lv] Street[li] disagrees with Hishikawa's suggestion so we believe that from the point of view of Raman studies the question of the strength of Si-Si bonds in a-Si:H remains open. We suggest that a more indicative quantity of an a-Si:H continuous random network with weak bonds, is the density of that structure. We will come back to this issue in a following paragraph.

Mathioudakis and Kelires[lxiv] have speculated that voids may be a source of reduction of rigidity in amorphous materials[lxiv] but the relation between the volume fraction of voids and the reduction of the Young's modulus, is still very unclear. All of our samples, which are considered as device quality in terms of electrical performance and stability, are reported[lxix] to contain a small volume fraction of voids (less than 1%). This fraction can contain molecular hydrogen,[lxx] and is generally too small to be responsible for any divergence of the network from its 'continuous random' elastic properties as Kushnereit *et al*[lix] pointed out. On the other hand there are many reports[lviii,lix,lxix] which prove that this fraction icreases dramatically with c_H for c_H

>10% causing a serious reduction of the material's density,[lviii] and E_f (Fig. 4.20). There are also preliminary reports of sizeable amounts of H_2 being present in two dimensional structures (platelets or *T*-like sites),[lxxi] which may have some relation with our observations, but this subject is not clarified yet.

When the volume fraction of voids increases, the density of the material must decrease. Furthermore, weakening of Si-Si bonds can occure when these bonds become more strained i.e. more elongated compared to the normal Si-Si bond (2.35 Å) of crystalline Silicon. This will also result in a decrease of the density of the material. We suggest that when voids and/or Si-Si bond weakening, reduce significantly the rigidity i.e. the Young's modulus of a-Si:H, then this must be accompanied by a significant decrease of the density of the material. This is the case for the HW2 material (Table 4.IV). Williamson[lxix] found that this material deposited at the same laboratory as ours exhibits a density of only 2.18 gr/cm^3 while HW samples deposited at elevated temperatures (such as the HW1 of Table 4.IV) have densities closer to 2.29 gr/cm^3. The best correlation however between rigidity and density can be made for the samples prepared under hydrogen dilution. Bauer *et al.*[lx] showed that the densest HW films are those prepared under a dilution ratio of 1 – 2 while the densest PECVD films were prepared with a dilution ratio of ~ 15. These ratios are very close to the ratios which produce the most rigid HW and PE films in our dilution series samples shown in Fig. 4.21 and Table 4.V.

Finally another plausible explanation comes from careful examination of the method yielding Eq. [4.83]: all networks with $r_{Si} < 4$ are simulated theoretically by *randomly* removing or substituting Si-Si bonds from a network with four-fold coordinated atoms. As we have already discussed in Section 3.14.3 when this action is not performed randomly but in a way that Si atoms with only two Si neighbors ($r_{Si} = 2$) are produced systematically or in a way that the broken Si-Si bonds are intentionally grouped to form tissues of low coordinated material, then the reduction of E_f may be more pronounced than expected from random network considerations. Non-random removal of bonds can also be conducted *anisotropically*, resulting in a network with different elastic properties along the three principal axes. All of the above processes produce an **inhomogeneous** material.

A dihydride is a Si atom bonded to two hydrogen atoms, while in a monohydride, Si is bonded to one hydrogen only. Dihydrides and chains of dihydrides, which are thought as polymeric structures, are the clasical examples of atoms with $r_{Si} = 2$. Kushnereit *et al*[lix] suggested that these structures cause significant reduction of E_f in low quality samples having hydrogen concentrations larger than 10% (Fig. 4.20). The reported[lxxii] decrease of the dihydride to monohydride ratio in HW samples with decreasing c_H, in the region of c_H = 1-10%, does not support the reduction of E_f towards low c_H (Fig. 4.20). On the other hand, Infra Red measurements showed that the PE-N film contains an appreciable amount of dihydrides contrary to the PE-L and PE-H samples. This may very well be a serious reason for the low E_f exhibited by this material (Fig. 4.21).

As we have already discussed in Section 1.3.2 device quality a-Si:H appears to be inhomogeneous at least with respect to the distribution of hydrogen. The material may consist of three different phases: a) hydrogen clusters, which comprise more than 50 % of the hydrogen content, b) randomly dispersed hydrogen regions of constant c_H = 2 – 4 % and c) hydrogen deficient material or pure amorphous Silicon. We suggest that clustered hydrogen regions can be a major source of rigidity reduction inside the material when they are organized in structures, which percolate the film. Percolation may be accomplished much more easily along the direction of growth since the thickness of a film is its smallest dimension. If this actually happens, then the film will behave like rigid H-dispersed or H-deficient columns, parallel to the growth axis, separated by weak intercolumnar material containing the hydrogen clusters. Such a structure is by definition anisotropic and is expected to give different Young's moduli for the directions parallel and perpendicular to the growth axis. A linear or "columnar" like structure has been actually observed in high quality PE material prepared under high dilution conditions (similar to our PE-H sample) both by Transmission Electron Microscopy (TEM) photographs[lv] and by a weak anisotropy detected in Small Angle X-ray Scattering (SAXS) in the directions along and perpendicular to the growth axis.[lxix] It is interesting to note also that high dilution PE material exhibits a low temperature effusion peak.[lxxiii] This is indicative of oriented features containing higher than average H concentration (i.e. H-clusters) which facilitate out-diffusion of hydrogen as discussed in Section 1.3.3. We speculate that a similar situation may exist in the high quality, low c_H, HW material (HW1) although

to a less extent due to the reduced total hydrogen concentration of these films. This might be the primary reason why this film exhibits lower E_f than that of the material with 9% of hydrogen (HW3) as observed in Fig. 4.20.

3.14.5. Conclusions

The study of the elastic properties of hydrogenated amorphous Silicon can provide useful information on the structure of the material especially if it is combined with measurements of other physical properties such as the density. This study resulted in the following conclusions:

a) A-Si:H material prepared without hydrogen dilution is closer to the continuous random network of atoms in terms of rigidity, when it contains approximately 10 % of hydrogen irrespectively of the deposition technique used.
b) A-Si:H material is generally softer than expected theoretically. Moderate hydrogen dilution can improve the rigidity of the structure but heavy dilution has a softening effect.
c) The best Hot-Wire and PECVD materials for solar cell applications -namely the low c_H HW and the PE prepared under high dilution- have a structure, which deviates from the continuous random network. These materials appear to be inhomogeneous.
d) An inhomogeneous hydrogen distribution inside a-Si:H must play a significant role in deteriorating the rigidity of the network especially if some sort of ordering of H-reach material occurs.
e) Dihydrides and voids play a significant role in rigidity reduction at hydrogen concentrations higher than 10 %. Material with $c_H > 10$ % is considered to be of low quality and can not be used in device applications.
f) Weakening of the bond bending and bond stretching force constants of the Si-Si bonds in general or in tissues surrounding rigid material, can play a significant role in the reduction of the Young's modulus of a-Si:H. Whether this weakening occurs or not, under certain deposition conditions, is still an open subject for experimental and theoretical research.

3.15. PHOTO-INDUCED STRESS IN a-Si:H.

3.15.1. Introduction

As we have already pointed out in Section 2.3.1, our study of the changes of internal stress after illumination was motivated by

a) the novelty of the phenomenon, since its presence was reported for the first time in 1998,[lxxiv,lxxv] b) the presence of contradictory reports[lxxiv,lxxv] on the type of the stress (compressive or tensile), which raised the suspicion that the phenomenon is sample dependent,

c) the fact that probing photo-induced structural changes through the measurement of mechanical properties is certainly more straightforward than the study of electronic properties, which offers greater sensitivity but is difficult to interpret and

d) the potential that the study of this phenomenon, could also improve our understanding of the Staebler-Wronski effect.

A great part of the 30-year research in a-Si:H was devoted to the study of the role of hydrogen in the stability of a-Si:H samples against the SW effect. The problems mainly arising in this study were a) that all device-quality[2] PECVD samples contain almost the same amount of hydrogen (c_H = 8-9 %) and b) that Nuclear Magnetic Resonance (NMR) and IR absorption techniques, which are used extensively to determine hydrogen concentration and bonding configurations, do not normally have the sensitivity to detect small changes that may be caused by illumination. In 1991 Mahan *et al.* reported on the development of device quality a-Si:H layers by the Hot Wire (HW) Chemical Vapor Deposition method.[liv] Since then, this technique has attracted considerable interest from many research groups because it produces material with a wide range of hydrogen concentrations from below 1 % to as high as 10 % and very low defect densities, at deposition rates higher than those achieved by PECVD. HW films are therefore the best candidates for the study of hydrogen in a-Si:H, in an attempt to understand its relation to the stability of the material.

In this section we present our experimental results regarding the stress induced in a-Si:H films deposited in c-Si micro-cantilevers (MCLs), after high intensity illumination. We have been able to obtain the highest possible intensity of monochromatic light without significant heating of the films thanks to the micron scale dimensions of the MCLs and the high focusing ability of the laser diode These produces easily detectable changes within reasonable exposure times. The stress is calculated from the measured deflection of their free end of the MCLs. The high length to thickness ratio of the MCLs, $L / t_s \cong 30$, offers great sensitivity as the detection limit in the relative change in length of the film, is only $\Delta L/L = 10^{-6}$. We

---

[2] By this term we denote samples, which, in their as-deposited state, have adequate opto-electronic properties for the production of solar-cell devices.

have used both HW films with c_H varying from 1 % to 10 % and device quality PECVD material in order to be able to observe the dependence of photo-stress on a) the hydrogen content on a series of films deposited by the same technique and b) possible systematic differences between HW and PE CVD samples. We have also re-measured the photo-stress kinetics in the same samples after annealing at various temperatures. This is very important in the establishment of the extend to which the effect is reversible.

3.15.2. Kinetics of photo-induced stress

The study of kinetics of photo-induced phenomena in a-Si:H generally ammounts to the determination of their dependence on exposure time, t, and the *generation rate*, G. This is the rate by which free carriers, electrons and holes, are generated when light is absorbed. G is always proportional to the absorbed light. Since absorption, reduces the light intensity exponentially with the distance traveled inside the material, the generation rate is taken as an average value by the simple formula:

$$G = (1-R)\frac{\Phi}{t_f}\left[1-\exp(-\alpha t_f)\right]$$

[4.86]

where Φ is the incident photon flux, and α, R, are absorption coefficient and reflectivity of the a-Si:H film respectively, at the wavelength of the light used (λ = 658nm in our case). $R \cong 0.35$ for all the samples studied. The derivation of Eq. [4.86] assumes that an electron-hole pair is generated for every photon absorbed i.e. quantum efficiency equal to unity.

For the study of the kinetics, we have used two MCLs on which device quality PECVD material was deposited at the same deposition run. The films' deposition characteristics, optical and elastic properties are identical to those of the PE material of Table 4.IV. We exposed one of the samples to 17 W/cm^2 of 658nm light, producing a $G_o = 2\cdot10^{23}$ cm^{-3}s^{-1}, and the other to light which was reduced to 1/13 of G_o. We have monitored the deflection of the MCLs' free end, after

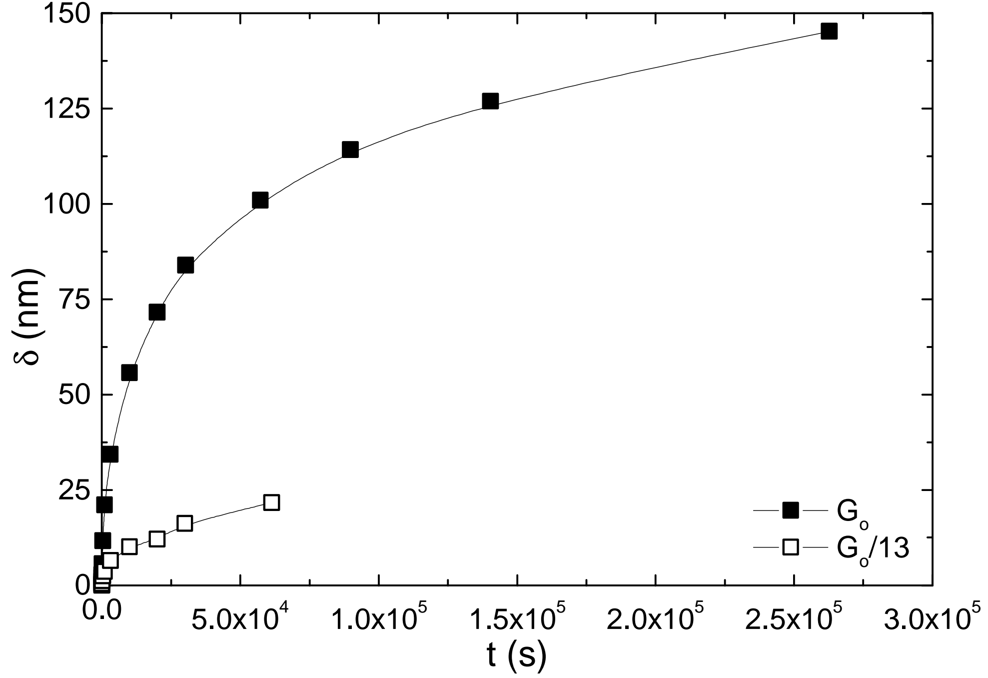

Fig. 4.22 *The deflection, δ, of the free end of two cantilevers, deposited with PECVD a-Si:H and exposed under different illumination conditions, as a function of exposure time, t.* $G_o = 2x10^{23}\ cm^{-3}s^{-1}$.

several logarithmically increasing time intervals, during these exposures. Each measurement was taken with the light turned off. We always allowed sufficient time in the dark for complete thermal equilibration, before measuring. This time was less than 5 min. The measuring procedure described above was followed in all the photo-induced stress experiments. In Fig. 4.22 we show the measured deflections, δ, of the cantilevers' free end as a function of exposure time, t. The positive sign of the deflection means that the cantilever bends upwards in Fig. 4.22. We remind here that the films are deposited on the bottom surface of the cantilevers (see Fig. 3.1) thus a positive deflection means that the film *expands*. We observe in Fig. 4.22 that both films expand under illumination but with a rate, which decreases with exposure time. The maximum deflection of the cantilevers is of the order of 150 nm, which is very small compared to their length. This ensures that we are within the limit of small deformations and that there is no permanent or plastic yield of the c-Si substrates due to bending. The relative position of deflection curves depends on the cantilevers' dimensions and thus can not be an absolute measure of strain or compressive stress increase in the film. Both quantities can be calculated from the deflection of the cantilevers through the formulae given in Section 3.1.6.2. At this point we wish to point out that, throughout this study, we never observed any contraction or expansion

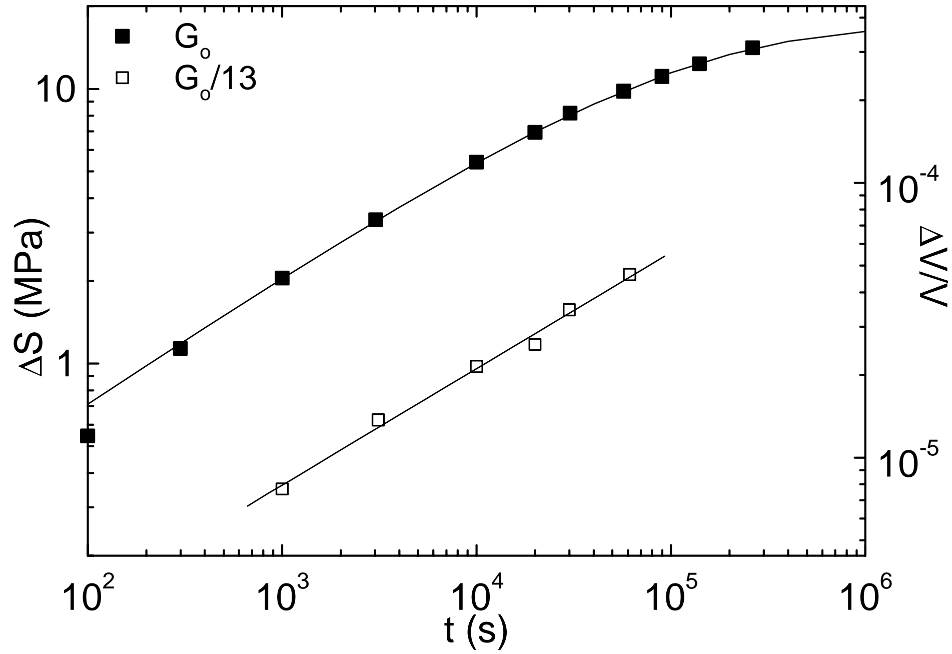

of the a-Si:H films, in the dark. We have also exposed uncoated c-Si cantilevers to the same illumination (17 W/cm^2) but we did not observe any deflection of their free ends.

Fig. 4.23 *Light-induced stress, ΔS, and volume expansion ΔV/V, as a function of exposure time, t, for the samples and illumination conditions shown in Fig. 4.22*

In Fig. 4.23 we present the results of our photo-induced stress, *ΔS*, kinetics experiments on a log-log scale. *ΔS*(t), was calculated from the deflection, *δ*, through Eqs. [3.58] and [3.60]. The right axis of Fig. 4.23 shows the light-induced volume change, *ΔV/V*, that the film would exhibit if it were detached from its substrate. Assuming that, in such a hypothetical situation, the strain produced in the film is isotropic, then *ΔV/V* will be three times higher than the strain produced by *ΔS* along the length of the lever, given by Eq. [3.51]:

$$\frac{\Delta V}{V} = 3\frac{1-\nu_f}{E_f}\Delta S$$

[4.87]

The detection limit of *ΔV/V* in our experiment is three times higher than that of the strain along the length, thus approximately equal to $3\cdot10^{-6}$.

Our first observation is that *ΔS* is compressive at any time. Therefore the film tends to expand monotonically at least in the time scale of our experiments. This agrees with

the results of Gotoh *et al.*[lxxiv] and disagrees with the observations of Shimizu *et al.*[lxxv] The second observation is that both curves show a clear "linear" region in the log-log diagram, indicating a power law time dependence, $\Delta S \sim t^r$. As both curves are parallel in this region, r appears to be independent of G, in the range of G's studied, and is found to be approximately equal to 0.45. The photo-induced stress increases with G. Assuming also a power law for $\Delta S(G)$ in accordance to many G-dependence studies of the SW effect in a-Si:H we find that $\Delta S \propto G^{0.7}$. This is the first and only available measurement of the generation rate dependence of ΔS because previous investigations lacked the necessary sensitivity and significantly higher generation rates would surely raise the temperature of the film on any substrate. We finally arrive to the conclusion that for $t \leq 3{\cdot}10^4$ s the photo-induced stress can by given by a relation of the form

$$\Delta S \propto G^{0.7} t^{0.45}$$

[4.88]

For times longer than $3{\cdot}10^4$ s, there is a continuous reduction of the rate exponent, r, in the high illumination regime, which suggests that ΔS saturates at very long exposure times. Although we prolonged the exposure up to approximately $3{\cdot}10^5$ s (3.5 days) a clear saturation was not observed.

3.15.3. Study on HW samples with variable hydrogen concentration

As mentioned before, a series of device quality samples with different H concentration prepared by the hot-wire technique offers a great opportunity to investigate the role of hydrogen in all photo-structural changes occurring in a-Si:H. The samples used are denoted as HW1, HW2 and HW3 and their properties are given in Table 4.IV. We note that the hydrogen concentration changes by an order of magnitude within the series. All of them are under a state of initial compressive stress, S_o given also in Table 4.IV. Its value is calculated from the curvatures of the cantilevers in the as-deposited state, through Eq. [3.62]. Compressive stress is a common characteristic of high quality a-Si:H material[lxxvi] and decreases almost linearly with increasing c_H.

Due to the small differences in the optical gap of the films, the absorption coefficient at 658nm varies from sample to sample. For better comparison of the samples, we

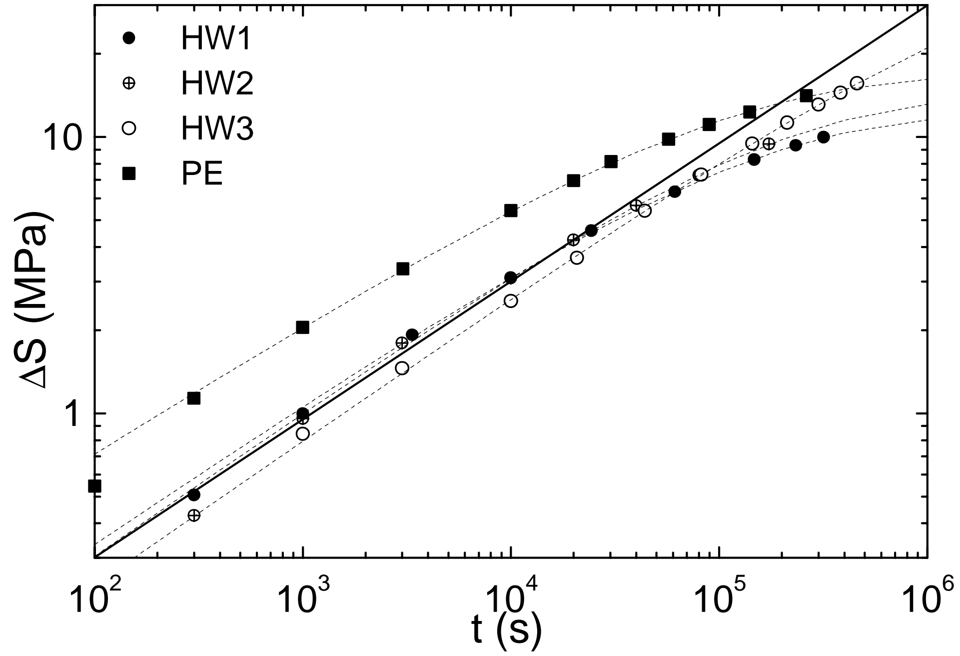

adjusted the light intensity of the laser (thus the flux, Φ, in Eq. [4.86]), so as to always yield the same generation rate. This rate was set equal to $G_o = 2 \cdot 10^{23}$ $cm^{-3}s^{-1}$. Our experimental results on the time evolution of ΔS in the HW samples, plotted on a log-log scale, are presented in Fig. 4.24. The PE sample of Fig. 4.23 is also plotted for comparison. We conclude that a-Si:H material always expands under illumination and that the stress increases with time having a relation $\Delta S \propto t^r$ for $t < 1\text{-}2 \cdot 10^4$ s. The time exponent r varies from 0.43 to 0.50. In the light of this impressive similarity in the form of $\Delta S(t)$, for samples with so different characteristics, we can assert for the first time that a common mechanism of light-induced expansion exists in all a-Si:H materials and not in some films prepared under particular conditions. On the other hand, the magnitude of

Fig. 4.24 *Photo-induced stress, ΔS, as a function of exposure time, t,* for samples with different hydrogen concentrations shown in *Table 4.IV*. The generation rate is $G_o = 2x10^{23}$ $cm^{-3}s^{-1}$. *The dash lines are guides to the eye. The solid line represents the* $\Delta S \sim t^{0.5}$ *relation.*

the photo-induced stress depends on the deposition technique used. A clear but quite unexpected result is that HW samples exhibit almost the same magnitude of ΔS irrespective of their hydrogen content, while the PECVD material shows approximately two times stronger phenomenon. This behavior covers a time range of three orders of magnitude: $10^2 < t < 10^5$. The absence of any clear change in the magnitude or time dependence of ΔS with hydrogen concentration, c_H, means that

either there is no relation between the two, or that the efficiency of stress induction per hydrogen atom increases with decreasing c_H due to possible differences in the H-bonding structure. We will come back to this issue later. It is also verified that, at this high generation rate, there is always a tendency of saturation with the exception of the HW sample with the highest hydrogen content (HW3). This sample presents a continuous $\Delta S \sim t^{0.5}$ relation, with a very weak indication of reduction of the rate exponent after 3 days of exposure.

3.15.4. Metastability

Light-induced defect (LID) creation in a-Si:H has the important feature of being a *reversible* phenomenon. Consider a film with initial defect density N_{Do} at room temperature, which is exposed to illumination. The defect density will increase with exposure time, t, to $N_D(t) = N_{Do} + \Delta N_D(t)$. The first manifestation of reversibility is that the room temperature defect density is restored to N_{Do} when this film is annealed at 190-200 ^oC in the dark for 1-2 hours. Furthermore, when the film is exposed for a second time, at the same temperature and illumination conditions, then the new LID creation curve $\Delta N_D(t)$, will be equal to that of the previous exposure. Reproducibility of $\Delta N_D(t)$ does not depend on the restoration of N_o, and is the second manifestation of reversibility. At this point we wish to note that full recovery is generally considered to depend on the samples characteristics and the intensity of the previous illumination. On the other hand reproducibility of the LID rate is always observed.

LID creation and the SW effect, in general, are most often called *metastable* phenomena. Metastability comes from the fact that the network in amorphous materials can have a large number of configurations with variable total energies and thus different macroscopically observed properties. In the presence of external factors, such as light, a-Si:H can jump from a lower to a higher energy configuration and stay there, presenting new properties. However when the temperature is raised suffociently, internal processes allow transitions among these configurations, then the material will naturally acquire a configuration for which its energy is reduced to its initial value and its properties are restored. Metastability is a major subject of study of the photo-induced structural changes in a-Si:H

A part of this study is devoted to the exploration of metastability on the photo-induced stress in a-Si:H. At first we wanted to find out whether the light-induced deflection of the free-end of a composite cantilever (MCL), disappears after annealing. For that purpose we have built an in-situ annealing apparatus with a heated gas nozzle brought very close to the MCL inside the SPM's head. In the first attempt, a composite MCL was surrounded for 30 min. by a nitrogen-hydrogen (forming gas) mixture coming out of the nozzle at a temperature of 190 ^{o}C. Although, there was a tendency of restoration of the MCL's original shape, we did not verify this result with other samples because we encountered two major problems. The first was the unwanted heating of the SPM's detection system by the hot gas. The second and most serious problem was the excellent thermal conductivity of c-Si. Its low value, which presented an advantage in the case of stress induction by intense illumination, was certain to produce a large temperature gradient between the free and the clamped end of the lever, the latter being always close to room temperature.

As described elsewhere[lxxvi] SEM images can be used in order to measure the curvature of an MCL when it is higher than the limiting value of 0.5 cm^{-1}. We have already shown in Fig. 4.22 that we observe maximum light-induced deflections of 150nm which correspond to curvatures (from Eq. [3.60] with L = 135μm) of the order of 0.05 cm^{-1}. This value is one order of magnitude lower than our SEM image detection limit. Therefore SEM images taken before and after exposure (or annealing) do not have sufficient resolution for detecting the minute changes in the curvature of the MCLs upon light soaking.

Another solution would have been to anneal the samples away from the SPM's holder and detect whether there is any reduction of stress, by measuring the difference in deflection signals before and after annealing. This requires a positioning accuracy of the free end of a MCL to better than 1 nm. Such accuracy cannot be achieved by hand. Therefore the difference in deflection signals before and after annealing is arbitrary and cannot be used as a measure of reversibility.

As it is virtually impossible to verify whether or not the curvature of the MCL i.e. the stress of the film is restored to its initial value within the accuracy of the ΔS measurement, we focused our interest on the study of the reproducibility of the $\Delta S(t)$

curve, after annealing at several different temperatures. The samples selected for the annealing experiments, were the HW1 and HW3 shown in Table 4.IV, because they are deposited at very different substrate temperatures and they exhibit hydrogen concentrations which are an order of magnitude apart. We also studied a cantilever with PECVD material having identical properties to the PE sample of Table 4.IV. The experimental sequence and the results, i.e. the $\Delta S(t)$ curves, for the three samples are given in Fig. 4.25. Annealing of the samples was always done in nitrogen gas environment, to prevent them from oxidization, and the transition from room to annealing temperature and back was done slowly, in order to avoid fracture of the cantilevers due to temperature gradients. Exposure was always done with a generation rate $G_o = 2 \cdot 10^{23}$ $cm^{-3}s^{-1}$.

A fully reversible phenomenon means that after annealing, the $\Delta S(t)$ curve is reproduced both in magnitude and time-dependence when the sample is exposed under the same temperature and illumination conditions. The first annealing was done at 190 ^{o}C. We started from this temperature because at this value all the SW defects disappear. We observe however that in all cases $\Delta S(t)$ is not restored. This is in fact the only common feature among these samples. Subsequent annealings at 235 and 270 ^{o}C for the same amount of time, reveal a very different behavior. HW1 exhibits almost full recovery at 270 ^{o}C while higher temperatures do not have any beneficial effect to the HW3 and PE films.

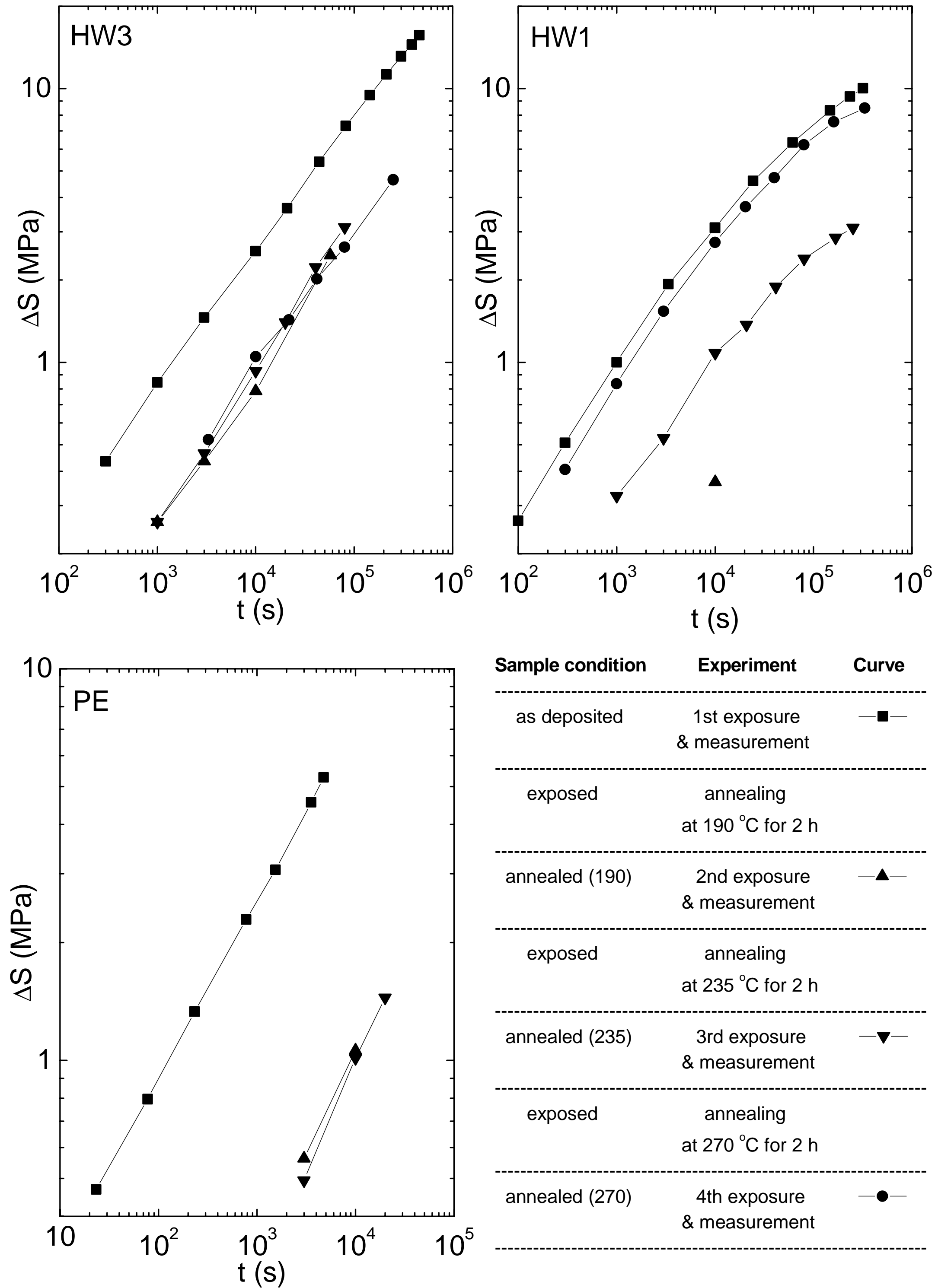

Fig. 4.25 *Annealing procedure and results for the HW and PE samples. The exposures are always done with generation rate* $G_o = 2x10^{23}$ $cm^{-3}s^{-1}$.

In fact we observed that **the latter have reached a new state** after their first annealing at 190 °C, **which is precisely reproduced with subsequent annealings** at the same T. We did not exceed 270 °C because at such elevated temperatures there is

a high probability that hydrogen rearranges inside the sample or even effuses out of it, producing irreversible changes of the structural and electronic properties (see Section 1.3.3).

We conclude that the *ΔS(t)* curve of the as-deposited state cannot generally be reproduced after annealing. The latter has been observed to occur only for the low-c_H HW sample and at very high temperatures. On the other hand, the first annealing at 190 ^{o}C seems to bring an a-Si:H film to a new state, which is characterized by a lower efficiency of stress induction under illumination and by *full* reproducibility of the *ΔS(t)* curve after subsequent annealings. This observation actually proves that the as-deposited and annealed states are not identical. We must also point out here that the intensity of monochromatic CW illumination used for the study of *ΔS(t)*, is much higher than the intensities used for the study of the SW effect. In fact there are no experimental data for the SW kinetics and metastability for CW generation rates of the order of 10^{23} $cm^{-3}s^{-1}$. It is very likely that the SW effect produced under extreme light intensities is not a fully reversible phenomenon.

3.15.5. Study of *ΔS*(*t*) in unhydrogenated a-Si

As *ΔS*(*t*) does not appear to depend on c_H, the question arises whether unhydrogenated amorphous Silicon presents any photo-induced stress. In order to answer this question we had, the cantilever named C3 of Table 4.III, deposited with a-Si, which was produced by e-gun evaporation of a c-Si target. The deposition temperature was 230 ^{o}C and the thickness of the evaporated film was approximately 0.9 μm. The Young's modulus of the material was found from oscillation frequency measurements to be ~ 90 GPa. Its low value, compared to the theoretically predicted 130-150 GPa (see Section 3.14.3), is due to the well established presence of a large volume fraction of voids.

The first difference of this film, compared to a-Si:H material, is that it exhibits **tensile** stress in its as-deposited state. Apart from that, this is the only sample for which we observed a deflection of the free end of the MCL **in the dark**. This deflection has the same direction with the light-induced deflection of a-Si:H and thus corresponds to a volume expansion of the material. In this case however, expansion does not

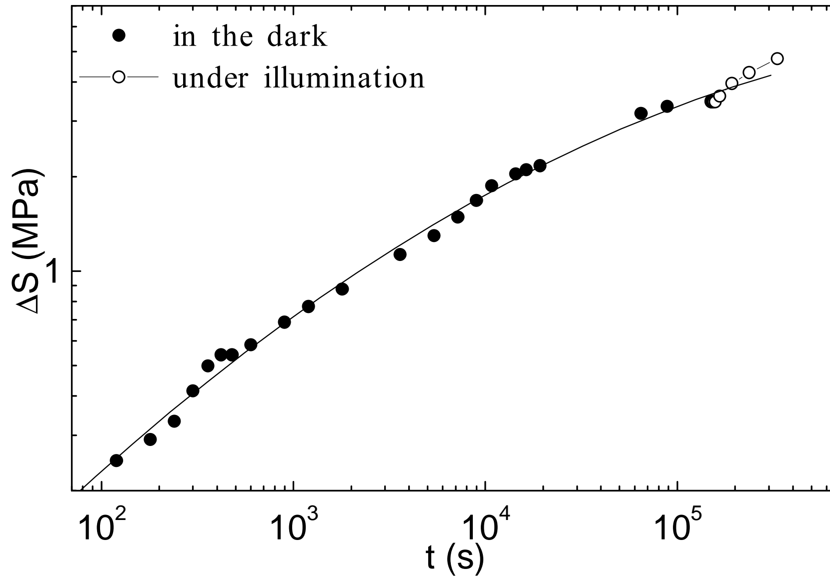

correspond to an increase of compressive stress but actually to a relaxation of the already present tensile stress. In Fig. 4.26 we plot the absolute decrease of tensile stress $\Delta S(t)$ with time.

Fig. 4.26 *Absolute decrease of the tensile stress, ΔS, of an evaporated a-Si sample with time, t. Solid circles are data taken in the dark and open circles are data taken under illumination of 17 W/cm^2. The lines are guides to the eye.*

The first measurement was made shortly after the sample was taken out of the deposition chamber. The solid line in Fig. 4.26 is a least-square 2nd order polynomial fit, plotted as a guide to the eye. Fig. 4.26 shows intense relaxation in the dark but with a clear tendency of stabilization at long times. The *ΔS* change in the dark is probably due to oxidization and moisture adsorption on the internal surfaces of the open network of voids.[lxxvii] This suggestion is supported by the observation that evaporated a-Si films are actually porous.[lxxvii]

After more than one and a half day in the dark, we exposed the sample in the 658nm light of 17 W/cm^2, used also for the experiments on the a-Si:H films, and we continued recording the change in stress, *ΔS*, with time. Our results are shown, with open circles, in Fig. 4.26. We observe that there is a slight enhancement of ΔS(t) at the early stages of exposure, however the *ΔS* increase rate falls back to its normal dark relaxation value after two days of exposure. We conclude that light has caused an extra stress change of approximately 1 MPa, after exposure of $1.8{\cdot}10^5$ s. This change is almost 20 times lower than the smallest *ΔS* change observed in a-Si:H for the same

light intensity and exposure time and is attributed to some activation of the oxidization of voids, by the release of energy upon carrier recombination. This "mobility" of the network may play some role to the photo-induced stress seen in a-Si:H but it is not the dominant mechanism behind the phenomenon.

3.15.6. Study of ΔS(t) in high temperature annealed a-Si:H.

This experiment was done in order to further explore more the role of hydrogen in the phenomenon of photo-induced stress in a-Si:H. We wanted to find out how if the photo-induced stress is affected by annealing the samples at temperatures high enough for hydrogen evolution. (see Section 1.3.3)

For the study of high annealing temperature effects we used the PE sample which was exposed to the low generation light (G_o/13) in Section 3.15.2. We selected this sample because it was the least degraded film of our series. We annealed the corresponding cantilever at 420 ^oC for 15 hours in high vacuum (approximately $5x10^{-6}$ mbar) together with a film, which was deposited under the same conditions and with the same technique onto a c-Si substrate. The latter was used for infrared absorption measurements in order to estimate the total change in the hydrogen concentration before and after the treatment. After cooling to room temperature we exposed the cantilever to the high intensity illumination $G_o = 2\cdot10^{23}$ $cm^{-3}s^{-1}$. To our surprise we observed that the sample has completely lost its ability to produce stress under illumination; after 2 days ($1.7x10^5$ s) of exposure there was no measurable deflection of the cantilevers' free end. Another effect of high temperature annealing was that the stress of the sample has changed from compressive to tensile. This means that the cantilever, which was initially bent upwards, was found to bend downwards after annealing (see Fig. 3.1).

As we have already discussed in Section 1.3.3, annealing at such high temperatures is characterized by a substantial motion of hydrogen. As a result of this motion, hydrogen can effuse out of from the sample. We measured IR absorption of the film deposited on the c-Si substrate before and after annealing, in order to estimate how much of the total hydrogen has effused. In Fig. 4.27 (A) we show the change in the

stretching mode absorption band (2000-2200 cm^{-1} see also the Section 1.3.1) due to annealing. We plot the absorption coefficient $a(cm^{-1})$ as a function of the wavenumber k(cm^{-1}). The straight lines are the sum of the least-square two-peak Gaussian fits presented in Fig. 4.27 (B). The integrated IR absorption is proportional to the total hydrogen concentration inside the sample as noted in section 1.3.1. Therefore the ratio of the integrated IR absorption before and after annealing can give an estimate on the amount of hydrogen that effused out of the film during the treatment. We calculated that only approximately 20 % of hydrogen has left the sample.

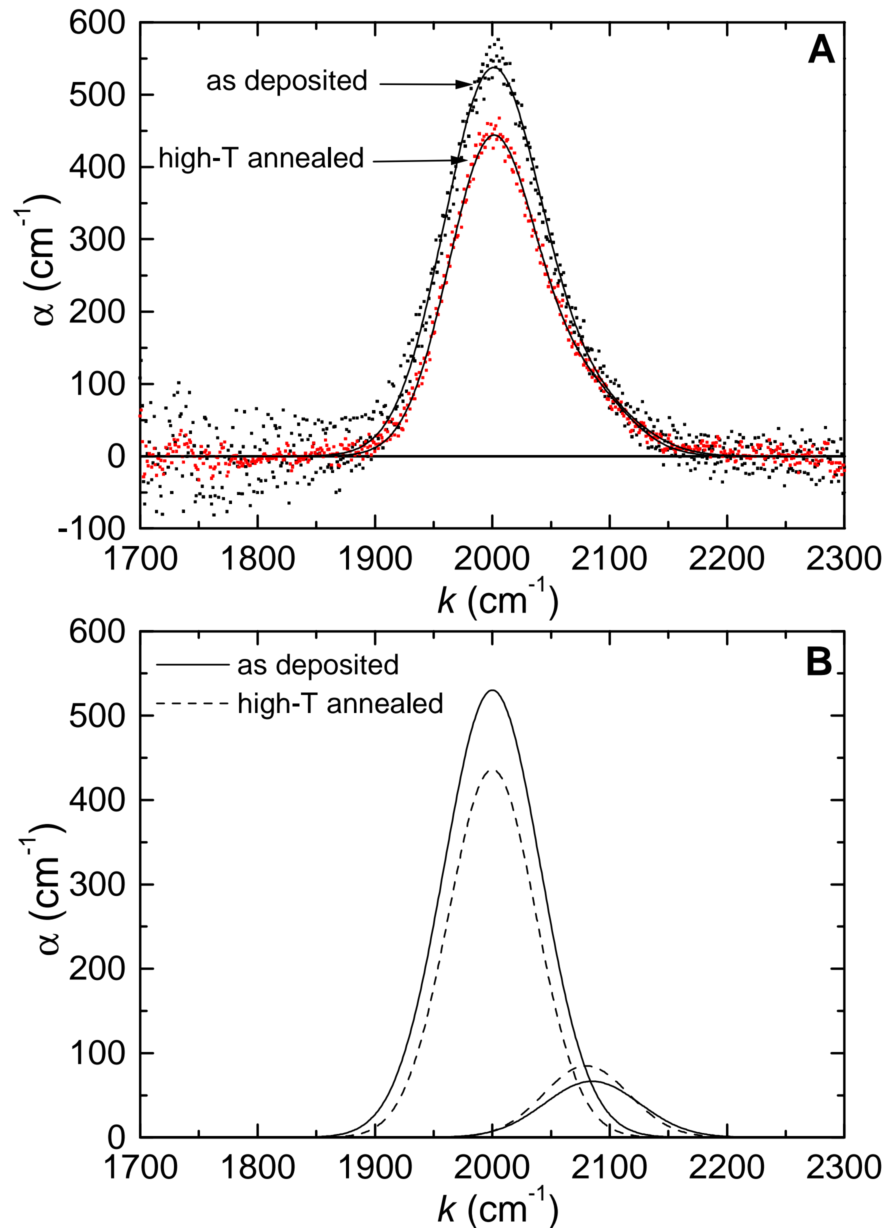

Fig. 4.27 *(A) Infrared absorption, a, as a function of the wavenumber, k, for the PE sample in the as-deposited and high temperature (420 °C) annealed state. The solid lines are least square two-peak Gaussian fits shown also in (B).*

This is consistent with the results of Mahan *et al.*[lxxviii] who found that at temperatures around 420 °C more than 80 hours are needed for the hydrogen to evolve completely out of device quality samples. We therefore conclude that it is not the loss of hydrogen that causes the absence of photo-induced stress in the high-T annealed sample.

In Section 1.3.1. we have seen that the stretching mode absorption band of a-Si:H consists mainly of two peaks: one centered at 2000 cm^{-1} and one at 2080-2100 cm^{-1}. The first peak is generally attributed to isolated mono-hydrides –i.e. dispersed Si-H bonds- or pairs of these and the second to clusters of such bonds. In Fig. 4.27 (B) we show the two Gaussian peaks that produce the best fit for the data of Fig. 4.27 (A) in the initial and the high-T annealed state. We also observe that these peaks are located at 2000 cm^{-1} and 2080 cm^{-1}. A striking feature of this figure is that high temperature annealing increases the ratio of the integrated absorption of the 2080 cm^{-1} peak to that of the 2000 cm^{-1} peak, I_{2080}/I_{2000}, by almost 50 %. This means that in the annealed state a larger percentage of hydrogen must be in the form of clusters compared to the initial state. This agrees with the results of Gleason *et al.*[lxxix] who observed that annealing at 387 ^{o}C causes either greater interactions between small clusters or the formation of larger clusters resulting from cluster migration or *coalescence*. Coalescence of voids is known to produce tensile stress in deposited films;[lxxx] two voids which coalesce have a tendency to produce a new void which has reduced volume compared to the sum of the two. Assuming that some of the H-clusters are located in internal surfaces of voids, then coalescence of these clusters may be a major cause for the change of intrinsic stress polarity (from compressive to tensile) observed after annealing. At this point we must point out that Padushek *et al.*[lxxxi] reported that the intrinsic stress of an a-Si:H sample can in fact change from compressive to tensile by annealing in the temperature region of 300-350 ^{o}C. These authors attributed this phenomenon to the contraction of the network at the origin of a very small percentage of effused H-atoms.

The absence of photo-induced stress after high-temperature annealing may correlate with two factors: a) the new hydrogen environment in the high-T annealed sample as established by the IR absorption measurement and b) the increased defect density of the high-T annealed sample compared to the initial low defect density state. From the data of Zhou *et al.*[lxxxii] we estimate that the defect density of the high-T annealed sample must be almost 100 times higher compared to that in the initial state. Defect creation has a detrimental effect on carrier lifetime and is a result of hydrogen atoms leaving Si-H bonds. The defects created are always fewer than the effused H-atoms because a large fraction of the dangling bonds can reform into weak Si-Si bonds

3.15.7. Discussion

3.15.7.1. Possible origins of photo-induced stress in a-Si:H

From our experimental results it clear that the phenomenon of creation or increase of **compressive** stress in a-Si:H under intense illumination is intrinsic to the material. This means that device quality a-Si:H films will always have a tendency to expand when exposed to bandgap light, irrespectively of the details of the deposition conditions and techniques utilized. Since this is such a universal effect, there must be a certain driving mechanism, common to all a-Si:H samples, behind it. In the following we examine three possibilities for this mechanism and evaluate their significance by immediate quantitative comparison with our experimental results.

A) **Defect creation.** The best known light-induced structural change in a-Si:H is the creation of additional dangling bonds (DBs). On this basis one could argue that the photo-induced stress is a consequence of DB creation. Each newly created dangling bond is accompanied by a local expansion of the lattice by Δu_l. The macroscopic volume expansion Δu_m is much smaller than Δu_l, since the latter is screened by the stress field surrounding the defect as we move away from it. The macroscopic volume change upon creation of N_D defects per unit volume should then be equal to $N_D \cdot \Delta u_m$. It is well established in the literature[li,lxxxiii] that the saturated defect density in device quality a-Si:H of the order 10^{17} cm^{-3}. The maximum volume change observed in our experiments is approximately $3x10^{-4}$ (see Fig. 4.23) which implies that $\Delta u_m \cong 3x10^{-21}$ cm^3. This volume is 200 times the volume per Si atom in c-Si. Δu_l should be even higher, which is clearly a non-realistic consequence of the creation of a single dangling bond.

B) *Increase of the H_2 gas pressure in voids.* ***In Section 2.2.2 we have introduced the H-collision model for defect creation. One of the basic assumptions of this model is that hydrogen atoms can be excited from Si-H bonds into a "mobile" state. The energy for this excitation is provided by carrier recombination in the vicinity of these bonds. Recombination energy also enhances the diffusion of mobile-H. It was suggested that a diffusing H-atom can find its way to the internal surface of a microvoid[lxxxiv] and that in the presence of another H-atom the two species can combine to form an H_2 molecule.[lxxxv] The formation and/or light-enhanced diffusion of molecular hydrogen inside a-Si:H[lxxxv] are also proposed theoretically but are not yet verified experimentally. What is interesting in these mechanisms is that there is the possibility that light increases the number of H_2 molecules inside the voids already present in a-Si:H. This would result in an increase of the gas pressure of these voids and thus in an increase in their volume. The question emerging is how much molecular hydrogen must accumulate inside voids in order to produce a volume expansion of the a-Si:H lattice of the order of $4x10^{-4}$ provided that the typical volume fraction of voids in device quality material is reported to be of the order of 0.1 %.[lxix] In order to answer this question, let us consider a sphere of radius*** **R** ***made out of a-Si:H material. Inside this sphere***

***there is a concentric spherical void of radius* R_v. *The void volume fraction in that case is* $f = (R_v/R)^3$. *Initially the pressure inside the void,* P_{in}, *and outside of the sphere,* P_{out}, *are assumed equal to 1 bar ≈ 100 kPa and no strain is present. Then we start filling the void with molecular hydrogen just as light is assumed to do. This will increase the pressure inside the void and its volume and therefore the volume of the a-Si:H sphere. Provided that the latter is under constant external pressure* P_{out} *= 100 kPa then the pressure inside the void will be given as a function of the radial strain of the sphere* $\varepsilon_R = \Delta R/R$ *by the relation:*[lxxxvi]**

$$P_{in} = 2\frac{1-f}{f}\left(1+\frac{2}{3}\frac{\mu}{\lambda}\right)\mu\varepsilon_R - \left(1-\frac{2}{3}\frac{\mu}{\lambda}\frac{1-f}{f}\right)P_{out}$$

[4.89]

where* λ, μ, *are the Lame's constants defined in Section 3.1.6.1. These constants are related to the Young's modulus* E *and the Poisson ratio* v *of a-Si:H through Eqs. [3.48]. The radial strain is equal to one third of the volume expansion of the sphere,* ΔV/V. *For an a-Si:H material with* E *= 100GPa and* v *= 0.2 (typical values) a volume expansion of 4x10*$^{-4}$ *will be induced only if the pressure inside the void reaches a value of* P_{in} *= 50 GPa ≈ 500 kbar. This is an extremely high value that would normally produce fracture of the material around the void. We conclude from this simple consideration that the observed

volume expansion cannot be due to increase in the gas pressure of voids. There are also other arguments against the mechanism of H_2 creation. The first is that if a considerable amount of bonded hydrogen turned to the molecular form, then this would induce an observable decrease in the Infrared absorption signal (see Section 1.3.1). Instead a light-induced increase of the stretching mode peak is observed (see Section 2.3). Furthermore there is considerable doubt whether molecular hydrogen could anneal back to the atomic form. Molecular hydrogen has a binding energy of 2.6 eV per atom and thus cannot account for even the partial annealing of the photo-induced stress described in Section 3.15.4.

***C*) The hydrogen flip mechanism.** Biswas and Li[lxxxvii] proposed in 1999 a simple "H-flip" model of rearrangements of bonded H-atoms that accounts naturally for many of the large scale structural changes observed recently in a-Si:H. They performed tight-binding molecular dynamics calculations on a 60-atom a-Si:H cell where all the H atoms are in monohydride (Si:H) groups. Their basic finding is that H-atoms in a-Si:H have two bonding configurations with different energies. The lower energy configuration is the normal tetrahedral bonding, with a H-Si_1 bond length of 1.48 Å and a distribution of H-Si_1-Si bond angles around tetrahedral (Fig. 4.28). In the higher energy configuration (Fig. 4.28), H is bonded to the same

Fig. 4.28 *The H-flip mechanism for light-induced volume expansion of a-Si:H.*

atom but in its "back-plane". Effectively, the H-atom is flipped to the backside of the H-Si bond. The Si_1 atom also moves about 0.5 Å into the back plane, resulting in a very similar H-Si_1 bond length. In the H-flip configuration the back bonds of the Si_1 atom become more planar, while the H-Si_1-Si bond angles deviate away

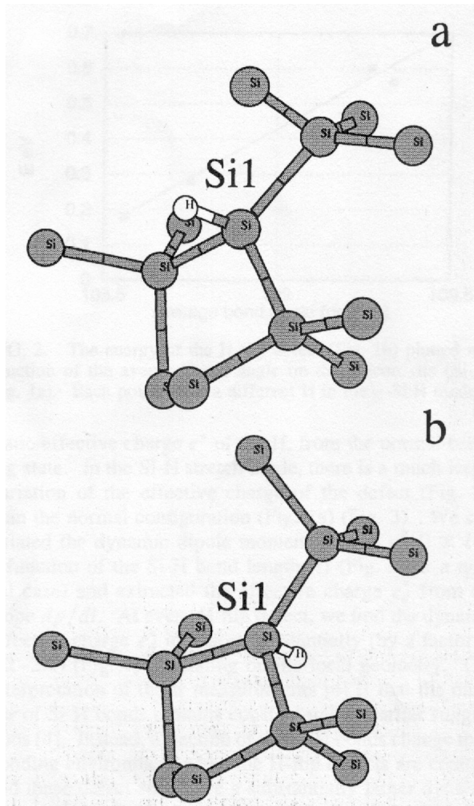

from tetrahedral towards 90°. The flipped configuration is a metastable local minimum calculated to be between 0.18 and 0.7 eV higher than the original configuration. It was also found that a H-atom must overcome a substantial energy barrier to move from the original to the flipped site which are separated by 3 to 4 Å. The barrier height is in the range of 1.5 to 1.8 eV. Since there is a substantial local motion of the H-atom it is found that the H-flip state significantly distorts the local atomic structure around it, through displacements of 0.1 – 0.2 Å for several neighboring silicon atoms and produces a small volume expansion of the network.

Biswas and Li[lxxxvii,lxxxviii] suggested that a density of H-flip states can be created by light-soaking. The energy needed for the H-atoms to surmount the barrier between the two configurations, can be provided by recombination events of photo-excited carriers which take place in the vicinity of these atoms. The authors estimated that light excitation can generate a saturated macroscopic fraction of 0.5% - 1% of H-flip states. For a typical H content of 10 % this predicts a macroscopic density of flipped H-atoms ($\sim 10^{19}$ cm^{-3}) much larger than the small density of metastable dangling bonds. They showed that this flipped hydrogen density could explain the experimental results of both the Infrared and NMR light-induced changes discussed in Section 2.3. The H-flip state induces volume expansion of the network. Since the Si-Si back bonds at this defect site are strained, the network expands to relieve the bond-angle strain. The authors also calculated that the light-induced fraction of H-flip states can produce a maximum volume expansion of 4×10^{-4} or an average value of $(1\text{-}2)\times10^{-4}$ for the material with 10 % hydrogen content. From their analysis it is obvious that volume expansion, will be proportional to the concentration of H-flip states in the sample. Finally they found with molecular dynamics that at annealing temperatures (T > 190 °C) where

hydrogen diffusion occurs, the state can flip back to its original configuration by a diffusing H-atom. When the latter approaches the backplane of a flipped bond it can break it and reform the normal Si-H bond.

3.15.7.2. H-flip in H-clusters: a modification of the Biswas model to account for our results.

There are some predictions of the Biswas mechanism, which are verified by our experimental results presented in the previous sections, provided that the photo-induced stress in a-Si:H remains proportional to the number of photo-generated flipped-H defects. At first we have seen that there is a general tendency of the *ΔS(t)* curves to saturate at long exposure times (Fig. 4.24) although we have not observed actual saturation as this would require maybe months of exposure. The H-flip model also predicts a maximum volume expansion of $4x10^{-4}$ for a typical a-Si:H sample with c_H = 10 %. This is in agreement with our results of Fig. 4.23 showing saturation between 3 and 4 x 10^{-4} for the PE sample with c_H = 8 %. On the other hand the Biswas model implies that there should be a significant change of the saturated value of the photo-induced stress when the total hydrogen concentration changes by an order of magnitude in a-Si:H; the films with higher hydrogen concentration should be able to produce proportionally higher H-flip states and thus stress, under illumination. This is not verified in our experiments. The series of HW samples with different c_H (see Table 4.IV) show ΔS(t) curves which are very close to one another (Fig. 4.23).

The lack of immediate correlation between the photo-induced stress and the total H-concentration is further established in PECVD films prepared under different hydrogen dilution ratios. Stratakis[lxxvi] showed that these samples exhibit great differences in their *ΔS*(t) curves although they have roughly the same hydrogen content. We suggest that the magnitude of photo-induced stress in device quality a-Si:H films is not proportional to the total hydrogen content inside the material but to a fraction of this hydrogen with a specific bonding configuration.

In our study of the elastic properties (namely the Young's modulus) of a-Si:H we have shown that the best HW material, i.e. that with the lowest c_H and the best PE material, i.e. that prepared under high dilution conditions appear to be softer than

expected from continuous random network considerations (see Section 3.14.4). We concluded then that both samples appear to have inhomogeneous H-bonding structure. The high-dilution sample (PE-H) appears to have a larger volume fraction of clustered hydrogen regions than the low diluted one (PE-L). These regions are large enough in PE-H to percolate through the thickness of the film giving a columnar morphology for this material. As we have pointed out in section 1.3.2 device quality HW and PE samples have comparable volume fraction of H-clustered regions although the total H concentration may vary from 1 - 10 %. We remind here that PE-H shows greater ΔS effect than PE-L[lxxvi] and that the HW samples show comparable effects (Fig. 4.24). This comparison leads us to suggest that it is highly probable that ΔS originates mainly from flipping of Si-H bonds inside H-cluster rich material. This means that it may be easier for H-atoms located in clusters to flip-out of these clusters than dispersed Si-H bonds. Jackson and Zhang[lxxxix] showed that H-atoms bonded to silicon in close vicinity to each other tend to remain apart due to electrostatic repulsion among them. Therefore the barrier that a H atom has to overcome to the flipped position may be smaller inside a cluster than when isolated among Si atoms only. We believe that flipping out of clusters merits further investigation both experimentally and theoretically.

Biswas[lxxxvii] has shown theoretically that the H-flip state is in a metastable high-energy configuration that can anneal back to the normal Si-H bond in temperatures where hydrogen diffusion is significant (T > 190 ^{o}C). This means that after annealing one should be able to reproduce fully the kinetics of photo-induced stress since the annealed normal Si-H bonds could be flipped again under illumination. This is not generally observed in our metastability experiments described in Section 3.15.4. Annealing at 190 ^{O}C and subsequent soaking does not reproduce the ΔS(t) curve of the as-deposited films. On the other hand the ΔS(t) curves of the samples annealed once at 190 ^{o}C are fully reproducible after subsequent annealings (Fig. 4.25). Therefore for an annealed sample the photo-induced stress phenomenon is fully reversible and this is consistent to the Biswas flip mechanism prediction. There is a difference, however, between the as deposited and annealed state. We suggest that there may be H-flip configurations stable enough not to anneal at the usual temperatures. If such configurations actually exist then they should be exhausted after

the first or second (at most) light-soaking runs under such high illumination intensities leaving behind only the metastable configurations.

Finally the high-temperature annealing experiment presented in Section 3.15.6 has shown that an a-Si:H film annealed at temperatures high enough for hydrogen effusion to occur (T > 400 ^{0}C for high quality samples) does not show any ΔS(t) with illumination even if a substantial amount of hydrogen is still present inside the material. Although we have shown that the hydrogen bonding configuration changes significantly after such a treatment it is not reasonable to conclude that there is no hydrogen left in such a form that can be flipped by illumination. It is most reasonable, however, to suggest that due to the high defect density created by the partial effusion of H, the recombination events that have enough energy to induce flipping, i.e. the bimolecular ones (see Section 1.3), become a negligible fraction of the total. Therefore the absence of the phenomenon is not due to the absence of the mechanism but due to insufficient activation energy.

3.15.7.3. Correlation of ΔS(t) with light-induced defect creation

In the previous section we have ruled out that defect creation is the origin of photo-induced stress. We must however examine the opposite mechanism namely that the SW effect is a secondary effect, a consequence of volume expansion. Certainly we do not have a proof that volume expansion and SW are linked with a cause-effect relation but a number of observations support this view.

The major source of disorder energy inside a random network of atoms is the bond strain. Philips[xc] proposed that a four-fold coordinated random network is overcoordinated in the sense that there are too many bonding constrains compared to the number of degrees of freedom. These constrains were attributed to bond stretching and bond bending forces. The topological constrains of the overcoordinated network promote processes which tend to reduce the lattice strain energy. The reduction of network coordination is the easiest and most efficient way to minimize the lattice strain energy. Reduction of the network coordination can be achieved only by breaking weak Si-Si bonds. Therefore it is expected that in response to a process

which increases the lattice strain energy the network will react in order to minimize this energy by *breaking* Si-Si bonds.

The possibility that defect creation is caused by increase of stress in the lattice under illumination, is a fascinating new approach to the problem of understanding the SW effect. Any light-induced bonding rearrangement at certain sites e.g. at Si-H bonds which turn to the H-flip configuration, can create stress which propagates easily throughout the network. Biswas and Li[lxxxvii] showed for example that the H-flip state significantly distorts the local atomic structure around it, through displacements of 0.1 – 0.2 Å for several neighboring silicon atoms. These atoms can be located as far as 6 – 8 Å away from the H-flip state. When distorted Si-Si bonds located in the vicinity of the stress origins are weak enough then they will break in order to minimize the increase in the strain energy of the network, producing dangling bonds (DBs). The candidates for DB creation may be further than 4 Å away from the stress origin and if the latter are Si-H flipped bonds this would explain the experimental observation that the light-induced DBs are far from hydrogen atoms.[xci] Furthermore, H-flips can store strain energy until the latter becomes sufficient for breaking bonds. This explains why as many as 10^{19} cm^{-3} H-flip sites in the Biswas model may produce only 10^{17} cm^{-3} dangling bonds. Dangling bonds created under such a procedure will not reform since this would be energetically unfavorable, but may move away from each other by bond switching.

Another fact established experimentally is the creation of DBs by strong illumination at temperatures from as low as 4 K. Authors advocating models requiring long range H-diffusion for the SW effect to proceed, have attempted to account for the 4 K degradation with the help of light activated H-diffusion. Light enhancement of H-diffusion is actually observed but only as a relatively minor acceleration at elevated temperatures. H-flipping only requires high energy recombination events of carriers to activate the expansion centers. The band-to-tail recombination processes described in Section 1.4 can provide this kind of energy.[3] Based on this assumption we will try to formulate the link between photo-induced stress and light-induced defect creation in

---

[3] One needs photon energy of more than 1.5 eV to initiate the SW effect.

the specific case where the carrier lifetime (see Section 1.4) is dominated by recombination through defects.

3.15.7.4. Linked kinetics of volume expansion and defect creation.

Let us consider a density N of sites in a-Si:H, which under illumination can potentially reach a new configuration that induces stress in the lattice. These sites may be the Si-H bonds which, in the Biswas mechanism, turn into the H-flip states. For the sake of simplicity and immediate comparison to the Biswas model, we will hereafter refer to the stress-inducing configuration as the “flipped” site or bond. After an illumination time *t,* a density N_f of flipped sites will be produced, leaving behind ($N-N_f$) normal sites. According to the prediction of Biswas the total stress induced in the film at that time will be proportional to the density of N_f

$$\Delta S(t) \propto N_f(t)$$

[4.90]

As the stress-inducing mechanism is activated by the energy dissipated in the immediate surrounding by photo-carriers recombining bimolecularly, we assume that the rate of creation, R_f, of N_f at a certain illumination time *t*, will be proportional to the bimolecular recombination rate *R* and the density of normal (non-flipped) sites ($N-N_f$):

$$R_f = k_1 R\left(N - N_f\right)$$

[4.91]

where k_1 is a proportionality constant.

The H-flip state in the Biswas model is a configuration, which has higher energy than the normal Si-H bond. An energy barrier separates the two states. This barrier is high enough to prevent thermal generation of H-flip states at temperatures T ≤ 300 K and also thermal annealing of the H-flip states back to normal Si-H bonds.[lxxxvii] On the other hand H-flip states can actually return to the normal configuration when recombination energy is supplied. This is the opposite mechanism of light-induced stress generation and it may be called light-induced annealing of stress. The rate of

annealing of N_f sites, R_f', will of course be proportional to the density of the existing sites and to the photo-carrier recombination rate, *R*:

$$R_f' = -k_2 R N_f$$

[4.92]

where k_2 is also a proportionality constant. The barrier is actually smaller for annealing than for creation of the flipped configuration due to the energy difference between the normal and the H-flipped site. Therefore we expect that $k_2 > k_1$ since there are recombination events which can anneal the N_f sites, but do not have an energy high enough to produce them.

The total rate equation for the creation and loss of the density of sites, N_f, inducing stress, or H-flip states in the Biswas theory, is the sum of the creation and annealing rates described above

$$\frac{dN_f}{dt} = k_2 R \left(\frac{k_1}{k_2} N - N_f \right)$$

[4.11]

The first prediction of this simple equation is that there will be a saturation of the photo-induced stress when a fraction of k_1 / k_2 of normal sites have turned into the flipped arrangement. According to Biswas[lxxxvii] only 1 % of the normal Si-H bonds can become flipped-H bonds under illumination and this fraction is high-enough to produce a volume expansion of the lattice of the order of 4×10^{-4}. As we observe from our experimental results of photo-induced stress vs illumination time (Fig. 4.23 - Fig. 4.24) there are signs of saturation of the stress only for exposure times higher than 5×10^4 s for all samples studied. This means that for $t < 3 \times 10^4$ s the density of flipped sites must be negligible compared to the density of normal sites that can be flipped or

$$N_f << \frac{k_1}{k_2} N$$

[4.93]

and in this case Eq. [4.11] can be simplified to

$$\frac{dN_f}{dt} = k_1 R N$$

[4.94]

It was shown by Tran[xcii] that under CW illumination with band-gap light, a steady state between trapped carriers in band tails (CBT, VBT) and free carriers in the respective bands (CB, VB) is established (see Fig. 1.2). Electrons and holes are generated by light in pairs, but more holes are captured in the wider VBT than electrons in the narrower CBT. This means that the free electron density, n, will be higher that the free hole density, p, and the trapped hole density, p_t, will be higher than the trapped electron density, n_t, i.e. the inequalities $n > p$ and $p_t > n_t$ are valid. From this follows that the bimolecular or band-to-tail recombination rate defined, as $R \propto np_t + pn_t$, will be simplified to

$$R = cnp_t$$

[4.95]

where c is a proportionality constant. For temperatures such that kT is at least two times lower than the slope kT_v of the exponential VBT (Fig. 1.2), the density of trapped holes can be related to the mobility edge, E_v and the trap quasi-Fermi level for holes, E_{fp}, by[xciii]

$$p_t \propto \exp\left(-\frac{E_{fp} - E_v}{kT_v}\right)$$

[4.96]

With the exception of extremely high illumination intensities or low temperatures, the trap quasi-Fermi levels for electrons and holes are far enough from the respective band edges for the Boltzmann approximation to hold for the occupancy of the respective bands, leading to the relation

$$p \propto \exp\left(-\frac{E_{fp} - E_v}{kT}\right)$$

[4.97]

Combining Eqs [4.96], [4.97] we find a general relation between the free and trapped holes inside the material[xciii]

$$p_t = \gamma(T) p^{kT/kT_v}$$

[4.98]

were $\gamma(T)$ is a proportionality constant that depends on the temperature. All samples used in this study of photo-induced stress have VBT slopes approximately equal to 50 meV (see Fig. 1.3) which is two times higher that kT at room temperature (25 meV).

Therefore Eq. [4.98] holds in our experiments. Substituting Eq. [4.98] into Eq. [4.95] and the latter into [4.94] we find an equation connecting the rate of increase of the density of stress-inducing states with the concentration of the photo-carriers at room temperature

$$\frac{dN_f}{dt} = k_1 \gamma(T) np^{0.5} N$$

[4.99]

This is a very useful equation since it connects the photo-carrier concentrations in a-Si:H with the flipping rate. In the previous section we have suggested, that the stress induced under illumination by these N_f sites may be the cause for dangling bond (DB) creation. On the other hand we do not know a-priori the relation between the DB density, N_D, and the photo-induced stress, ΔS, or, in other words, the relation between N_D and N_f. This relation can be established only by combined experimental results from photo-induced stress and light-induced defect creation for a wide range of samples, generation rates and temperatures. Eq. [4.99] derived from simple considerations, in combination with our experimental results on ΔS(t), gives us the opportunity to find this relation only in the specific case in which the carrier lifetime, defined in Section 1.4, is determined by recombination through defects. In this case the photo-carrier densities are given by

$$n,p \propto G / N_D$$

[4.100]

Inserting the above into Eq. 4.17 we find

$$\frac{dN_f}{dt} \propto \left(\frac{G}{N_D} \right)^{3/2}$$

[4.101]

Our experimental results on the time and photocarrier generation rate, G, dependence of ΔS together with Eq. [4.90]

$$N_f \propto G^{0.7} t^{0.5}$$

[4.102]

The experimental uncertainty on the t exponent is much lower than on the G exponent as explained in section 3.15.2. Solving Eq. [4.101] for N_D with Eq. [4.102] for N_f we find that

$$N_D \propto G^{0.5} t^{0.33}$$

[4.103]

which is very close to the experimental results on the SW effect under CW illumination. The implied relation between N_D and N_f is then

$$N_D \propto N_f^{\;2/3}$$

[4.104]

We propose the following explanation for the 2/3 exponent. Photogenerated volume expansion ΔV occurs only in particular regions of the network as are the Si-H clusters in our modification of the Biswas model (see section 3.15.7.2). Dangling bonds are created at the outskirts of the expanding regions where tensile stress is larger. This means that the probability of defect creation is roughly proportional to the increase of a loosely defined surface area of interface between expanding and non-expanding regions while photo-dilatation is proportional to the increase of the volume of the expanding regions.

Assuming that the relation [4.104] is valid also for the long exposure times, where ΔS tends to saturate, we insert it into Eq. [4.100] and through the photo-carrier recombination rate, $R = c\gamma(\mathrm{T})np^{0.5}$, into the total rate equation for N_f, (Eq. [4.11]) to arrive to a new differential equation:

$$\frac{dN_f}{dt} = \frac{N_{sat}}{\tau}\left(\frac{N_{sat}}{N_f} - 1\right)$$

[4.105]

where, N_f, is the only unknown. The above equation, in which $N_{sat} = (k_1 / k_2)\, N$ and $\tau = N_{sat} / (k_2 c\gamma(\mathrm{T})G^{1.5})$, can be solved analytically to give the following formula:

$$x + ln(1 - x) + t / \tau = 0$$

[4.106]

where $x = N_f / N_{sat} = \Delta S / \Delta S_{sat}$. Eq. [4.106] may be used to describe the full kinetics of ΔS in which ΔS_{sat} is the saturation value of photo-induced stress and τ is a characteristic time (needed to reach 84 % of this value). In Fig. 4.29 we re-plot the data of ΔS(t) for the HW and PE samples in the as-deposited state, along with the best least-square fits using Eq. [4.106]. The values of τ and ΔS_{sat} for these fits are given in Table 4.VI We conclude from Fig. 4.29 that Eq. [4.106] can describe adequately our

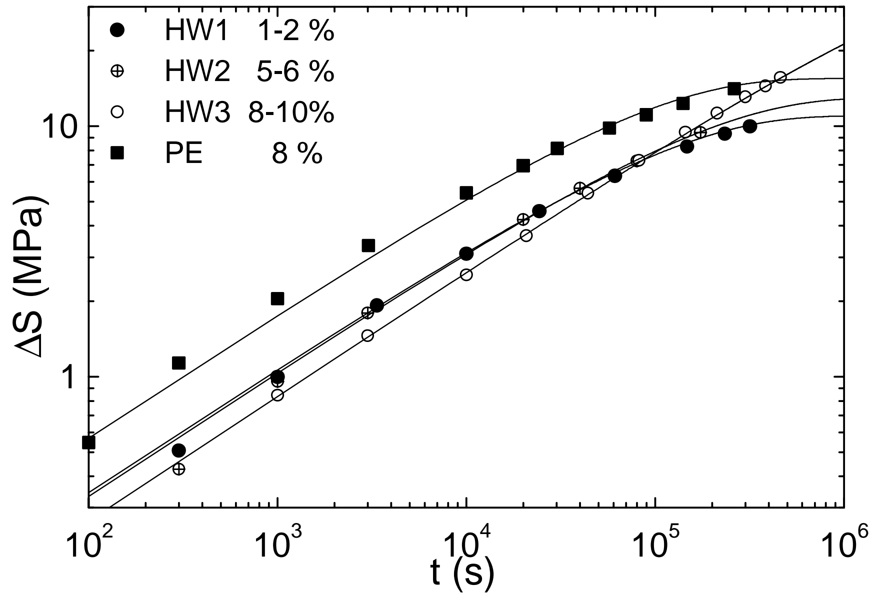

experimental results with only two fitting parameters. This indicates that the reasoning behind our analysis is valid at least in our experimental conditions and can serve as a good starting point for further investigation of ΔS and its relation to the SW effect, in

Fig. 4.29 *Least square fits of the data for the HW and PE samples according to* Eq. [4.106].

	HW1	HW2	HW3	PE
ΔS_{sat} (Mpa)	11	13	42	15
τ ($\times 10^5$ s)	2	3	50	1.5

Table 4.VI *Values of parameters used in the fits of* Fig. 4.29.

other temperature and illumination regimes where the latter has already been extensively studied.

3.15.8. Conclusions

The study of photo-induced stress (ΔS) or volume expansion (ΔV/V) in hydrogenated amorphous silicon provides new insight on structural modifications of the amorphous lattice under intense illumination, which may lead to improvement of our present understanding of the Staebler-Wronski (SW) effect. The basic conclusions of this work can be summarized as follows:

a) Device grade a-Si:H **always expands** under band-gap illumination, irrespective of the films' characteristics and deposition parameters. No volume change is observed in the dark.

b) There is always a tendency of **saturation** of the effect at long exposure times.

c) The magnitude of the effect is $\Delta V/V \sim 10^{-4}$–10^{-3}. It reveals the occurrence of **large-scale structural modifications** and excludes the possibility that these are limited to the vicinity of defect sites.

d) Before saturation, the phenomenon is characterized by the kinetics $\boldsymbol{\Delta S \sim t^{0.5}}$, in the temperature and illumination regime of our experiments.

e) Unhydrogenated a-Si and dehydrogenated a-Si:H, show no effect.

f) The phenomenon observed in the as-deposited state of a-Si:H samples is not fully metastable. On the other hand annealing at 190 ^{o}C brings the films to a new state in which the effect can be fully reversed.

g) The magnitude of ΔS does not correlate with the total hydrogen concentration of the films.

h) An H-flip mechanism of volume expansion, as proposed by Biswas and Li[lxxxvii], may be valid only if the main contribution to ΔS is from **flips of H atoms inside Si-H clusters**. This is an intriguing concept that needs further exploration.

i) Photo-induced stress and light induced defect creation kinetics have been linked through a simple model involving photo-carrier recombination.

Finally we wish to point out that this study introduces for the first time the possibility that the SW effect is a **result** of the photo-induced stressing of the a-Si:H network, a mechanism completely different from what has been proposed until today. We believe that this possibility must be further explored both theoretically and experimentally and that it might lead to the complete understanding of the microscopic mechanisms of light-induced degradation of Hydrogenated Amorphous Silicon.

Publications (April 2001)

1. "Light-induced defect creation in Hydrogenated Amorphous Silicon in the presence of positive space charge" E.Spanakis, E.Stratakis and P.Tzanetakis, 11th Workshop on Quantum Solar Energy Conversion, 14-20 March 1999, Wildhaus, Switzerland.

2. "Space charges resulting from photocurrents exceeding the thermionic emission currents in a-Si:H", E. Spanakis, E. Stratakis, N. Kopidakis, P. Tzanetakis and H. Fritzsche, J. Non-Cryst. Solids **266-269** (2000) 247 - 252.

3. "Stress and internal friction associated with light-induced structural changes of a-Si:H deposited on crystalline silicon microcantilevers" E. Stratakis, E. Spanakis, H. Fritzsche and P. Tzanetakis, J. Non-Cryst. Solids **266-269** (2000) 506 - 510.

4. "Elastic properties, intrinsic and photo-induced stress in a-Si:H thin films with different hydrogen content" E. Spanakis, E. Stratakis, P. Tzanetakis and Qi Wang, J. Appl. Phys. **89** [8] (2001) 4294 - 4300.

5. "Photoinduced stress in hydrogenated amorphous silicon films" E. Stratakis, E. Spanakis, P. Tzanetakis, H. Fritzsche, S. Guha and J. Yang, submitted for publication.

References (Chapter 1)

[i] J.C. Phillips, J. Non - Cryst. Solids **34** 153 (1979).

[ii] S.T. Pantelides, Phys. Rev. Lett. **42** 1151 (1979).

[iii] A. H. Mahan and M. Vanecek, in *Amorphous Silicon Materials and Solar Cells*, edited by B. L. Stafford, AIP Conf. Proc. No. 234 (AIP, New York 1991), p. 195.

[iv] A. H. Mahan, J. Carapella, B. P. Nelson, I. Balberg and R. S. Crandall, J. Appl. Phys. **69** [9] 6728 (1991)

[v] G. Lucowsky, R. J. Nemanich and J.C. Knights, Phys. Rev. B **19** 2064 (1979)

[vi] H. Shanks, C. J. Fang, L. Ley, M. Cardonna, F. J. Demond and S. Kalbitzer, Phys. Stat. Sol. B **100** 43 (1980)

[vii] A.A. Langford, M. L. Fleet, B. P. Nelson, W. A. Lanford and N. Maley, Phys Rev. B **45** [22] 13367 (1992).

[viii] J. D. Ouwens and R.E.I. Shropp, Phys. Rev. B **54** [24] 17759 (1996)

[ix] D. Han, J. Baugh, G. Yue and Qi Wang, Phys. Rev. B **62** [11] 7169 (2000).

[x] P. C. Taylor “Magnetic Resonance Measurements in a-Si:H” in *Semiconductor and Semimetals* Part C, edited by J.I. Pankove (Academic Press, New York, 1984).

[xi] K. K. Gleason, M.A. Petrich and J. A. Reimer, Phys. Rev. B **36** [6] 3259 (1987).

[xii] R.A. Street *Hydrogenated Amorphous Silicon* (Cambridge University Press,Cambridge,1991).

[xiii] Y. Wu, J. T. Stephen, D. X. Han, J. M. Rutland, R. S. Crandall and A. H. Mahan, Phys. Rev. Lett. **77** 2049 (1996).

[xiv] W. B. Jackson and S.B. Zhang “Hydrogen Complexes in Amorphous Silicon” in *Transport Correlation and Structural Defects* edited by H. Fritzsche (World Scientific, 1990)

[xv] J. B. Boyce and M. Stutzmann, Phys. Rev. Lett. **54** [6] 562 (1985).

[xvi] T. Su, P. C. Taylor, S. Chen, R. S. Crandall and A. H. Mahan, J. Non-Cryst Sol. **266-269** 195 (2000).

[xvii] A.H. Mahan, E. J. Johnson, R. S. Crandall and H. M. Branz, Mat. Res. Soc. Proc. Vol 377 (1995) p. 413.

[xviii] S. Zafar and EA. Schiff, Phys. Rev. Lett. **66** 1493 (1991).

[xix] S. Zafar and EA. Schiff, Phys. Rev. B **40** 5235 (1989).

[xx] D.L. Staebler and C.R. Wronski, Appl. Phys. Lett. **26** 292 (1977).

[xxi] H. Fritzsche, Mat. Res. Soc. Symp. Proc. Vol. 467 (1997) p.19.

[xxii] H. Fritzsche, Solid State Comm. **94** [11] 953 (1995).

References (Chapter 2)

[xxiii]M. Stutzmann, W.B. Jackson and C.C. tsai, Phys. Rev. B **32** 23 (1985).

[xxiv] P. Stradins and H. Fritzsche, J. Non-Cryst. Solids **198-200** 432 (1996).

[xxv] N. Kopidakis, PhD thesis, May 1998.

[xxvi] H.M. Branz, Phys. Rev. B **59** [8] 5498 (1999).

[xxvii] T. Kamei, N. Hata, A. Matsuda, T. Uchiyama, S. Amano, K. Tsukamoto, Y. Yoshioka and T. Hirao, Appl. Phys. Lett. **68** 2380 (1996).

[xxviii] P. Stradins and H. Fritzsche, Philos. Mag. B **69** 121 (1994).

[xxix] H. Fritzsche, *Development in Understanding and Controlling the Staebler-Wronski Effect* to appear in "Annual Review of Material Science" Vol. 31.

[xxx] J. Isoya, S. Yamasaki, H. Okushi, A. Matsuda and K. Tanaka, Phys. Rev. B **47** 7013 (1993).

[xxxi] D. Han and H. Fritzsche J. Non-Cryst. Solids **59-60** 397 (1983).

[xxxii] P. Tzanetakis, N. Kopidakis, M. Androulidaki, C. Kalpouzos, P. Stradins and H. Fritzsche, J. Non-Cryst. Solids **198-200** 458 (1996).

[xxxiii] H. Fritzsche, Solid State Comm. **94** [11] 953 (1995).

[xxxiv] G. L. Kong, D. L. Zhang, G. Z. Yue, Y. Q. Wang and X. B. Liao, Mat. Res. Soc. Symp. Proc. Vol. 507 (1998) p. 697.

[xxxv] P. Hari, P.C. Taylor and R.A Street, in "Amorphous Silicon technology – 1994", edited by E.A. Schiff, M. Hack, A. Madan, M. Powell and A. Matsuda Mat. Res. Soc. Vol. 336, p. 329.

[xxxvi] T. Gotoh, S. Nonomura, M. Nishio, N. Masui, S. Nitta, M. Kondo and A. Matsuda, J. Non-Cryst. Solids **227-230** 236 (1998).

[xxxvii] K. Shimizu, T. Tabuchi, M. Ida and H. Okamoto, J. Non-Cryst. Solids **227-230** 267 (1998).

References (Chapter 3)

[xxxviii] T. Gotoh, S. Nonomura, M. Nishio, N. Masui, S. Nitta, M. Kondo and A. Matsuda, J. Non-Cryst. Solids **227-230** 236 (1998).

[xxxix] K. Shimizu, T. Tabuchi, M. Ida and H. Okamoto, J. Non-Cryst. Solids **227-230** 267 (1998).

[xl] J. R. Barnes, R. J. Stephenson, C. N. Woodburn, S. J. O'Shea, M. E. Welland, T. Rayment, J. K. Gimzewski and Ch. Gerber, Rev. Sci. Instrum. **65** 3793 (1994).

[xli] D. G. Gahill, M. Katiyar and J. R. Abelson, Phys. Rev. B **50** 6077 (1994).

[xlii] *CRC Handbook of Chemistry and Physics*, 60th Edition, 1979-1980.

[xliii] E. J. Hearn, *Mechanics of Materials* (Pergamon Press, Oxford,1977) Chapters 1,4,5.

[xliv] H. Kolsky, *Stress Waves in Solids* (Dover, New York, 1963) Chapters II,III.

[xlv] U. Rabe, K. Janser and W. Arnold, Rev. Sci. Instrum. **67** [9] (1996) 3281.

[xlvi] K. E. Petersen and C. R. Guarnieri, J. Appl. Phys. **50** [11] (1979) 6761.

[xlvii] *Handbook of Thin Film Technology* edited by L. I. Maissel and R. Glang (McGraw-Hill, 1970) p.12-29.

[xlviii] G. C. Stoney, Proc. Roy. Soc. London **A32** (1909) 172.

[xlix] A. Brenner and S, Senderoff, J. Res. NBS **42** (1949) 105.

[l] P. M. Marcus, Phys. Rev. B **53** [11] (1996) 7460.

References (Chapter 4)

[li] R. A. Street, *Hydrogenated Amorphous Silicon* (Cambridge University Press, Cambridge, 1991).

[lii] *CRC Handbook of Chemistry and Physics*, 60th Edition, 1979-1980.

[liii] W. A. Brantley, J. Appl. Phys. **44** [1] (1973) 534.

[liv] A. H. Mahan, J. Carapella, B. P. Nelson, I. Balberg and R. S. Crandall, J. Appl. Phys. **69** 6728 (1991).

[lv] D. V. Tsu, B. S. Chao, S. R. Ovshinski, S. Guha and J. Yang , Appl. Phys. Lett. **71** 1317 (1997).

[lvi] S. Guha, J. Yang, D. L. Williamson, Y. Lubianiker, J. D. Cohen and A. H. Mahan, Appl. Phys. Lett **74** 1860 (1999).

[lvii] P. Stradins and H. Fritzsche, Philos. Mag. B **69** 121 (1994).

[lviii] Z. Remes, M. Vanecek, A. H. Mahan and R. S. Crandall, Phys. Rev. B **56** 12710 (1997).

[lix] R. Kuschnereit, H. Fath, A. A. Kolomenskii, M. Szabadi and P. Hess, Appl. Phys. A **61** 269 (1995).

[lx] S. Bauer, B. Schroeder and H. Oeshner, J. Non-Cryst. Solids **227-230** 34 (1998).

[lxi] H. He and M. F. Thorpe, Phys. Rev. Lett. **54** 2107 (1985).

[lxii] J. Robertson, Phys. Rev. Lett. **68** 220 (1992).

[lxiii] M. D. Kluge and J. R. Ray, Phys. Rev. B **37** [8] (1988) 4132.

[lxiv] C. Mathioudakis, P.C. Kelires, J. Non-Cryst. Solids **266-269** 161 (2000).

[lxv] S.I. Tan, B.S. Berry and B.L. Crowder, Appl. Phys. Lett. **20** [2] 88 (1972).

[lxvi] A. C. Ferrari, J. Robertson, M. G. Beghi, C. E. Bottani, R. Ferulano and R. Pastorelli, Appl. Phys. Lett. **75** 1893 (1999).

[lxvii] Y. Hishikawa, J. Appl. Phys. **62** 3150 (1987).

[lxviii] S. Gupta, R. S. Katiyar, G. Morell, S. Z. Weisz and I. Balberg, Appl. Phys. Lett **75** 2803 (1999).

[lxix] D.L. Williamson Mat. Res. Soc. Symp. Proc. Vol. 377 (1995) p. 251.

[lxx] R. S. Crandall, X. Liu and E. Iwaniczko, J. Non-Cryst. Sol. **227-230** 23 (1998) and references therein.

[lxxi] P. A. Fedders, D. J. Leopold, P. H. Chan, R. Borzi and R. E. Norberg, Phys. Rev. Lett. **85** 401 (2000).

[lxxii] K. F. Feenstra, R. E. I. Schropp and F. Van der Weg, J. Appl. Phys. **85** 6843 (1999).

[lxxiii] X. Xu, J. Yang and S. Guha, J. Non-Cryst. Solids **198-200** 60 (1996).

[lxxiv] T. Gotoh, S. Nonomura, M. Nishio, N. Masui, S. Nitta, M. Kondo and A. Matsuda, J. Non-Cryst. Solids **227-230** (1998) 236.

[lxxv] K. Shimizu, T. Tabuchi, M. Ida and H. Okamoto, J. Non-Cryst. Solids **227-230** (1998) 267.

[lxxvi] M. Stratakis, PhD Thesis

[lxxvii] H. Fritzsche, private communication.

[lxxviii] A. H. Mahan, E. J. Johnson, R. S. Crandall and H. M. Branz, Mat. Res. Soc. Symp. Proc. Vol 377 (1995) p. 413.

[lxxix] K. K. Gleason, M. A. Petrich and J. A. Reimer, Phys. Rev. B **36** [6] 3259 (1987).

[lxxx] *Handbook of Thin Film Technology* edited by L. I. Maissel and R. Glang (McGraw-Hill, 1970) p.12-29.

[lxxxi] P. Padushek and Ch. Hopfl, thin Solid Films **110** 291 (1983).

[lxxxii] J. H. Zhou, M Kumeda and T. Shimizu, J. Non-Cryst. Solids **195** 76 (1996).

[lxxxiii] H. R. Park, J. Z. Liu, P. Roca I Cabarrocas, A. Maruyama, M. Isomura, S. Wagner, J. R. Abelson and F. Finger, Appl. Phys. Lett. **57** [14] 1440 (1990).

[lxxxiv] D. E. Carlson, Appl. Phys. A:solid Surf. **41**, 305 (1986).

[lxxxv] P.A. Fedders, Phys. Rev. B **61** [23] 15797 (2000).

[lxxxvi] A. E. H. Love "A treatise on the mathematical theory of elasticity" (Dover, New York, 1944) p. 142.

[lxxxvii] R. Biswas and Y.-P. Li, Phys. Rev. Lett. **82** [12] 2512 (1999).

[lxxxviii] R. Biswas and Y.-P. Li, J. Non-Cryst. Solids **266-269** 401 (2000).

[lxxxix] W. B. Jackson and S. B. Zhang, "Hydrogen complexes in Amorphous Silicon" in *Transport, Correlation and Structural Defects*, edited by H. Fritzsche (World Scientific, 1990) p. 63.

[xc] J.C. Philips, J. Non-Cryst. Solids **34** 153 (1979).

[xci] J. Isoya, S. Yamasaki, H. Okushi, A. Matsuda and K. Tanaka, Phys. Rev. B **47** 7013 (1993).

[xcii] M. Tran, Phil. Mag. B **72** 35 (1995).

[xciii] K.C. Kao and W. Hwang *Electrical Transport In Solids* (Pergamon, Oxford, 1981) p. 159.